

UNCLASSIFIED

AD NUMBER

ADB014238

LIMITATION CHANGES

TO:

Approved for public release; distribution is unlimited.

FROM:

Distribution authorized to U.S. Gov't. agencies only; Test and Evaluation; MAR 1976. Other requests shall be referred to Air Force Materials Laboratory, MXS, Wright-Patterson AFB, OH 45433.

AUTHORITY

afwal ltr, 19 nov 1982

THIS PAGE IS UNCLASSIFIED

THIS REPORT HAS BEEN DELIMITED
AND CLEARED FOR PUBLIC RELEASE
UNDER DOD DIRECTIVE 5200.20
NO RESTRICTIONS ARE IMPOSED
ON ITS USE AND DISCLOSURE.

DISTRIBUTION STATEMENT A

APPROVED FOR PUBLIC RELEASE;
DISTRIBUTION UNLIMITED.

ADB014238

DDC FILE COPY

AFML-TR-76-41 ✓

[Handwritten signature and scribble]

VAPORIZATION OF GRAPHITIC MATERIALS AT HIGH MASS TRANSFER RATES

✓
AEROTHERM DIVISION/ACUREX CORPORATION
485 CLYDE AVENUE
MOUNTAIN VIEW, CALIFORNIA 94042

MARCH 1976

TECHNICAL REPORT AFML-TR-76-41
FINAL REPORT FOR PERIOD APRIL 1974 - MARCH 1976

Distribution limited to U.S. Government agencies only (test and evaluation). Other requests for this document must be referred to Air Force Materials Laboratory, Wright-Patterson Air Force Base (MXS), Ohio 45433.

28 OCT 1976

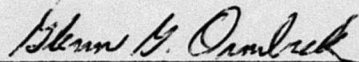
AIR FORCE MATERIALS LABORATORY
AIR FORCE WRIGHT AERONAUTICAL LABORATORIES
AIR FORCE SYSTEMS COMMAND
WRIGHT-PATTERSON AIR FORCE BASE, OHIO 45433

[Handwritten 'f' and 'DDC']
RECEIVED
OCT 28 1976
D

NOTICE

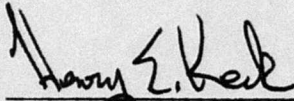
When Government drawings, specifications, or other data are used for any purpose other than in connection with a definitely related Government procurement operation, the United States Government thereby incurs no responsibility nor any obligation whatsoever; and the fact that the government may have formulated, furnished, or in any way supplied the said drawings, specifications, or other data, is not to be regarded by implication or otherwise as in any manner licensing the holder or any other person or corporation, or conveying any rights or permission to manufacture, use, or sell any patented invention that may in any way be related thereto.

This technical report has been reviewed and is approved for publication.



GLENN G. ORMBREK
Project Officer

FOR THE DIRECTOR:



HENRY E. KECK, MAJOR, USAF
Chief, Space and Missile Branch
Systems Support Division
AF Materials Laboratory

Copies of this report should not be returned unless return is required by security considerations, contractual obligations, or notice on a specific document.

19 REPORT DOCUMENTATION PAGE		READ INSTRUCTIONS BEFORE COMPLETING FORM	
18 RESEARCH REPORT NUMBER AFML-TR-76-41 ✓	2. GOVT ACCESSION NO.	3. REPORT NUMBER 9	
4. TITLE (and Subtitle) VAPORIZATION OF GRAPHITIC MATERIALS AT HIGH MASS TRANSFER RATES		5. TYPE OF REPORT & PERIOD COVERED Final Report, Apr 1974 - Mar 1976	
6. AUTHOR(s) R. E. Maurer, T. F. Foster G. Hartman C. A. Powars		7. PERFORMING ORG. REPORT NUMBER Aerotherm Final Report 76-185	
8. PERFORMING ORGANIZATION NAME AND ADDRESS Aerotherm Division/Acurex Corporation 485 Clyde Avenue Mountain View, CA 94042		9. CONTRACT OR GRANT NUMBER(s) F33615-74-C-5094	
10. CONTROLLING OFFICE NAME AND ADDRESS Air Force Materials Laboratory AFML/MXS Wright-Patterson Air Force Base Ohio 45433		11. REPORT DATE Mar 1976	
12. MONITORING AGENCY NAME & ADDRESS (if different from Controlling Office)		13. SECURITY CLASS. (of this report) Unclassified	
14. Aerotherm-76-185		15. DECLASSIFICATION/DOWNGRADING SCHEDULE	
16. DISTRIBUTION STATEMENT (of this Report) Distribution limited to U.S. Government agencies only (test and evaluation). Other requests for this document must be referred to Air Force Materials Laboratory, Wright-Patterson Air Force Base (MXS), Ohio 45433.		17. DISTRIBUTION STATEMENT (of the abstract entered in Block 20, if different from Report) 28 OCT 1976	
18. SUPPLEMENTARY NOTES		19. KEY WORDS (Continue on reverse side if necessary and identify by block number) 1. Ablation testing of ATJ-S graphite 2. Carbon sublimation 3. High temperature carbon response 4. Sublimation kinetics	
20. ABSTRACT (Continue on reverse side if necessary and identify by block number) The thermochemical sublimation response of ATJ-S graphite in both low and high mass transfer convective environments was studied both experimentally and analytically. ATJ-S graphite models were ablation tested in the NASA Ames Advanced Entry Heating Simulator (AEHS) test facility at 0.1 and 1.0 atmosphere impact pressure test conditions. Ablation tests were run under both subsonic and supersonic flow conditions at both pressures. High quality recession rate and surface temperature from the ablation tests		21. NUMBER OF PAGES 121p	

407435

YB

UNCLASSIFIED

SECURITY CLASSIFICATION OF THIS PAGE (When Data Entered)

20.

were correlated with various thermochemical ablation predictions. Results from the low subsonic flow conditions (low mass transfer rates) exhibit good agreement with the JANAF thermochemical model for carbon vapor species ($C_1 - C_5$). Results from these tests under supersonic flow conditions (high mass transfer) show the data to exhibit slight kinetic sublimation effects compared to JANAF equilibrium sublimation predictions. Extrapolation of the inferred kinetic sublimation effects to the high pressure regime of interest (10 - 300 atmospheres) shows the uncertainty in both surface temperature and recession rates to be less than 1 percent. The conclusion is made that the JANAF equilibrium sublimation model is most appropriate for graphite thermochemical ablation predictions under high pressure reentry conditions.

FOREWORD

This Final Report documents the results of research performed by the Aerotherm Division of Acurex Corporation, Mountain View, California, for the Air Force Materials Laboratory, Systems Support Division, Space and Missiles Branch, under Contract F33615-74-C-5D94. The AFML Project Engineer was initially Capt. G. Y. Jumper, Jr. (AFML/MXS) and this responsibility was subsequently assumed by Mr. G. G. Ormbrek (AFML/MXS). The Aerotherm Project Manager was Mr. C. A. Powars. This research was conducted during the period April, 1974 through January, 1976. This report was submitted to AFML in January 1976.

The experimental portion of this program was accomplished using NASA Ames test facilities, equipment, and personnel, through a cooperative arrangement between the Air Force Materials Laboratory and NASA Ames Research Center. The NASA Ames Advanced Entry Heating Simulator facility was used to conduct the tests, and certain required modifications to this facility were provided by NASA Ames and Aerotherm under AFML sponsorship. The cooperation of Mr. Howard Larson (Branch Chief) and Dr. Philip Nachtsheim (Assistant Branch Chief) of the Thermal Protection Branch in making available the NASA facilities, equipment, and personnel to support this program is gratefully acknowledged. Valuable technical assistance was provided by Mr. John Lundell. Mr. David Peterson and Mr. Frank Nichols provided assistance relative to test equipment utilization and modification. Finally, the services of Mr. Jack Hagan and Mr. Harry Simmon in operating the test facility and associated equipment is most gratefully acknowledged.

ACCESSION for		
NTIS	White Section	<input type="checkbox"/>
DDC	Buff Section	<input checked="" type="checkbox"/>
UNANNOUNCED		<input type="checkbox"/>
JUSTIFICATION.....		
BY.....		
DISTRIBUTION/AVAILABILITY CODES		
Dist.	AVAIL. REQ./OF SPECIAL	
B		

DDC
RECEIVED
 OCT 28 1976
RECEIVED
 D

TABLE OF CONTENTS

Section		Page
1	INTRODUCTION	1
2	CARBON SUBLIMATION UNCERTAINTIES	3
	2.1 Carbon Sublimation Thermochemistry	3
	2.2 Carbon Melting and Condensed Phase Polymorphic Forms	4
	2.3 Carbon Sublimation Rate Uncertainties	10
	2.3.1 Mass and Energy Transfer Models for Graphite Ablation	10
	2.3.2 Background and Modeling of Sublimation Kinetics	15
	2.3.3 Effect of the Surface Carbon Vapor State	16
	2.4 Particulate Mass Loss Uncertainties	21
3	EXPERIMENTAL APPROACH	24
	3.1 Experimental Approach	24
	3.2 Test Equipment	25
	3.2.1 AEHS Facility	25
	3.2.2 Facility Modifications	30
	3.2.3 Instrumentation	34
	3.3 Test Plan	40
	3.3.1 Checkout, Proof and Calibration Tests	42
	3.3.2 Sublimation Tests	43
	3.4 Test Results	52
	3.4.1 Test Matrix and Test Conditions	52
	3.4.2 Data Reduction Techniques	52
	3.4.3 Ablation Results	64
4	SUBLIMATION DATA ANALYSIS	66
	4.1 Data Comparison with Equilibrium Carbon Vapor Phase Models	66
	4.2 Data Comparison with Equilibrium and Rate Controlled Models	68
5	ABLATION DATA COMPARISON WITH PREVIOUSLY PUBLISHED RESULTS	76
	5.1 Wakefield and Peterson's AEHS Ablation Test Series	76
	5.2 Davy and Bar Num's AEHS Ablation Test Series	77
	5.3 Lundell and Dickey's ATJ Ablation Test Series	79
6	IMPLICATIONS of SUBLIMATION KINETICS ON HIGH PRESSURE ABLATION RESPONSE	85
	6.1 Generalized Kinetic Sublimation Ablation Predictions	86
	6.2 Kinetic Sublimation Predictions Applied to 50 MW Ablation Data and Flight	91
7	CONCLUSIONS	95
8	RECOMMENDATIONS	97
	APPENDIX A — DESIGN DETAILS OF AEHS CONSTRICTOR ARC MODIFICATION	A-1
	APPENDIX B — COMPLETE DATA SET FROM CALIBRAITON AND ATJ-S ABLATION TESTS IN THE NASA AMES AEHS FACILITY	B-1
	REFERENCES	R-1

LIST OF ILLUSTRATIONS

Figure		Page
1	Variation in the carbon phase diagram with C_3 species thermochemistry	6
2	Thermochemical mass balance for an ablating graphitic material	11
3	Mass transfer (B') curves for equilibrium and kinetic sublimation models	12
4	Thermochemical energy balance for an ablating graphite material	14
5	Sensitivity of kinetic sublimation predictions to the carbon vapor state	18
6	Radiative radial distributions at different axial positions	26
7	Advanced entry heating simulator	27
8	Spectral distribution, Ames 125 kw radiation source	29
9	Modified NASA Ames constrictor arc heater used for graphite sublimation kinetics study (46 segment configuration)	33
10	Gas metering board schematic	35
11	Thermogage pyrometer spectral response	37
12	Pyrometer alignment -- top view	38
13	Typical pyrometer output on CEC oscillograph	39
14	Ablation Model Configuration	41
15	Radiation contributions of surface gas cap and ablation products from AFML-TR-70-133	58
16	Pyrometer/recording system response to the reflected incident radiation on a "cold" calorimeter	60
17	Post-test ablation models from the four primary test conditions	62
18	Technique used to correct \dot{S} and B'_0 due to asymmetric ablation	63
19	Comparison of phase equilibrium sublimation data with four carbon vapor thermochemical models	69
20	Comparison of ATJ-S ablation data from the AEHS test series with the JANAF equilibrium predictions	70
21	Measured temperature shift with p_{eueCM} for ATJ-S ablation tests in the pressure range of 0.1 to 0.3 atmospheres	72
22	Measured temperature shift with p_{eueCM} referenced to experimental equilibrium graphite ablation temperatures in the pressure range 0.1 to 0.3 atmospheres	73
23	Measured temperature shift with p_{eueCM} for ATJ-S ablation tests in the pressure range 0.8 to 1.0 atmospheres	74
24	Comparison of Wakefield and Peterson's ablation data from the AEHS facility with ablation data from this series	78
25	Comparison of phase equilibrium sublimation data from Davy and Bar Nun's tests with data from this series	80

LIST OF ILLUSTRATIONS CONCLUDED

Figure		Page
26	Comparison of ablation data from this series with the data of Lundell and Dickey	82
27	Mass transfer predictions for graphite ablation in air assuming equilibrium and frozen carbon vapor species with kinetically controlled sublimation	87
28	Effect of sublimation kinetics on predicted graphite ablation temperatures in the 50 MW arc	93

LIST OF TABLES

Table		Page
1	Comparison of Experimental and Theoretical Values for Entropy of $C_{c(g)}$ Molecule	5
2	Summary of Carbon Triple Point Measurements Made to Date	8
3	Description of AEHS Constrictor Arc Heater Configurations	31
4	Summary of 0.1 ATM, Supersonic Sublimation Tests (Configuration 3)	45
5	Summary of 0.1 ATM, High Velocity, Subsonic Sublimation Tests (Configuration 2)	47
6	Summary of 0.1 ATM, Low Velocity, Subsonic Sublimation Tests (Configuration 1)	49
7	Summary of 1.0 ATM, Supersonic Sublimation Tests (Configuration 6)	50
8	Summary of 1.0 ATM, Low Velocity, Subsonic Sublimation Tests (Configuration 4)	51
9	Test Conditions and ATJ-S Surface Temperature Data	53
10	Ablation Results	65
11	Comparison of 1 Atmosphere Supersonic Flaw Convective Environmental Parameters	83
12	Sensitivity of Carbon Vapor Species Concentrations and Sublimation Rates with the Assumed Carbon Vapor State and with Pressure	92
13	Comparison of Equilibrium and Kinetically Controlled Sublimation Predictions for a Typical High β High Reentry Condition	94

SECTION 1

INTRODUCTION

The purpose of this study was to examine the sublimation* response of graphitic materials in the high convective mass transfer rate regime, i.e., the regime of primary interest relative to the application of these materials to reentry vehicle thermal protection systems. The specific objectives were to (a) design and demonstrate an experimental procedure for isolating the effects of sublimation kinetics in the high convective mass transfer rate regime, (b) analyze the resultant data to determine the importance of sublimation kinetics in controlling the rate of graphite ablation in this regime, and (c) analyze these experimental data in conjunction with the results of other recent investigations to better establish the correct equilibrium carbon vapor pressure law.

Important uncertainties currently exist regarding the sublimation of graphitic materials due primarily to uncertainties in the carbon vapor equilibrium thermochemical properties (i.e., the carbon equation of state) and the quantitative importance of sublimation kinetics relative to boundary layer diffusion in controlling the material ablation rate. Uncertainties also exist regarding carbon melting and particulate mass loss from graphitic materials during ablation. These uncertainties are reviewed in Section 2. In this section, the relevant findings of prior investigations of carbon sublimation are reviewed and compared. Also, current mathematical modeling of graphitic material ablation is reviewed (both with and without sublimation kinetics). This serves to establish the requirements for experimentally investigating sublimation kinetic effects in the high convective mass transfer regime.

The experimental approach used to study graphite sublimation kinetic effects is described in Section 3. Since this experimental approach was both unique and complex, details regarding the test facility, instrumentation, and test procedures are carefully documented in this section. Section 3 also includes a detailed summary of the resultant test data. An analysis of the experimental data is presented in Section 4. Consideration is given to the implications of the data relative to both the carbon vapor pressure law and the effects of sublimation kinetics.

*Throughout this report, the term "sublimation" is used (rather than "vaporization" which is often used in the carbon literature) to emphasize that it is the solid to gaseous phase change which is being studied.

In Section 5, the results of this study are compared with the findings of prior relevant investigations. Particular emphasis is given to those instances where the data generated on this program are in disagreement with prior data, and the potential reasons for the disagreement are discussed. The implications of this study relative to predicting the ablation response of reentry vehicle graphitic nosetips and heat shields is discussed in Section 6. The principal conclusions to be drawn from this study are summarized in Section 7, and recommendations for future work in this area are presented in Section 8.

SECTION 2

CARBON SUBLIMATION UNCERTAINTIES

The hyperthermal ablative response of carbon and graphitic materials continues to be controversial due principally to uncertainties in (1) the carbon equation of state, (2) the chemical and/or diffusional rate processes controlling sublimation, and (3) the significance of particulate mass loss from high temperature graphite surfaces. This section will present an overview of work in the field of high temperature carbon thermochemical response from an engineering perspective. Topics reviewed will include (1) carbon sublimation thermochemistry (Section 2.1), (2) carbon melting and solid polymorphic phases (Section 2.2), (3) carbon sublimation rate uncertainties (Section 2.3), and (4) particulate mass loss from polycrystalline graphites and carbon/carbon materials (Section 2.4).

2.1 CARBON SUBLIMATION THERMOCHEMISTRY

Extensive work in the area of equilibrium carbon sublimation has been conducted within the past two and a half decades (Reference 1-20). The purpose of these studies has been to identify the significant carbon vapor species and to evaluate their thermochemical properties in the hyperthermal regime of interest (i.e., $T_s > 5400^\circ\text{R}$). The procedure generally used to study equilibrium carbon sublimation is mass spectrometric analysis of the vapor species effusing from a Knudsen cell. Some experimental programs however, have studied sublimation as free vaporization directly from the surface of the specimen.

The most recently completed program utilizing the Knudsen cell approach was that of Milne, et al., (Reference 14) under AFML sponsorship. Milne's apparatus was unique in that the Knudsen cell was operated at temperatures approaching 6000°R . Their measurements of ion species ratios at 17 eV showed good agreement with the results of Drowart, et al., (Reference 1) for species C_1 - C_3 and C_5 although their values for C_4 were somewhat lower. Milne's results do therefore essentially substantiate the carbon vapor thermochemistry reported by JANAF (Reference 21). These results in turn tend to refute the theoretical carbon equations of state of Dolton, et al., (Reference 22) and Kratsch, et al., (Reference 23) recommended several years earlier.

Wachi and Gilmartin (Reference 15) also studied carbon sublimation using the technique of free vaporization. These researchers studied the free vaporization of ATJ, ZTA, TU-6, and pyrolytic graphites.

Relative ion intensities, apparent rates of vaporization, and activation energies of vaporization were measured for species C_1 - C_5 in the temperature range 5000°R - 5400°R. Some differences in the free vaporization of polycrystalline and pyrolytic graphites were noted. These differences were apparent at temperatures above 5200°R where the polycrystalline graphites would exhibit rapid increases in their vaporization rates with an attendant ejection of crystallites. (Note that Milne's results did not exhibit this behavior.) Wachi and Gilmartin attributed this behavior to the two phase nature of polycrystalline graphites although they could not provide a precise explanation. Interestingly, this observation of increased mass loss with a substantial particulate component has been observed by others (References 19, 24, 25) and relates to the uncertainty of carbon melting which is reviewed in Section 2.2.

Wachi and Gilmartin conclude from their results that for conventional graphites, the sublimation of carbon species from the crystalline phase is the predominant process, and at temperatures above 5300°R + 90°R the vaporization of species from the amorphous carbon binder is the predominant process. In addition, Wachi and Gilmartin observed a time dependency of the relative ion intensities of carbon species at a given surface temperature, which they attribute to changes in surface area and surface morphology. Their findings relate to the subject of carbon melting in Section 2.2 and specifically the results of Whittaker, et al., (Reference 19).

In summary, the results of their research substantiate the JANAF thermochemical models for vapor species C_1 - C_5 . Thus, the recent carbon sublimation studies whether using a Knudsen cell approach or free vaporization support the JANAF thermochemical model for the vapor species C_1 - C_5 (Reference 21). The predominant species is C_3 with C_1 and C_2 both about a factor of 5 below C_3 in concentration. Species C_4 and C_5 are about two orders of magnitude below the concentration of C_3 . Wachi, in a later paper (Reference 20) reports a C_3 thermochemical model which exhibits agreement from both the second law and third law analyses and also with the theoretical C_3 model of Strauss and Thiele (Reference 26). This model is compared with the JANAF values and other experimental and theoretical results in Table 1. The difference between the two C_3 models is slight as shown by the carbon phase diagram in Figure 1. These results certainly provide a valid experimental basis for the JANAF carbon vapor thermochemistry. One must bear in mind however that the JANAF predicted triple point ($P \sim 100$ atm; $T \sim 7400^\circ\text{R}$) exhibits poor agreement with reported triple point states (References 10, 12, 13). This controversy is reviewed in the next section.

2.2 CARBON MELTING AND CONDENSED PHASE POLYMORPHIC FORMS

Konig (Reference 18) in his review of carbon melting states that "although the melting temperatures reported by various authors, with few exceptions, are in good agreement, the question as to whether carbon is meltable at atmospheric pressure has not yet been answered satisfactorily."

TABLE 1. COMPARISON OF EXPERIMENTAL AND THEORETICAL VALUES FOR ENTROPY OF $C_3(g)$ MOLECULE

Type of $S_T^0(C_3)$	$S_T^0(C_3), eu$				Remarks	Reference
	2400°K	2500°K	2600°K	2700°K		
Experimental	76.1	-	-	-	$\Delta H_f^0(C_3) = 183.7 \text{ kcal/mole}$ $T = 2400^\circ K$	1, Drowart, et al.
Experimental	77.41	-	-	-	$\Delta H_f^0(C_3) = 184.4 \text{ kcal/mole}$ $T = 2400^\circ K$	4, Thorn & Winslow
Experimental	78.99	79.71	80.41	81.09	$\Delta H_f^0(C_3) = 189.4 \text{ kcal/mole}$ $T = 2700^\circ K$	7, Zavitsanos
Experimental	81.47	82.22	82.91	83.58	$\Delta f^0(C_3) = 195.2 \text{ kcal/mole}$ $T = 2579^\circ K$	20, Wachi & Gilmartin
Theoretical	81.41	81.94	82.46	82.95	Strauss & Thiele	26
Theoretical	78.04	78.92	79.41	79.89	JANAF	21

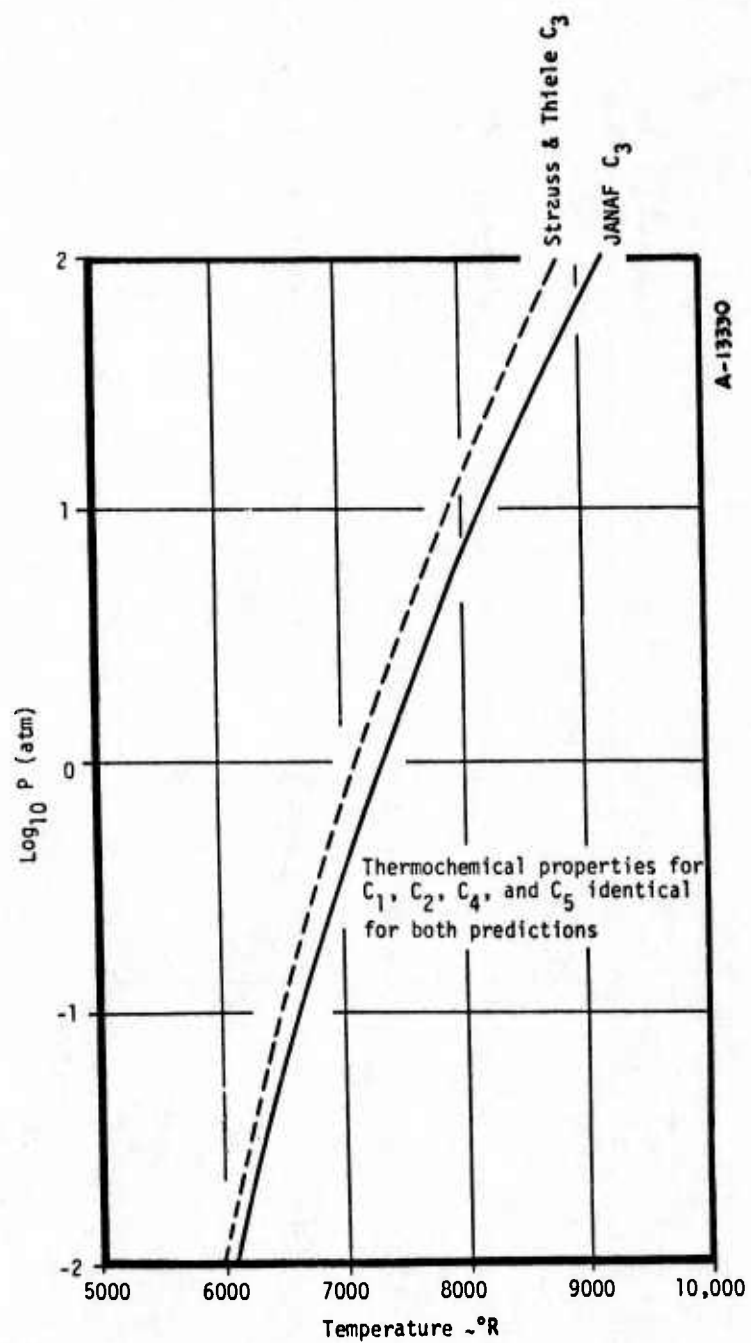


Figure 1. Variation in the carbon phase diagram with C₃ species thermochemistry.

König stated this observation in 1947 and in the nearly thirty years hence the uncertainty regarding the melting response of carbon is not much improved. Many researchers have studied the high temperature and pressure phase equilibrium of carbon with the intent of locating the triple point. These results are summarized in Table 2. The high pressure triple point data in Table 2 below 7400°R are felt to be of doubtful validity for the following reasons.

- Data below 7400°R have generally been derived from resistively heated specimen which exhibit internal temperature profiles which peak in the center. Since the melting occurs at the specimen's center, and the measured temperatures are surface or near surface values, they are probably low.
- No allowance was generally made for carbon vapor absorption of the surface radiative flux, again causing the measured temperature to be below the actual surface temperature.

Most notable among the recent work in this area is that of Schoessow (Reference 10), Diaconis, et al., (Reference 27) and Whittaker, et al., (Reference 19).

Schoessow's experimental technique reduced the effects of carbon vapor absorption on temperature measurements by defining a power/temperature correlation for the black body hole in the resistively heated specimen. The correlation was defined at the lower power/temperature levels where carbon vapor effects are minimal. By extrapolating the correlation to higher power levels, the melt temperature was evaluated from the input power at melt. Two potential effects which would cause the measured temperatures to be lower than actual are:

- The large size of the internal black body cavity and geometry of the specimen so as to allow substantial thermal gradients to exist within the cavity. Such thermal gradients would tend to reduce the measured black body temperature.
- Although precautions were taken, use of a disappearing filament pyrometer for black body temperature measurements is such that any radiation absorption by the carbon vapor in the cavity would be maximized because of the wide wavelength band of these instruments.

Although it is difficult to assign quantitative values to these uncertainties in Schoessow's temperature data, one concludes that these data are probably the best available.

The arc heating technique employed by Diaconis, et al., (Reference 27) to measure the melt temperature of ATJ-S and pyrolytic graphite proved reasonably successful and substantiates the data of Schoessow. The primary uncertainty in this experimental technique results from the uncertainty in the surface emissivity. By measuring the back surface of the ablating specimen, the carbon vapor absorption effects were minimized, although uncertainties resulting from temperature gradients within the material were introduced.

TABLE 2. SUMMARY OF CARBON TRIPLE POINT MEASUREMENTS MADE TO DATE

Principal Investigator	Reference	Triple Point Temperature °R	Pressure	Experimental Technique	Comments
Basset, J.	16	7200°R	100 atm	resistance heating	Small specimen limited the quality of black body hole - temperature measurement inaccuracies
Beque	6	7340°R	100 atm	unknown	Work similar to that of Basset's. Surface temperature measurement with calibrated optical pyrometer
Noda, T.	5	7235 ± 90°R	100-110 atm	resistance heating	Similar expt. tech. employed by Basset. Black-body hole was not high quality - no corrections for vapor absorption included
Jones, M. T.	11	7250°R	100 atm	resistance heating	Based on Basset's work - although the triple point temp. was evaluated by relating the eng. input $\oint C_p dT$, carbon (C_p is uncertain)
Bundy, F. P.	12	7200°R	102 atm	resistance heating	Earlier reported temp. was erroneous because of calibration errors
Fateeva, N. S.	13	7272°R	102 atm	resistively heated specimen in an argon environment	Thermal gradients within bb cavity could cause low temp. readings - also the use of a disappearing filament pyrometer is probably not too good
Schoessow, G. J.	10	7645°R	103 atm	resistively heated specimen with large black body cavity	Some questions regarding the quality of black body hole and carbon vapor absorption in the resistively heated specimens
Diaconis, N. S.	27	7380°R (resistively heated ATJ-S & pyrolytic) 7560°R (arc/ATJ-S) 7740°R (arc/pyrolytic) 6800 ± 54°R	102 atm	both resistively heated ATJ-S and pyrolytic graphite arc heated ATJ-S and pyrolytic graphite	Main question regarding arc heated specimen is the surface emissivity uncertainty
Whittaker, A. G.	19		~0.2 atm	CO ₂ laser heated spinning pyrolytic graphite rods	Uncertainty regarding the local carbon vapor pressure at the surface of the ablating specimen.

Van Vechten (Reference 28) has recently developed a scaling theory for predicting the melting temperatures of covalent crystals. He predicts a carbon melt temperature of 8746°R which is substantially above any of the experimental measurements. This predicted melt temperature is about 600°R above the highest measured graphite ablation temperatures in both the AEOL aeroballistic range (Reference 29) and the AFFOL 50 MW arc (Reference 30). Graphite and carbon/carbon ablation temperatures in the high pressure regime ($P_{t_2} \sim 100$ atm) in both facilities are in the range of 7800°R - 8100°R.

Whittaker's (Reference 19) experiments with laser heated spinning cylindrical samples of pyrolytic graphite have resulted in a unique set of carbon melting response data. Whittaker observes at a total chamber pressure of 0.2 atmospheres and a temperature of 6800°R \pm 54°R a liquid phase on the surface which can be observed flying from the spinning rod. Whittaker, however, does estimate the local vapor pressure to be 150 times the static pressure which implies a local pressure of 30 atm. Smaller droplets thrown off by the spinning rod are observed to maintain their integrity while vaporizing, whereas larger droplets break-up into 20-30 fragments about 0.3 msec after leaving the sample. Whittaker has captured the carbon matter leaving the spinning rods on copper slabs. At static pressures above 0.2 atmospheres, the material deposited on the slab has a uniform black appearance. When this material is removed from the surface of the slab and the surface is examined it exhibits a cratered appearance. These craters are felt to result from bombardment of the copper slab with globs of liquid carbon. At pressures below 0.2 atmospheres the deposit has a distinct silvery appearance and a considerably different character. It consists of a relatively dense sheet that breaks into strips which consist mainly of chaoite, α carbyne, and several other linear forms of polymorphic carbon.

The linear transitional polymorphic forms of carbon identified by Whittaker provide heretofore unavailable insight into the high temperature response of the carbon crystalline structure. Whittaker has observed that the solid phase transformations are slow at low temperature, and the rate increases as the triple point is approached. Whittaker believes the linear carbon polymorphs are confined to the temperature regime of 4600°R - 6850°R. To date eight polymorphic forms are known, and it is felt there may be others yet unidentified. Evidence exists which indicate that graphite transforms to chaoite at 4700°R and that it is β carbyne which melts to produce liquid carbon at 6850°R.

It is apparent that Whittaker's results are in conflict with the results of Schoessow and others who have placed the triple point pressure at 100 atm, although there is some uncertainty regarding the local carbon vapor pressure in his tests. In addition, the linear polymorphic forms of carbon above 4700°R identified by Whittaker are a unique finding. Whittaker is quick to point out that these linear forms are extremely unstable upon cooldown and therefore are not readily available to be identified on a post-test specimen. Cooldown rates of 3500°R/sec must be increased to 50,000°R/sec to freeze the linear polymorphic forms.

The review of work relating to carbon melting and the high temperature and pressure regime of the carbon phase diagram is presented to illustrate the uncertainty which currently exists in establishing the high temperature thermochemical response of graphitic materials. Whittaker's results which show an unstable met formation at 6850°R must be rationalized with the high pressure graphite ablation data which consistently show surface brightness temperatures in the range 7800°R - 8100°R. Possibly the rates controlling the transformation to the various linear polymorphic carbon states are such as to allow the material to be heated above the equilibrium melt temperature. It is obvious that questions regarding the mechanisms of carbon melt will persist for some time. At the present time, however, the ablation test data must be relied on for predictions of carbon and graphite ablation during reentry.

2.3 CARBON SUBLIMATION RATE UNCERTAINTIES

This review of graphite sublimation, the rate physics, and the current modeling techniques is presented in four subsections. Section 2.3.1 presents an overview of the mass and energy transfer models used to predict the thermochemical ablation response of graphitic materials. Section 2.3.2 reviews background and development of carbon kinetic sublimation models. Section 2.3.3 addresses the uncertainty associated with the state of the carbon vapor species adjacent to the ablating material when sublimation is kinetically controlled. Some models assume the gaseous carbon vapor species equilibrate while other models assume no gas phase reactions. Finally, the experimental verification of sublimation kinetics in the intermediate temperature regime is reviewed in Section 2.3.4.

2.3.1 Mass and Energy Transfer Models for Graphite Ablation

This section presents a brief review of the heat and mass transfer models and assumptions implicit in the thermochemical ablation predictions subsequently presented. The differential equations used to describe the thermochemical ablation of graphitic materials reviewed herein are based on the hypersonic approximation of Lees (Reference 31). Further assuming boundary layer similarity and unity Lewis-Semenov number, results in a direct solution of the mass and energy balance relations. Details of this reduction are outlined below.

Mass Transfer

The mass loss from a graphitic surface (assuming no particulate mass loss) is directly related to the surface recession rate by the simple expression

$$\dot{m}_s = (\rho u)_w = \rho \dot{s} \quad (1)$$

which is illustrated by the mass balance in Figure 2.

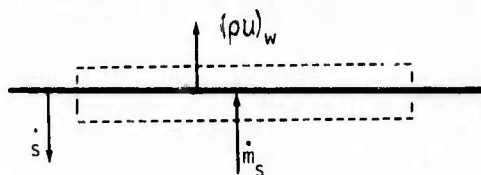


Figure 2. Thermochemical mass balance for an ablating graphitic material.

For graphite ablation in air the mass conservation is described by the following set of equations

$$\tilde{K}_{N_w} + \tilde{K}_{O_w} + \tilde{K}_{C_w} = 1 \quad (2)$$

$$(\rho u)_{C_w} = \rho \dot{s} = \rho \dot{s} \tilde{K}_{C_w} - (\rho D \frac{\partial \tilde{K}_C}{\partial y})_w \quad (3)$$

$$(\rho u)_{O_w} = 0 = \rho \dot{s} \tilde{K}_{O_w} - (\rho D \frac{\partial \tilde{K}_O}{\partial y})_w \quad (4)$$

$$(\rho u)_{N_w} = 0 = \rho \dot{s} \tilde{K}_{N_w} - (\rho D \frac{\partial \tilde{K}_N}{\partial y})_w \quad (5)$$

The gradients of the individual chemical elements at the wall are given by an equation of the form, e.g., carbon.

$$\left(\frac{\partial \tilde{K}_C}{\partial y} \right)_w = \left(\frac{\tilde{K}_{C_e} - \tilde{K}_{C_w}}{H_{S_e} - H_w} \right) \left(\frac{\partial H}{\partial y} \right)_w \quad (6)$$

where for unity Lewis-Semenov number the convective heat transfer to the wall by conduction and diffusion, based on a Stanton number becomes

$$\dot{q}_{\text{conv.}} = \left(\frac{k}{c_p} \frac{\partial H}{\partial y} \right)_w = \rho_e u_e c_H (H_{S_e} - H_w) \quad (7)$$

Thus, combining equations (6) and (7) to solve for $(\partial \tilde{K}_i / \partial y)_w$ in terms of the enthalpy potential and the Stanton number yields an expression for any of the elemental constituents at the wall

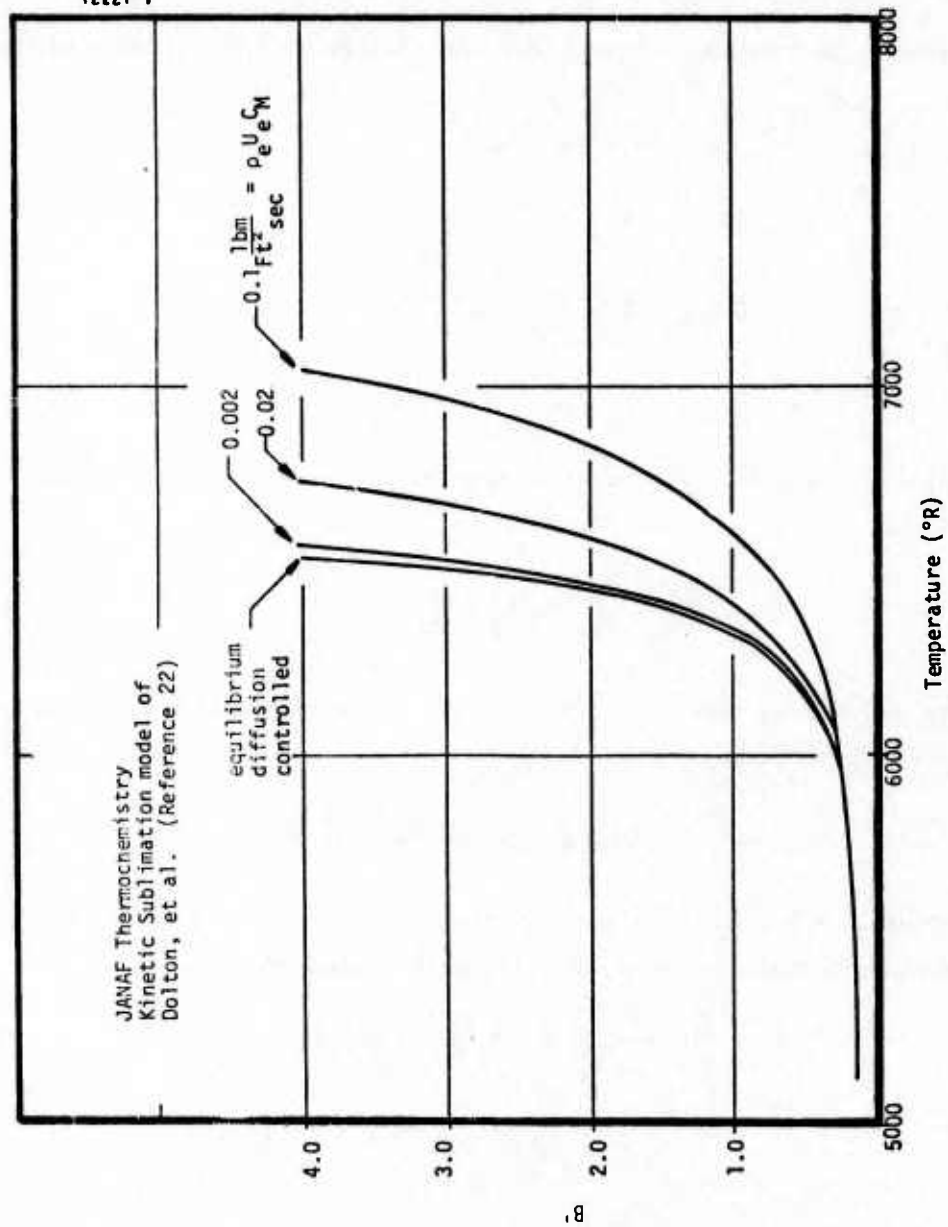
$$K_{i_w} = \left(\tilde{K}_{i_e} + \frac{\rho \dot{s}}{\rho_e u_e c_H} \tilde{K}_{C(s)} \right) / \left(1 + \frac{\rho \dot{s}}{\rho_e u_e c_H} \right) \quad (8)$$

where

$$B' = \frac{\rho \dot{s}}{\rho_e u_e c_H}$$

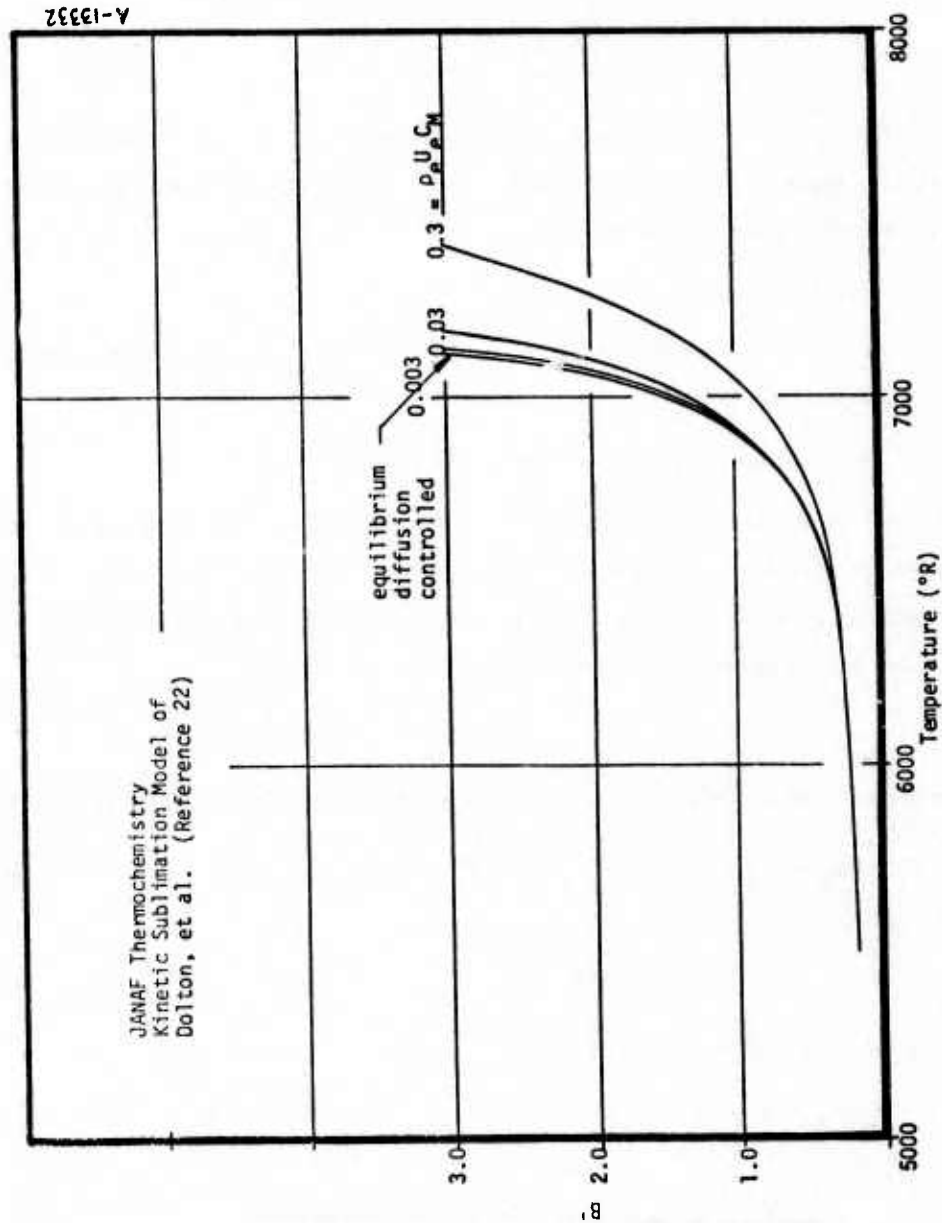
and the following boundary conditions are imposed for carbon ablation in air,

$$\tilde{K}_{C_e} = 0 \quad \tilde{K}_{N_e} = 0.768 \quad \tilde{K}_{O_e} = 0.232 \quad \tilde{K}_{C(s)} = 1$$



(a) Pressure = 0.1 atmosphere

Figure 3. Mass transfer (B') curves for equilibrium and kinetic sublimation models.



(b) Pressure = 1.0 atmosphere

Figure 3. Concluded.

Equation (8) shows that the mass fraction of the element carbon at the wall is determined solely by the mass flux of elemental carbon injected at the surface as vapor. Likewise, equation (8) specifies the elemental mass fraction of both oxygen and nitrogen at the wall in terms of the nondimensional mass transfer parameter B' . A stoichiometric expression then directly relates the elemental mass fractions to the chemical composition of the ablation species at the surface.

$$\tilde{k}_{iW} = \sum_j \frac{v_j M_i}{M_j} K_j \quad (9)$$

With the mass transfer equations complete the classical B'/T ablation curves can be specified by defining the thermochemical state of the ablation products. Much flexibility exists when specifying the thermochemical state of the ablation species, such as

1. chemical equilibrium
2. kinetic controlled sublimation (which imposes an additional constraint on the carbon vapor species surface mass transfer), frozen carbon vapor
3. kinetic controlled sublimation, equilibrium carbon vapor.

Examples of B'/T ablation curves are presented in Figure 3, showing the variation in the predicted surface temperature with variations in the assumed thermochemistry. To predict the graphite ablation response a surface energy balance must be coupled to both the mass transfer equations and the in-depth heat conduction. The energy balance expressions are developed subsequently.

Energy Transfer

The thermochemical energy balance equation for an ablating graphite surface is given below.

$$\rho_e U_e C_H (H_{se} - H_w) + \dot{q}_{rad_{in}} - \epsilon \sigma T_w^4 - (\rho u)_w H_w + \dot{m}_s H_s - \dot{q}_{cond} = 0 \quad (10)$$

where

$$H_w = \sum_j K_j H_j \quad (11)$$

This surface energy balance is shown in Figure 4.

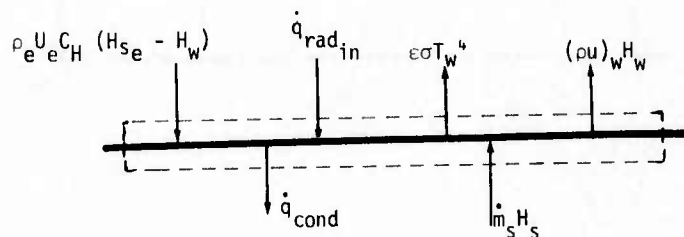


Figure 4. Thermochemical energy balance for an ablating graphite material.

The blowing to nonblowing heat and mass transfer ratio for laminar flow over an ablating graphite surface is best correlated by (Reference 32)

$$\frac{C_H}{C_{H_0}} = \frac{2\lambda B'_0}{(e^{2\lambda B'_0} - 1)} \quad \text{where } \lambda = 0.7 \quad (12)$$

Equation 10, when coupled to a standard finite difference solution to the indepth conduction equation enables a description of the thermochemical ablation response of a graphitic surface. Specific modeling techniques for predicting the kinetic sublimation response of a graphitic surface are reviewed in the next section.

2.3.2 Background and Modeling of Sublimation Kinetics

Graphite sublimation is kinetically controlled under free-molecular flow conditions and vaporization coefficients have been measured at these low temperature and pressure sublimation states (Reference 7). Before further consideration is given to the sublimation response in the free molecular regime, one must establish the need for modeling sublimation kinetics in the high pressure/highly convective regime of interest. To demonstrate how the existence of sublimation kinetics can be established, the process first must be described.

Kinetic controlled sublimation is modeled by using a Knudsen-Langmuir expression of the form.

$$\dot{m}_{C_i_w} = \alpha_{C_i} (P_{C_i_{\text{equil}}} - P_{C_i_w}) / \sqrt{\frac{2\pi RT_w}{m_{C_i}}} \quad (13)$$

which requires that the i^{th} carbon vapor species partial pressure is always below the equilibrium value for a non-zero mass flux. Because the species partial pressures at the wall must be below the equilibrium values, the rate controlled sublimation temperature must always be above the equilibrium diffusion controlled value. The fact that recent high quality graphite ablation temperatures are above the values predicted by either the Dolton or Kratsch equilibrium diffusion controlled ablation models suggests that either the diffusion controlled assumption is invalid or the thermochemical data are incorrect.

The early modeling of carbon sublimation kinetics was done by Dolton, et al., (Reference 22). This initial model was simplified by limiting ablation products to the following species N_2 , O_2 , CO, CN, C_2N_2 , C_1 - C_{16} where the production of CN was assumed to be equilibrium controlled and CO production was equilibrium/diffusion controlled. Carbon sublimation was controlled by the Knudsen-Langmuir rate equations shown above. In addition the carbon vapor species were assumed to not react in the gas phase (i.e., the carbon vapor concentrations were controlled by the sublimation process). Application of this model illustrated the controlling effects which sublimation kinetics have on the predicted graphite

ablation response. Sensitivity studies were even made to assess the significance of uncertainties in the species vaporization coefficients (α_{ci}) on the ablation predictions.

Subsequent graphite kinetic sublimation models developed by Zering (Reference 33) and Kratsch, et al., (Reference 34) were less restrictive with respect to the number of ablation products (CN, C_2N_2 , C_2N) and the reactivity of the carbon vapor species (i.e., equilibrium carbon vapor). Both models are considered an improvement over the initial modeling of Dolton, et al. Recent application of the Aerotherm Chemical Equilibrium (ACE) computer code (Reference 35) to graphite kinetic sublimation predictions has further advanced the generality of these calculations. No restriction exists with respect to the number of ablation products and the sublimation products can either be assumed to equilibrate or be frozen. Application of this ablation model has provided some insight into the significance of the assumed carbon vapor state at the surface (Reference 36). These results are reviewed in the subsequent section.

2.3.3 Effect of the Surface Carbon Vapor State

Graphite ablation predictions in Reference 36 illustrate the sensitivity of kinetic sublimation predictions to the assumed state of the carbon vapor species at the surface. Results of these calculations show that at pressures below one atmosphere the shift to higher temperatures with increasing $\rho_e U_e C_m$ (at constant B') is relatively insensitive to the state of the carbon vapor species at the surface. This result is shown in Figure 5. However, at pressures above 10 atmospheres, the sensitivity of B' /temperature curves to the assumed carbon vapor state at the surface increases substantially. This result is shown in Figure 5 at 100 atmospheres. In other words, at high pressures, if carbon sublimation is kinetically controlled, but the vapor species equilibrate in the gas phase the theoretical B' /temperature curve approaches the equilibrium diffusion controlled curve, as shown in Figure 5. Thus, the low to moderate pressure sublimation tests in the NASA Ames AEHS facility will not be sensitive to uncertainties in the carbon vapor state at the ablating surface. A more complete discussion of the carbon vapor state uncertainties and implications thereof as this relates to ablation predictions for flight is presented in Section 6.

2.3.4 Experimental Identification of Vaporization Kinetics Effects

It is apparent from the discussions in the previous two sections that kinetically controlled sublimation has the effect of reducing the sublimation rate from an ablating surface under a fixed set of environmental conditions. This result will cause: (1) the surface ablation temperature to rise and (2) the surface recession rate to decrease. These effects depend on the convective mass transfer rate

within the boundary layer. This behavior is evident in the comparison of equilibrium diffusion controlled and kinetically controlled B' curves shown in Figures 3 and 5. This section is designed to show how the kinetic sublimation shift to higher temperatures varies with the convective heat and mass transfer rate within the boundary layer. Physically one would expect the kinetic sublimation predictions to agree with the equilibrium-diffusion controlled predictions when the mass transfer rate approaches zero. The analysis developed below illustrates this result by considering the sublimation kinetics and boundary layer diffusion to be two resistances in series. Such an approach yields the following implicit expression for the ratio $B'_{\text{rate}}/B'_{\text{equilibrium}}$ (Reference 37)

$$\frac{B'_{\text{rate}}}{B'_{\text{equilibrium}}} = \frac{1}{1 + \frac{\rho_e U_e C_M}{\alpha \mu} K \frac{B'_{\text{rate}}}{B'_{\text{equilibrium}}}} \quad (14)$$

where

α = vaporization coefficient

$$K = \frac{\sum K_{i \text{ equil}}}{\left\{ \sum K_{i \text{ equil}} + \left[\frac{M_c}{M_o} \tilde{K}_{O_e} + \frac{M_c}{M_o} \tilde{K}_{N_e} \right] \right\}}$$

$$\mu = \sum p_{i \text{ equil}} \sqrt{\frac{m^*}{2\pi RT_w}}$$

Since $B'_{\text{equilibrium}} = \text{fn}(T, P)$ this expression shows that for the two limiting conditions of $\rho_e U_e C_M \rightarrow 0$ and $\rho_e U_e C_M \rightarrow \infty$ the following values of $B'_{\text{rate}}/B'_{\text{equilibrium}}$ are attained.

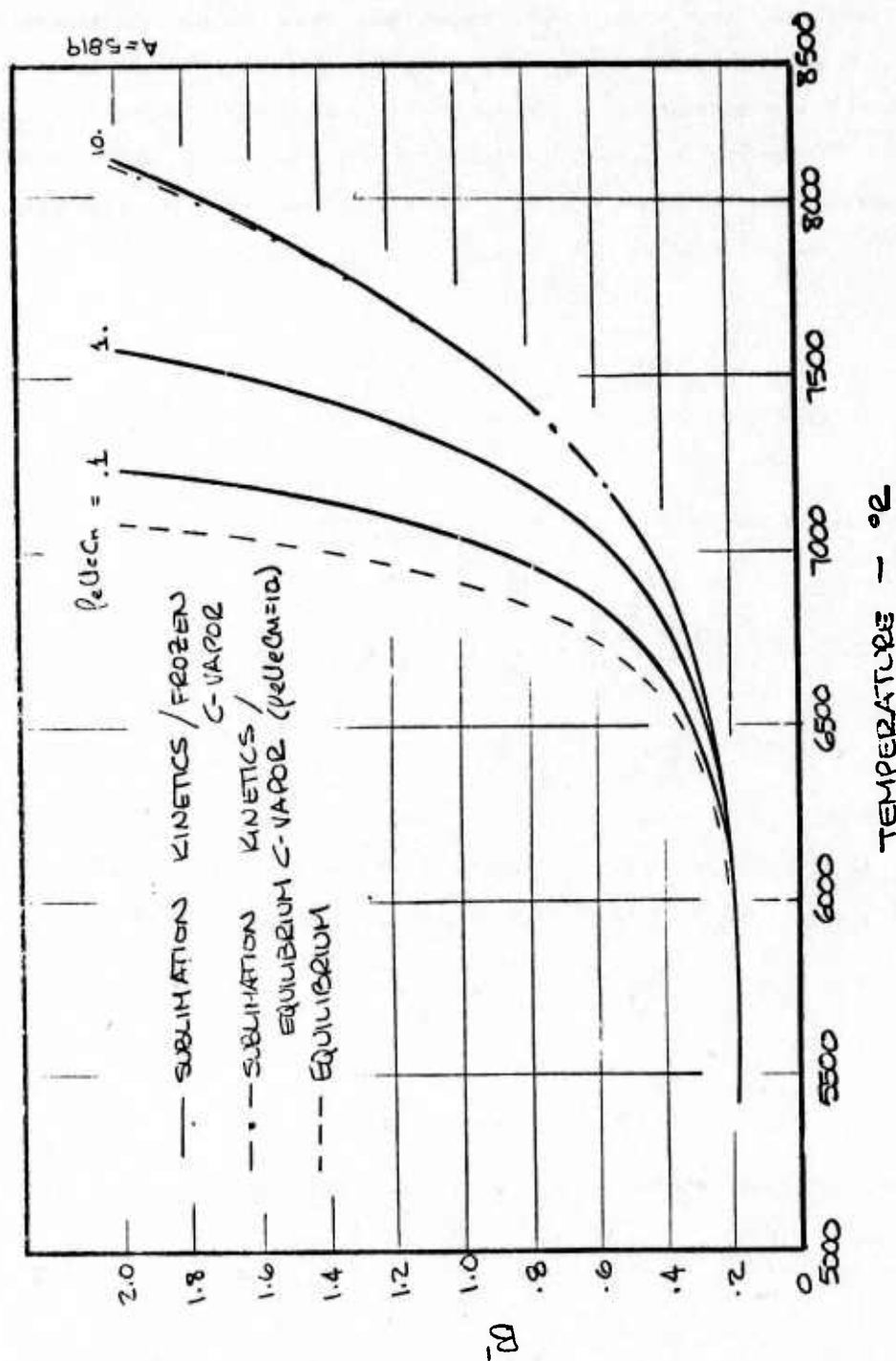
$$\text{Limit}_{\rho_e U_e C_M \rightarrow 0} \frac{B'_{\text{rate}}}{B'_{\text{equilibrium}}} = 1$$

$$\text{Limit}_{\rho_e U_e C_M \rightarrow \infty} \frac{B'_{\text{rate}}}{B'_{\text{equilibrium}}} = 0$$

These limits are readily derived from expanded forms of the above expressions.

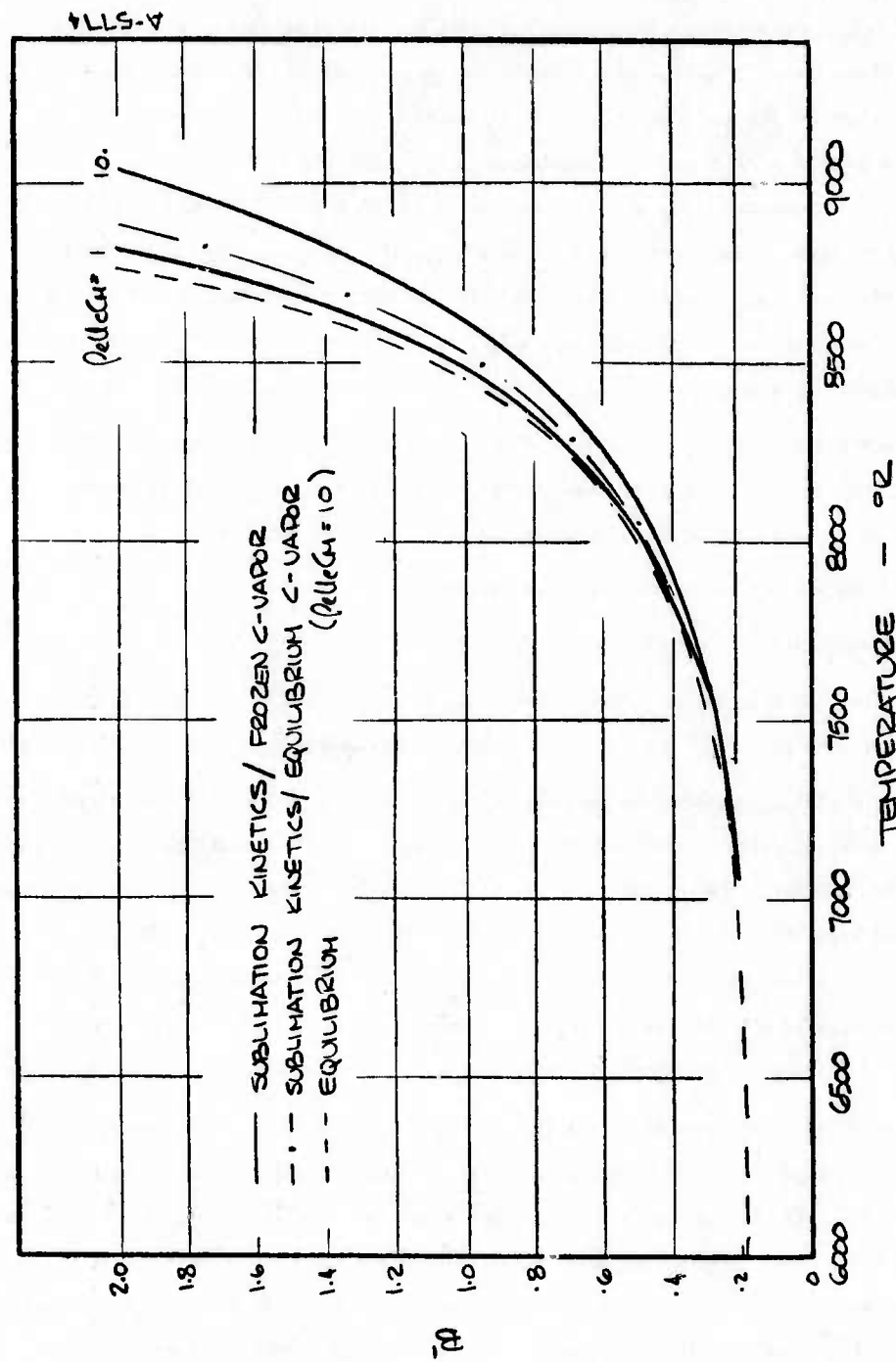
$$\text{Limit}_{\rho_e U_e C_M \rightarrow 0} \left[\left(\frac{B'_{\text{rate}}}{B'_{\text{equil}}} \right) \frac{\rho_e U_e C_M}{\alpha \mu} K + \frac{B'_{\text{rate}}}{B'_{\text{equil}}} = 1 \right] \rightarrow \frac{B'_{\text{rate}}}{B'_{\text{equil}}} = 1$$

$$\text{Limit}_{\rho_e U_e C_M \rightarrow \infty} \left[\frac{B'_{\text{rate}}}{B'_{\text{equil}}} = \frac{1}{2} \left\{ \sqrt{\left(\frac{\alpha \mu}{\rho_e U_e C_M K} \right)^2 + \frac{4\alpha \mu}{\rho_e U_e C_M K}} - \frac{\alpha \mu}{\rho_e U_e C_M K} \right\} \right] \rightarrow \frac{B'_{\text{rate}}}{B'_{\text{equil}}} = 0$$



(a) 1.0 Atmosphere

Figure 5. Sensitivity of kinetic sublimation predictions to the carbon vapor state.



(b) 100 atmospheres

Figure 5. Concluded.

Thus, properly designed experiments which cover a large range in the value of the convective mass transfer coefficient $\rho_e U_e C_M$ can establish the existence of rate controlled sublimation response for ablation conditions of interest. Figure 3 shows that if the kinetic sublimation model recommended by Dolton, et al., (Reference 22) using the JANAF data is assumed, a factor of 5 variation in $\rho_e U_e C_M$ is required to produce a 200°R shift in temperature at 0.1 atmosphere for $B' \approx 1.5$. To achieve a factor of 5 variation in $\rho_e U_e C_M$ in the stagnation region of a blunt cylindrical model by geometric variations, the model diameter would have to vary by about a factor of 25. It is immediately obvious that this is not possible within the constraints of most test facilities. Therefore, the best means of achieving the desired variation in $\rho_e U_e C_M$ is by varying the velocity of the convective flow from subsonic to supersonic.

In order to maintain the surface temperature at sufficiently high values to sustain sublimation while varying the convection energy and mass transfer coefficients, an additional source of energy flux into the surface must be available. Two means of achieving this are:

- Incident radiation combined with convective heating
- Resistively heated sample with convective heating

Both means of conducting such ablation experiments were thoroughly studied. It was established that the combined radiative/convective technique is superior to the combined resistive/convective technique.

Properly designed radiative/convective heating tests can provide a sufficiently large variation in the convective coefficient while maintaining the ablation state at sufficiently high B' values in the sublimation regime. In fact, the equilibrium diffusion limited condition ($\rho_e U_e C_M \rightarrow 0$) is approached at one atmosphere test conditions with only radiative heating. The results of Davy and Bar-Nun (Reference 38) substantiate this as a viable technique for measuring the equilibrium vaporization temperature at pressures above 0.1 atmosphere, although free convection currents and carbon vapor condensation tend to complicate the interpretation of the results at the one atmosphere test condition.

The only combined radiative/convective facility currently in existence with the required flexibility for such a test program is the Advanced Entry Heating Simulator (AEHS) at Ames Research Center (Reference 39). This facility was used by Davy and Bar-Nun to conduct "radiative-only" ATJ-S ablation experiments and by Wakefield and Peterson for combined radiative/convective ATJ-S ablation tests. The ablation test program described in Section 3 has extended the work of these investigators by combining high enthalpy supersonic and subsonic flow conditions with the radiative heat flux maintaining the ablation response at sufficiently high B' values to observe the potential temperature shifts with $\rho_e U_e C_M$.

2.4 PARTICULATE MASS LOSS UNCERTAINTIES

Accurate interpretation of ablation test data depends on one's ability to accurately assess the state of matter removed during the ablation process. This question has been addressed by nearly all researchers who have worked with the hyperthermal response of graphitic materials. The question also relates closely to the uncertainty of the high temperature phase equilibrium of carbon.

Lundell and Dickey (Reference 24) devised a technique to photograph the particulate mass loss from ATJ graphite models tested in the NASA Ames Heat Transfer Tunnel. They estimate from their results that the particulate flux becomes a significant component of the total mass loss at temperatures above 6650°R. Because of the two phase nature of ATJ graphite (i.e., filler particles held together in a binder matrix) it was rationalized that preferential ablation of the binder material allowed filler particles to be released and thus removed in the solid state.

Lundell and Dickey performed a similar set of ablation experiments using over 80 different types of graphitic materials with the intent of evaluating the role of the material microstructure in controlling particulate mass loss (Reference 25). This second series of ablation tests was similar to the previous series in all respects. The graphitic materials tested included commercial and developmental grades of artificial graphites, both two and three dimensional carbon/carbon composites seeded with refractory compounds, and several special materials such as pyrolytic graphite, mesophase graphite, glass carbon, and natural graphite. Results of these tests showed

1. The extreme variation in these materials' microstructure has little effect on their ablation performance at these low pressure (~4 atm) test conditions.
2. The observed particulate mass loss from single phase carbon materials indicates preferential ablation is not the only explanation for particulate mass loss.
3. No correlation relating the microstructure of commercially available graphites to the particulate mass loss was evident from these tests.

These results of Lundell and Dickey show that for the low to moderate pressure test conditions considered, particulate mass loss from graphitic materials does exist, but does not correlate with the materials' microstructure. One must keep in mind, however that the particulate mass loss observed by Lundell may be unique of the test technique employed

Whittaker interprets these results to show the effect of carbon melting at 6850°R, since the sharp rise in particulate mass loss observed by Lundell and Dickey occurs at a surface temperature of 6650°R. Whittaker and Kintner (Reference 40) also observed particulate mass loss at temperatures above 6650°R and cite similar observations by Maahs and Schryer (Reference 41) and Wachi and Gilmartin

(Reference 15). It is only natural that Whittaker explains the phenomena of particulate mass loss in this temperature regime to result from carbon melting, since the results of his research show a carbon melt phase to exist.

A substantial amount of work was done under the Air Force sponsored Passive Nostip Technology (PANT) Program to evaluate the effects and probability of particulate mass loss from ATJ-S graphite under high pressure hyperthermal environments (Reference 42). Ablation test data from both the AFFDL 50 MW arc and the AEDC Aeroballistic Range were thoroughly analyzed based on the JANAF thermochemical ablation model with particulate mass loss and rough wall convective heating sensitivity studies. These ablation data were the first high pressure graphite ablation data with both high quality surface temperature and surface recession data. The surface temperature and recession data made it possible to assess the significance of particulate mass loss under these high pressure ablation test conditions. These analyses consistently showed particulate mass loss to be small.

Kratsch, et al., within a subtask of the ASML Exploratory Development Program (EDP) titled, "The Erosion Mechanisms and Improvement of Graphitic Materials," (Reference 34), studied at the macro and micro-structural response of graphitic materials under hyperthermal ablation conditions. A segment of this program specifically studied the ablation response of bulk graphitic materials including ATJ-S graphite.

This micromechanical erosion model was applied and evaluated on the PANT program. The MDAC/EDP micromechanical ablation model is summarized below.

- The surface thermochemical ablation response is kinetically controlled.
- Subsurface sublimation occurs by diffusion of equilibrium carbon vapor through the porous microstructure in the near surface material.
- Subsurface sublimation weakens the surface structure. If sufficiently weakened, the surface material can be mechanically removed.

Application of the micromechanical ablation model to both 50 MW and ballistic range ablation data resulted in no predicted particulate mass loss. Kratsch, et al., report that their use of the model showed particulate mass loss to generally be less than 10 percent of the total with no particulate mass loss often being predicted.

Review of this work is included in this discussion to illustrate the uncertainty which currently exists regarding the existence and significance of particulate mass loss from hyperthermal ablating graphite materials. To quantitatively assess the significance of particulate mass loss it must be directly measured. To date no technique has been devised to accomplish this task, thus the precise amount of particulate mass loss cannot be measured. Because of this limitation one must infer the

significance of particulate mass loss from measured surface temperatures and recession rates. All efforts at inferring a particulate mass flux from available ablation data show it to be a small contribution to the total mass flux.

SECTION 3

EXPERIMENTAL APPROACH

The experimental approach utilized in the carbon sublimation study is described in this section. Section 3.1 discusses the test procedure and approach as related to the objectives of the study. Section 3.2 is a description of the test equipment employed for the experimental portion of the study. Section 3.3 reviews the test program including both calibration and sublimation tests while the test results are presented in Section 3.4.

3.1 TEST PROCEDURE/APPROACH

The review of the Knudsen-Langmuir kinetic sublimation model in Section 2.3 shows that sublimation reactions which are kinetically controlled exhibit a dependence on the convective mass transfer coefficient ($\rho_e u_e C_M$). Because of this dependence the best way to assess the existence and significance of sublimation kinetics is to perform carbon sublimation tests under varying convective conditions. In order to maintain ablation in the sublimation regime, some means of augmenting the convective heat input (such as incident radiation or inductive heating) is required as discussed in Section 2.3.

A review of available test facilities with multiple heating modes identified the NASA Ames Advanced Entry Heating Simulator (AEHS) as the optimum facility for this test series. The AEHS facility has the capability to subject a test specimen to simultaneous convective and radiative heating. The peak radiation flux which can be generated with its argon driven arc imaging radiation source is approximately 2500 Btu/ft² sec which is adequate to maintain carbon in its sublimation state under a near zero convective heating environment.

Therefore the ablation test procedure used on this program was to expose models to two nominal pressure conditions (i.e., ~ 0.1 and ~ 1.0 atmospheres) and various convective conditions. The variation in the convective heat and mass transfer rate was achieved by varying the arc heated air velocity over the models. This procedure was used since it was impossible to vary the model size sufficiently to gain the desired variation in $\rho_e u_e C_M$. The size of the radiation beam with a

90 percent uniformity is shown in Figure 6 to be 0.5 inch in diameter at a 0.25 inch standoff. Thus, the 0.5 inch diameter corresponds to an upper limit on the model size. Since the pyrometer which views the ablating surface is located ~ 30 inches from the model, the model diameter can't be much smaller than 0.25 inch with any assurance of measuring accurate surface temperature data. Thus, the practical size range available for models lies between 0.25 and 0.5 inch. A factor of two variation in nose radius corresponds to a 40 percent variation in $\rho_e u_e C_M$ which is insufficient for studying sublimation kinetics as discussed in Section 2.3.4.

The flow over the models in this test series was varied from low subsonic velocities (~ 100 ft/sec) to supersonic flow. The variation in $\rho_e u_e C_M$ at the ~ 0.1 atmosphere and ~ 1.0 atmosphere test conditions was approximately a factor of ~ 40 and ~ 30 respectively. Since the supersonic flow condition controls the maximum temperature shift due to kinetic sublimation response with a fixed configuration, a 0.5-inch diameter model at 0.1 and 1.0 atmosphere test conditions experiences peak heat and mass transfer rates of ~ 0.09 and ~ 0.19 lbm/ft²sec respectively. Thus the predictions in Figure 3 show that at a nominal B' value of unity, the maximum shift in surface temperature anticipated at the ~ 0.1 and ~ 1.0 atmosphere conditions are ~ 220°R and ~ 120°R, respectively. It was known from the inception of this program that these potential temperature shifts were close to the anticipated ±2 percent uncertainty in the pyrometer data.

3.2 TEST EQUIPMENT

This section describes the facility hardware, equipment modifications required for this program, and the instrumentation used in data acquisition. The ablation model configuration is also presented and the procedures used to establish the specific model design employed for this test series are discussed. The AEHS facility is described in Section 3.2.1, the facility modifications are discussed in Section 3.2.2, the instrumentation and models are described in Sections 3.2.3 and 3.2.4, respectively.

3.2.1 AEHS Facility

The experimental portion of this program was performed in the Advanced Entry Heating Simulator (AEHS) facility at the NASA Ames Research Center. The AEHS facility is shown in Figure 7 and described in more detail in Reference 39. It consists of four main subsystems: the convective source, the radiant source, test chamber/vacuum system and the test model support and insertion system.

The convective heating source is provided by an arc heater coaxially mounted on the test chamber/radiant source centerline (see Figure 7). Several arc heaters are available for use in this

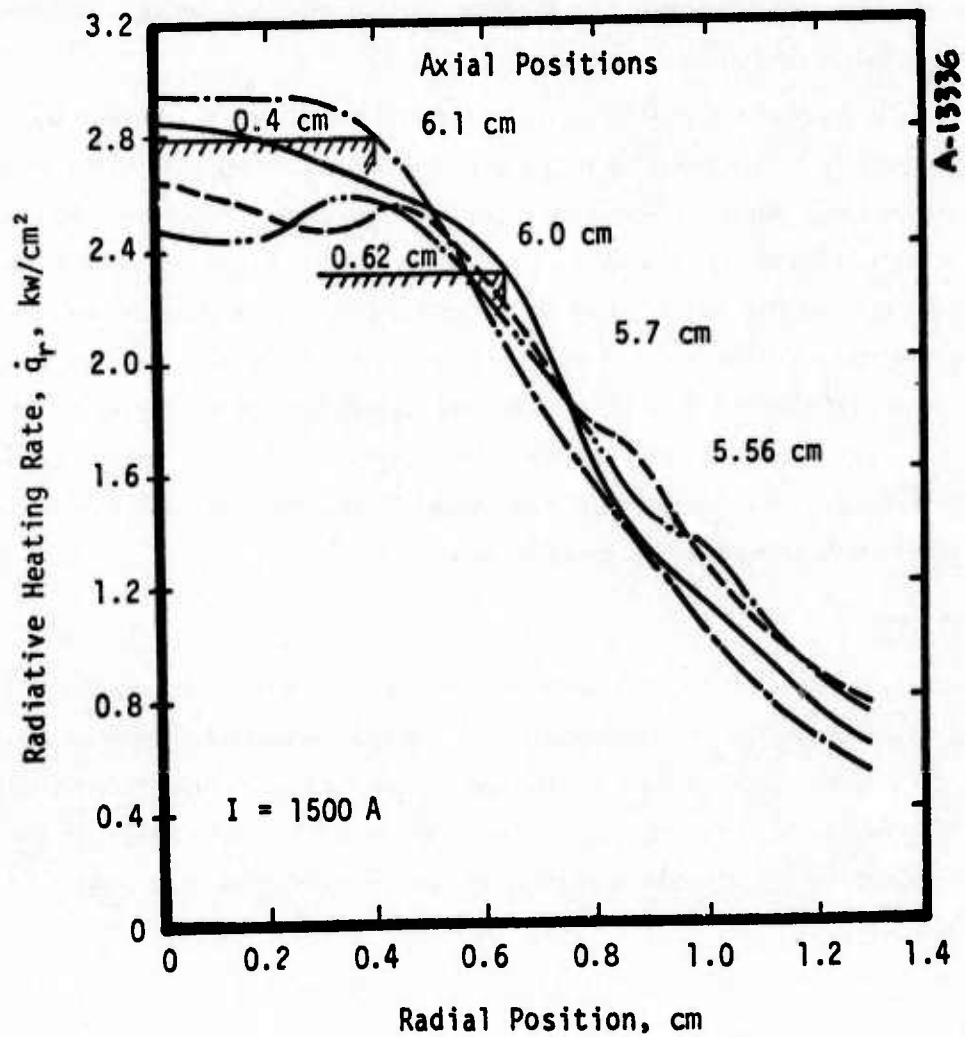


Figure 6. Radiative radial distributions at different axial positions.

ADVANCED ENTRY HEATING SIMULATOR

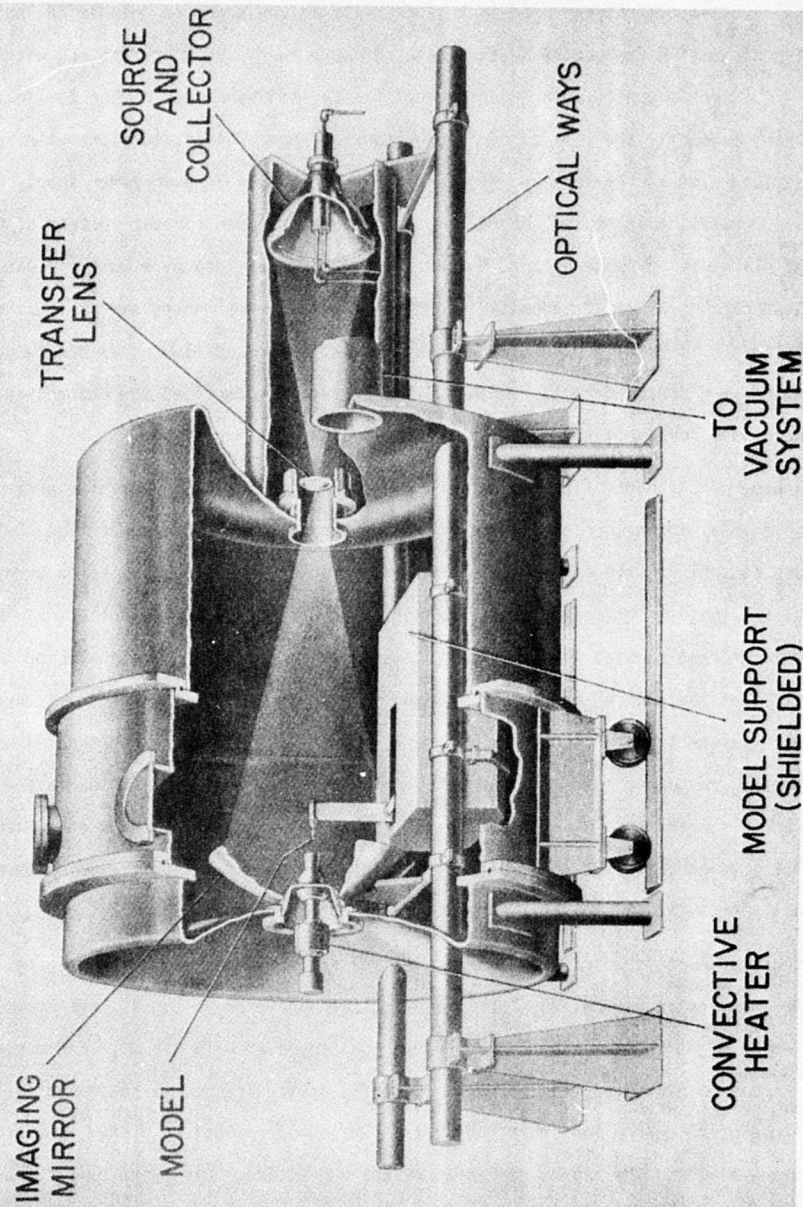


Figure 7. Advanced entry heating simulator.

facility and consist of both the Linde type (i.e., N-4001) and the Ames developed constricted type. The typical convective test stream used in this facility is low pressure, high enthalpy, supersonic flow providing stagnation convective heating rates of more than $\sim 2500 \text{ Btu/ft}^2 \text{ sec}$ with a nominal model size of 0.5 inch diameter. In order to meet the objectives of the carbon sublimation study, it was necessary to modify the constricted arc heaters. These modifications are discussed in the following section. The arc heaters are electrically powered by a 3 MW dc power supply consisting of 8 rectifier modules, each capable of 600 amp output with an open circuit voltage of 1125 volts. Simulation of planetary atmosphere (air, N_2 , He, CO_2 , AR) is provided by a multiple gas mixing and metering system capable of simultaneously injecting three different gases over a 100:1 mass-flow range of 1.1 lbm/sec to 0.011 lbm/sec. The dc arc current and mass-flow rates can be continuously varied and maintained during operation. The following section describes the changes in the metering system necessary for the lower mass flow requirements of this test series.

The independently controlled radiant source can provide incident radiant energy to the model surface while maintaining reasonable target uniformity in a low pressure convective environment. The system consists of an Ames developed 125 kw, argon vortex-stabilized radiation source and quasi-bifocal arc imaging optical system. The optical components (source, collector, transfer lens, and imaging mirror) are coaxial with respect to the tunnel centerline. The collector mirror captures the output of the source transferred arc and directs the energy towards the 1 meter diameter imaging mirror via the transfer lens (see Figure 7). The imaging mirror, constructed around the arc heater nozzle, in turn focuses the radiation onto the model surface. The surface contours of the mirrors are distorted from a simple elliptical shape to affect increased arc utilization and radiation distribution uniformity. Complete interruption and/or exposure of radiation is controlled manually or automatically by a pneumatically operated douser (shutter).

The radiant source spectral characteristics are shown in Figure 8. This figure shows that at 0.9μ (the peak sensitivity of the Thermogage optical pyrometer) a significant amount of reflected radiation might be picked up by the Thermogage pyrometer. To minimize incident radiation reflectance errors in pyrometer measurements a chopping device is used which periodically occludes the incident radiative energy for short intervals. The chopper consists of two 1-meter radius counter-rotating blades. The blades rotate at 20 cps and entirely block the beam for 3 msec intervals, during which time, the temperature measurements are taken.

The 3-meter diameter test chamber provides a low pressure nozzle discharge environment and houses both the convective and radiative systems as well as the model support system. The chamber is connected to a series of vacuum spheres with a 20.129 ft^3 capacity.

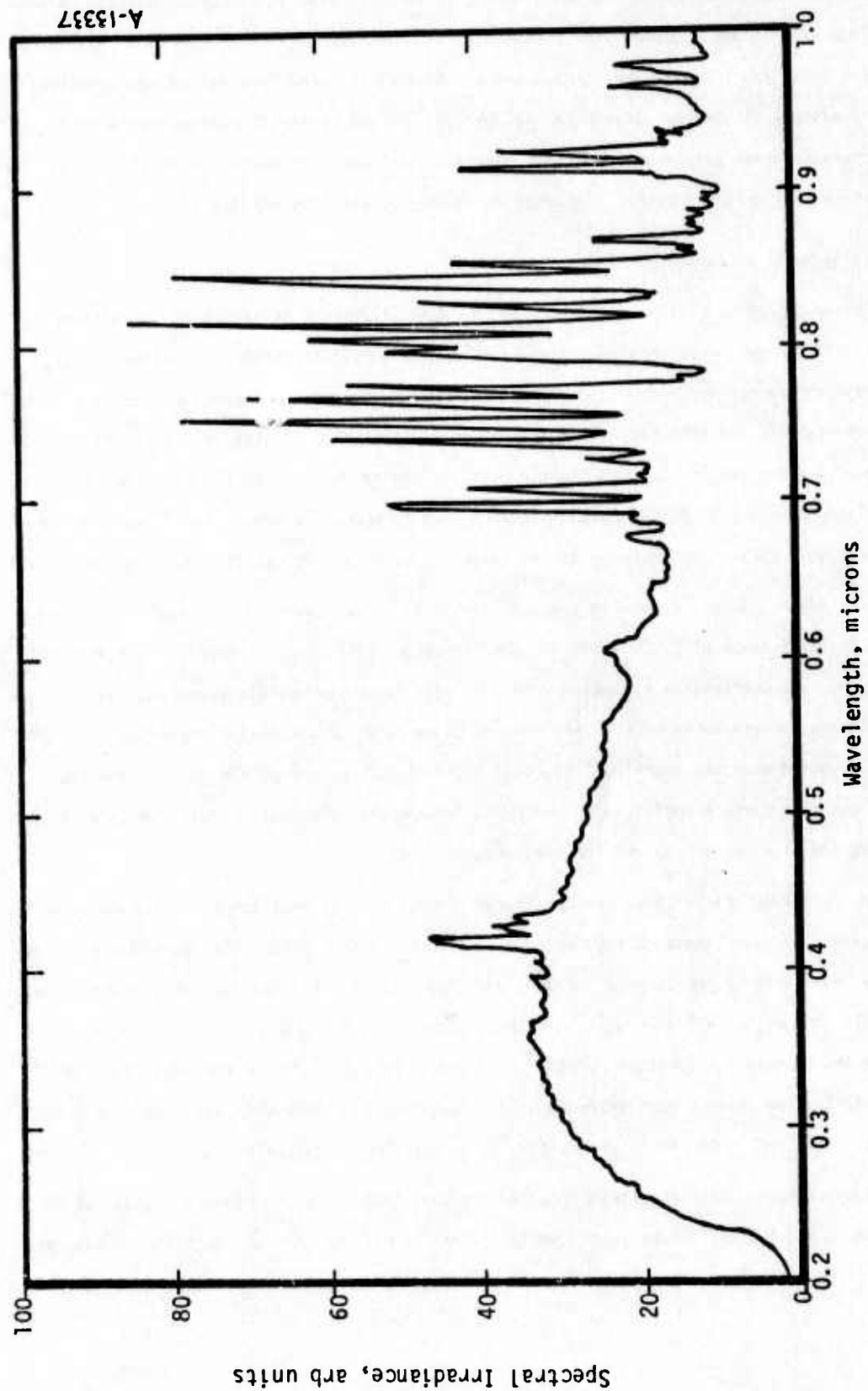


Figure 8. Spectral distribution, Ames 125 kw radiation source.

A multiple model support system provides for insertion of test models or calibration probes into the combined convective-radiative environment. A total of nine models or probes can be automatically inserted, in any sequence, for preselected exposure times. Total insertion time is less than 1 second including transit time through the arc heated, expanded free jet of approximately 200 msec. The model struts are aligned to the optical axis and convective stream centerline. A laser monitored feedback servo-control system maintains the model stagnation point at a fixed location from the nozzle exit and within the focal point of the radiation imaging mirror.

3.2.2 Facility Modifications

The basic objective of the experiments was to demonstrate the existence or nonexistence of carbon sublimation kinetics by providing large variations in mass transfer coefficient ($\rho_e u_e C_M$) while maintaining the surface temperature in the sublimation regime. The combined radiative/convective environment in the AEHS facility was capable of maintaining a relatively constant surface temperature with variation in the mass transfer coefficient by varying the flowrate over the model. Pretest analyses showed that this objective could be met by providing convective flows from subsonic to supersonic with a gas enthalpy in the range of 20,000 Btu/lbm as discussed in Section 3.1.

The arc heater generally used in the facility is the Linde N-4001. This heater provides total enthalpy gas streams of 2,000 to 20,000 Btu/lbm (supersonic only) at model stagnation pressures to 1 atm. The constricted heater, however, is capable of gas enthalpies as high as 40,000 Btu/lbm at stagnation pressures to 0.3 atm. The required range of arc heater operation (subsonic-supersonic) combined with the enthalpy level desired, dictated the use of the constrictor heater. Further, it was felt certain modifications were required before this heater could run in a stable mode with the low flow rates required for the subsonic cases.

The principal modification to the constricted heater was the replacement of the existing pin electrode/ballast resistor anode configuration with a combined anode/nozzle design which enhanced the enthalpy capability by providing a "peaked" enthalpy profile. The peaking was considered necessary to provide the enthalpy level required without exceeding safe current limits at the flowrates required for the supersonic operating points. This operating procedure had the added benefit of maintaining a very low level of contaminants in the test stream. These modifications also provided the necessary facility/arc heater interface for proper mounting to the test chamber.

The six arc heater configurations required for this test series are summarized in Table 3. Configurations 3 and 6 are the supersonic configurations at 0.1 and 1.0 atm stagnation pressures, respectively. The enthalpy levels noted for these configurations assume a peaking ratio of 2. The

TABLE 3. DESCRIPTION OF AEHS CONSTRICTOR ARC HEATER CONFIGURATIONS

Configuration	Model Stagnation Pressure P_{t2} (atm)	Diameter d_e (Inch)	Gas Flow Rate \dot{m}_t (lbm/sec)	Mass Average Enthalpy H_{ave} (Btu/lbm)	Operating Mode	Arc Chamber Pressure P_{t1} (atm)	Constrictor Length (Segments)	Primary Gas Injection Slots	Secondary Gas Injection Slots
1	0.1	2.75	0.00084	20,000	Subsonic	-0.1	5	$\begin{smallmatrix} 4 \\ (0.125 \times 0.005) \end{smallmatrix}$	$\begin{smallmatrix} 4 \\ (0.125 \times 0.005) \end{smallmatrix}$
2	0.1	1.00	0.00084	20,000	Subsonic	-0.1	5	$\begin{smallmatrix} 4 \\ (0.125 \times 0.005) \end{smallmatrix}$	$\begin{smallmatrix} 4 \\ (0.125 \times 0.005) \end{smallmatrix}$
3	0.1	2.75	0.02100	10,000	Supersonic	2.3	23	$\begin{smallmatrix} 4 \\ (0.125 \times 0.015) \end{smallmatrix}$	$\begin{smallmatrix} 4 \\ (0.125 \times 0.005) \end{smallmatrix}$
4	1.0	2.75	0.0084	20,000	Subsonic	-1.0	46	$\begin{smallmatrix} 4 \\ (0.125 \times 0.015) \end{smallmatrix}$	$\begin{smallmatrix} 4 \\ (0.125 \times 0.005) \end{smallmatrix}$
5	1.0	1.00	0.0084	20,000	Subsonic	-1.0	46	$\begin{smallmatrix} 4 \\ (0.125 \times 0.015) \end{smallmatrix}$	$\begin{smallmatrix} 4 \\ (0.125 \times 0.005) \end{smallmatrix}$
6	1.0	1.00	0.033	10,000	Supersonic	3.5	46	$\begin{smallmatrix} 4 \\ (0.125 \times 0.015) \end{smallmatrix}$	$\begin{smallmatrix} 4 \\ (0.125 \times 0.005) \end{smallmatrix}$

existing facility 2.75-inch nozzle extension was augmented with a new, 1.0-inch nozzle, thus significantly lowering the required flowrate to achieve the 1.0 atm stagnation pressure. This configuration also determined the longest constrictor required, 46 segments. The reduced flowrate for the 0.1 atm stagnation pressure allowed the constrictor to be shortened to 23 segments. The flowrates noted in this table were calculated from best estimates of arc heater performance. During actual checkout/calibration runs, the flowrates were modified as required to produce optimum arc heater operation.

Configurations 4 and 5 provided the 1.0 atm, subsonic conditions. Low and high velocity streams were achieved by using the two nozzles. The low flowrate noted was necessary to prevent sonic conditions at the nozzle throat. The 0.1 atm subsonic conditions were provided by Configurations 1 and 2. For these conditions, the arc heater constrictor was shortened to 5 segments, reducing the arc voltage so that the arc current levels could be maintained at reasonable levels. In addition, this increased the ability of the very low flow to stabilize the arc column, providing stable arc operation. As noted in the table, the gas injection rings of the arc heater were modified to maintain sonic gas injection to the arc chamber over the large flow range required.

The reconfigured constricted arc heater (46 segments) is shown in Figure 9. The design of the required arc heater parts was done by Aerotherm with all fabrication provided by NASA Ames. The heater parts required for the modifications are listed below. Drawings of these parts are included in Appendix A.

<u>Drawing No</u>	<u>Description</u>
7111-033	Downstream Housing, Anode
7111-004	Upstream Housing, Anode
7111-005	Split Core, 0.50-2.0 Liner
7111-006	0.50-2.0 Liner, Nozzle
7111-007	Split Ring
7111-009	Split Core, 0.5-0.75 Liner
7111-010	0.50-0.75 Liner, Nozzle
7111-011	0.75-1.0 Nozzle Extension
7111-012	Insulator, Bolt
7111-013	Insulator, Stud
7111-014	Outer Insulator

The range and low level of gas flow rates required for these arc heater configurations required the addition of a gas metering board to augment the facility gas system. The metering board

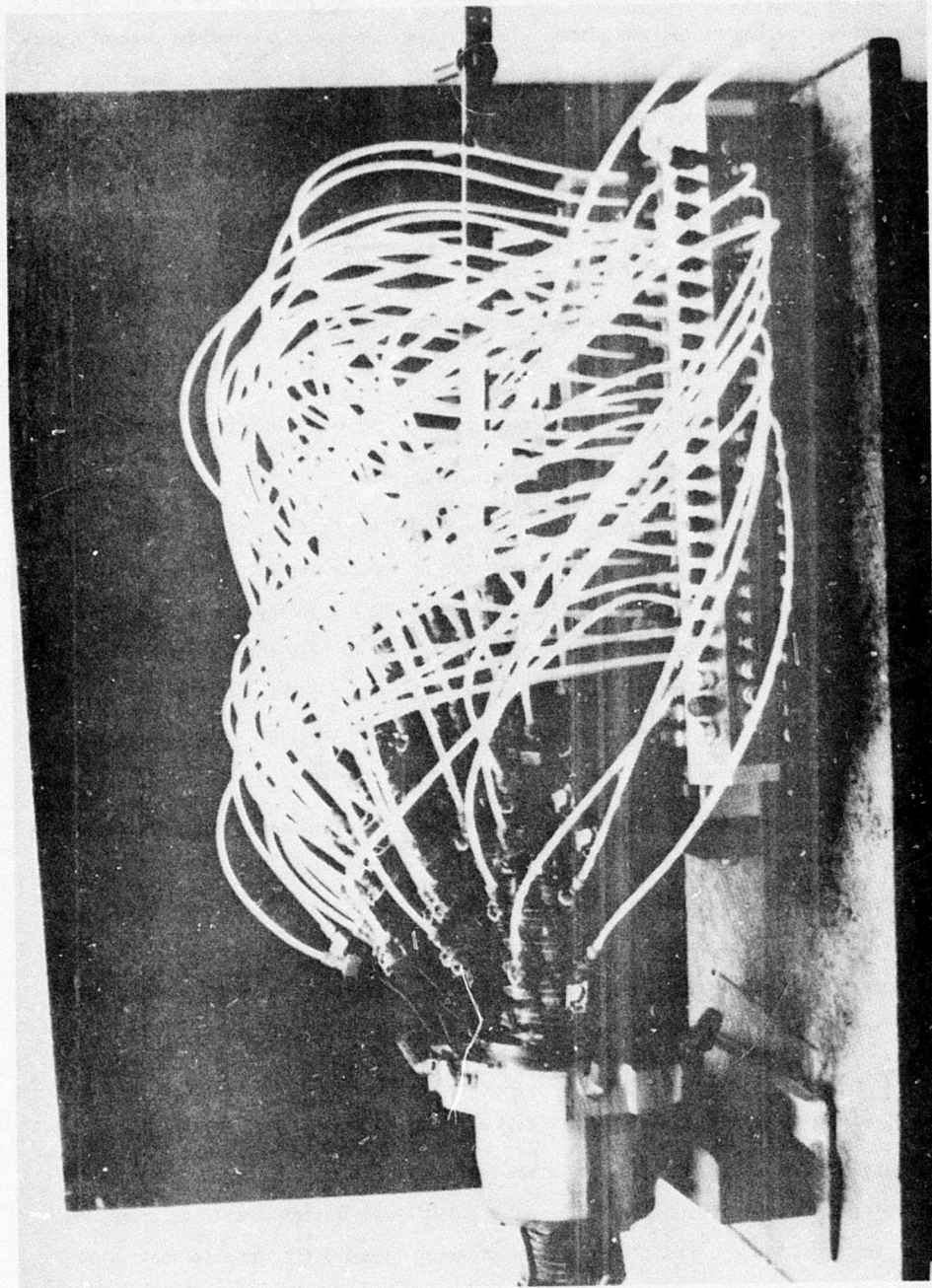


Figure 9.

Modified NASA Ames constrictor arc heater used for graphite sublimation Kinetics study (46 segment configuration).

provided the necessary gas regulation and monitoring equipment to meter nitrogen and oxygen separately, as required by the constricted arc heater. In addition necessary valving and control equipment was included to provide the argon start gas to the heater. The metering board schematic is shown in Figure 10. The design, assembly and checkout of the metering board was accomplished by Aerotherm. The board was delivered to Ames and is now a permanent part of the AEHS facility.

3.2.3 Instrumentation

The following data were recorded for the various test systems:

- Arc heater - voltage, current and arc chamber pressure
- Radiation source - voltage and current
- Convective stream - heating rate, stagnation pressure and test cabin pressure history
- Model - surface recession, surface temperature

The normal procedure for determining the arc heater efficiency in facilities of this type is to measure the energy loss to the arc heater wall by monitoring the cooling water temperature change and mass flowrate. With the heater efficiency known, the stream bulk enthalpy can be determined from the power input and gas mass flowrate. The AEHS facility did not have this capability and the stream enthalpy was, therefore, backed out from the measured stagnation point heat flux through use of the Fay and Riddell stagnation point heat transfer correlation for the supersonic test cases and by an iteration technique described in Section 3.4.2.1 in the case of the subsonic test points.

All the above mentioned pressure, heating rate, voltage and current data, and pyrometer output were recorded on a high speed CEC oscillograph system for later reduction by Aerotherm personnel. The arc voltage, current, chamber pressure, and test cabin pressure were also monitored by facility gauges and recorded photographically and/or manually for comparison to the CEC data. Model recession data were recorded by a high speed Photo-sonics 16mm motion picture camera viewing the model in the horizontal plane 180° from the pyrometer viewing location.

Pressure data were measured by Statham absolute and differential pressure transducers of various ranges to cover the different operating regimes experienced in this test series.

Heating rate data were measured by steady-state circular foil heat flux gages as well as an Ames manufactured copper slug, capacity type calorimeter. Two types of steady-state calorimeters were available. The Hycal was a 0-5000 Btu/ft² sec calorimeter intended for the supersonic high heat flux portion of the test series. A number of Medtherm calorimeters were available in ranges of 0-1000 Btu/ft² sec and 0-3000 Btu/ft² sec for the lower heating rates. However, these devices

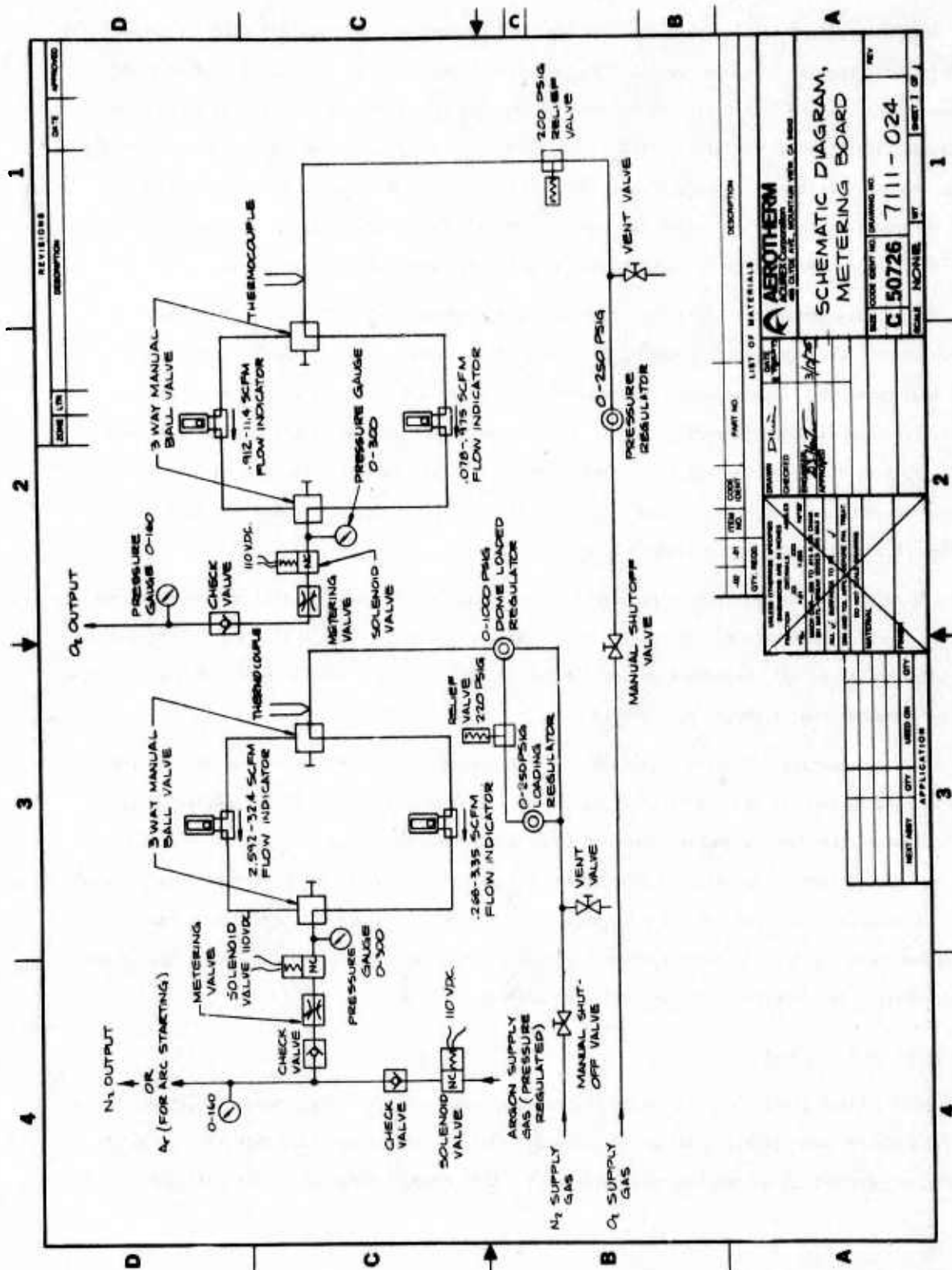


Figure 10. Gas metering board schematic.

showed little repeatability and erratic response during calibration runs. The data from these devices were ignored and the Hycal and slug calorimeter became the primary source of heating rate data.

Accurate radiant heating rate data was obtained by coating the transient calorimeter with a high emissivity coating (camphor soot) before each run. Comparison of the coated slug data with the steady-state calorimeter measurements made in the same environment during the same run provide an in-situ calibration of the steady-state calorimeter. This comparison was most useful since the radiant heating levels were capable of altering the transient calorimeter coating characteristics (i.e., removal of some coating) after only one insertion. The steady-state calorimeter then became the primary measurement device for subsequent radiant data during the same test run.

The surface temperature data were recorded by a Thermogage (S/N 422) optical pyrometer. The instrument viewed the model through a barium-fluoride window and an aperture in the large "elliptical" imaging mirror. The viewing angle was 45° off of the model axis with an approximate spot size of 1/16-inch diameter at a focal length of 30 inches. The sensing wavelength of this pyrometer is centered at 0.8 micron and falls almost entirely within the band from 0.4 to 1.1 microns. The pyrometer spectral response is shown in Figure 11. A neutral density filter was used to extend the range of the pyrometer to the 7600°R level.

The relative size of the sensing area and the model size required careful alignment of the pyrometer to insure accurate temperature data. To this end, the Thermogage standard "light-source-replacement-of-the-sensor" technique was used prior to each test run. The location of the resulting pyrometer sensing area is shown in Figure 12.

The model surface reflective component from the radiation source was eliminated from the pyrometer data by the source chopper as discussed earlier (Section 3.2.1). The relatively fast response time of the Thermogage pyrometer and associated electronics (on the order of ~ 3 msec) allow the surface temperature data to be obtained during this "blocked" interval during each chopper cycle. An example of a pyrometer trace is shown in Figure 13. Note the plateau corresponding to the combined model surface emission and radiant source reflected components; the difference between "peak-to-valley" levels represents the reflected component.

3.2.4 Ablation Model Design

The principal thermal consideration of the model design was to reduce heat conduction through the model material and radiation losses from the cylindrical surface and thus maintain the stagnation area temperature at the maximum possible level. This criterion had to be met while maintaining

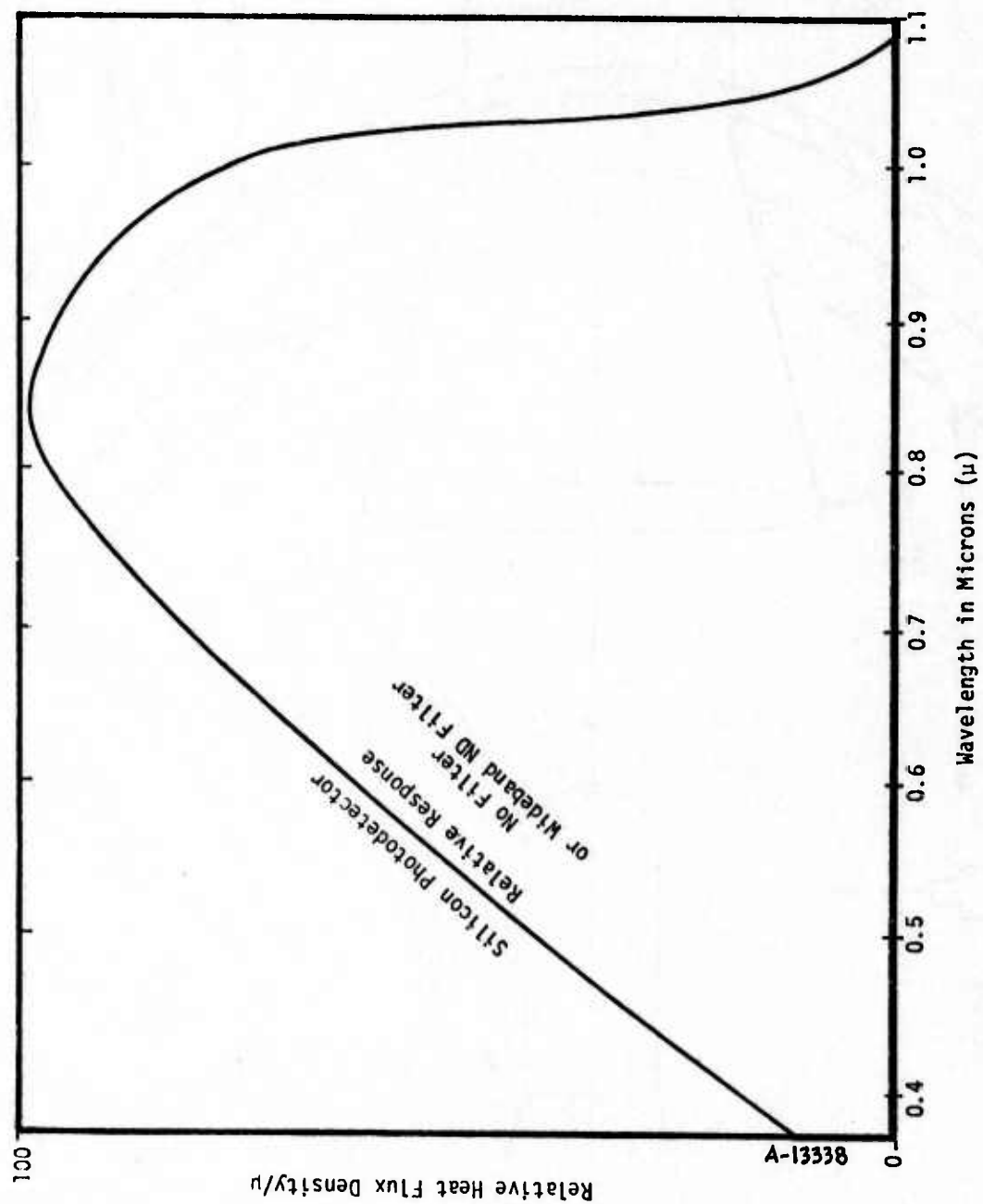


Figure 11. Thermogage pyrometer spectral response.

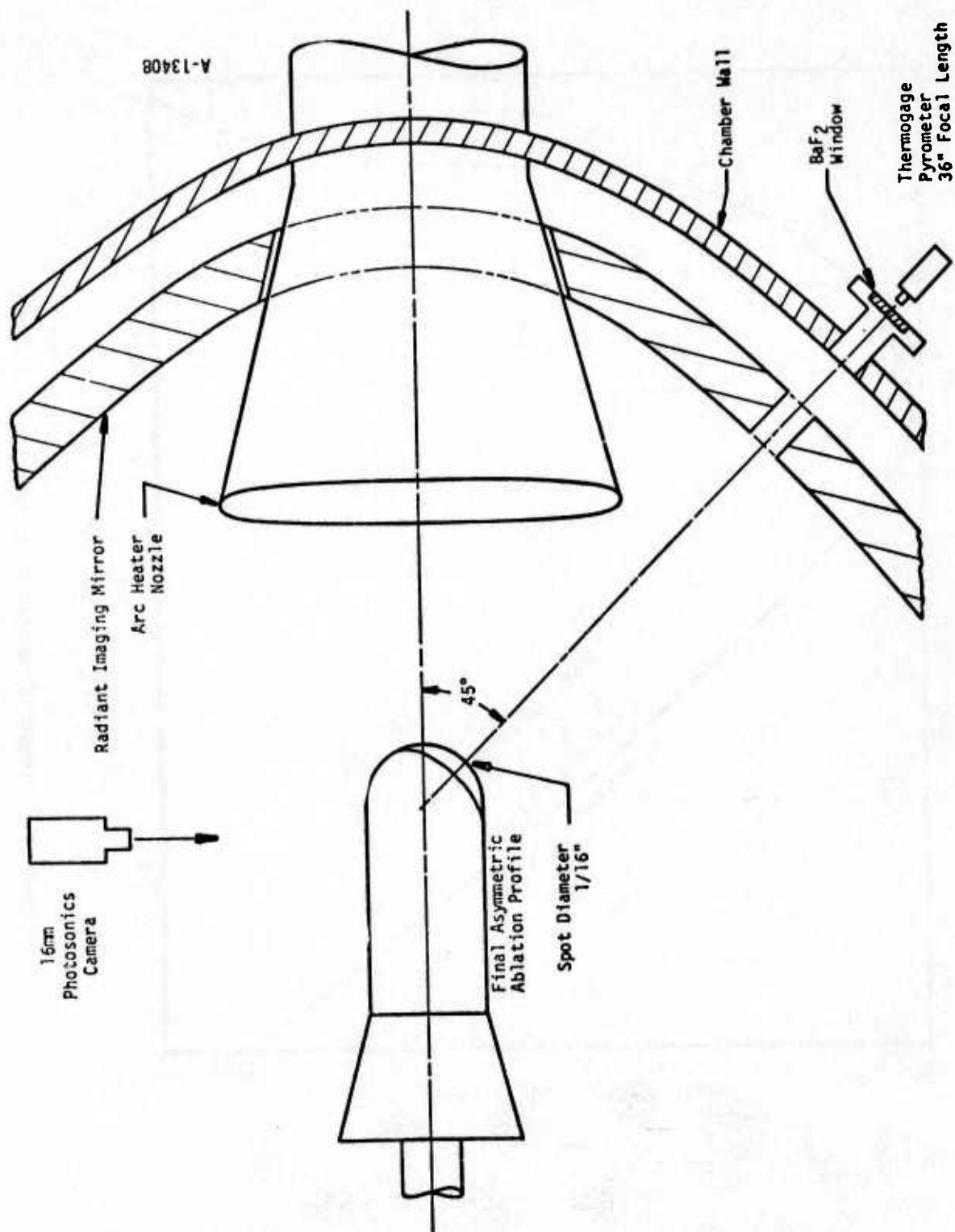


Figure 12. Pyrometer alignment — top view.

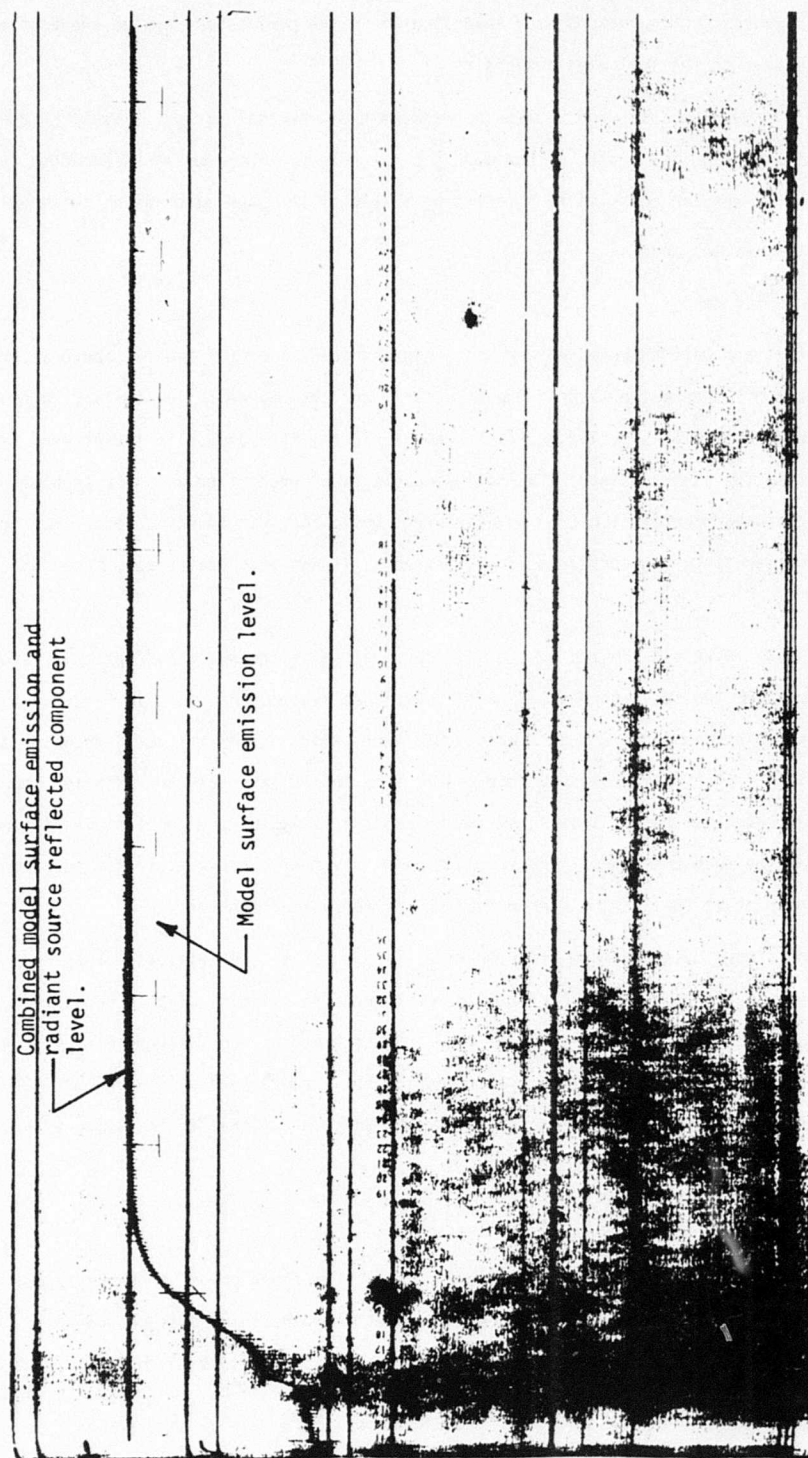


Figure 13. Typical pyrometer output on CEC oscillograph.

the structural integrity of the model during injection pressure loading and the initial thermal shock conditions. Several configurations were investigated in the preliminary system checkout tests by exposing proof models of the following designs:

1. "Mushroom" shaped models with a 0.25-inch radius hemispherical tip and a small (0.25-inch) stem running the length of the model to the holder. The stem was surrounded by a concentric annular cross section radiation shield of the same material as the model.
2. Hollow thin-walled models
3. Baseline solid design

Various stem diameters and wall thicknesses were investigated in designs (1) and (2) above attempting to limit the conduction losses while maintaining structural and thermal design criterion. Although the solid model was structurally superior and easier to fabricate, the conduction losses were significantly higher than the other designs. The hollow models experienced thermal shock problems (i.e., cracked) and proved more difficult to manufacture. Design one was found to be optimum from thermal response and manufacturing considerations; therefore, it was used exclusively throughout the test series.

The overall model size was limited by the size constraints of the radiation/optical system and the axial movement of the servo-controlled model positioner system. As shown in Figure 6, imaging mirror focal point diameter is approximately 0.5 inch, which limits the model diameter to approximately 0.5 inch for uniform heating of the model. The focal length of the radiation imaging mirror and the axial range of the positioning system define the limits of the model's overall length. The model length must be such that there is sufficient axial movement capability to actively control the stagnation point at the imaging mirror focal point throughout the test.

The test models were machined from Union Carbide ATJ-S graphite ("P" billet). They were 0.25 inch R_N hemispherically tipped cylinders 1.5 inches long. The cylindrical body consisted of an inner stem and a surrounding "sleeve." Figure 14 is a sketch of the model assembly. The model was mated to the facility water cooled sting by a carbon phenolic model holder (MX-4926 or FM5790). The model was cross-pinned to the holder and the holder was in turn attached to the sting by a set screw.

3.3 TEST PLAN

The test program was completed in two distinct phases. The first phase, checkout, proof and calibration tests, was designed to "debug" the operation of the arc heater and is described in Section 3.3.1. The second phase consisted of the actual sublimation tests, as discussed in Section 3.3.2.

3.3.1 Checkout, Proof and Calibration Tests

The objective of this initial test series was to fully characterize the operation of the newly configured arc heater while generating the data necessary to select the model design and facilities optimum operating conditions. Since this arc heater had never been operated in the AEHS facility, and further, the expected convective levels were much higher than those produced with previous heaters, certain operational problems had to be overcome in the initial checkout tests. These problems are summarized as follows:

1. Verification of arc starting technique
2. Verification of power supply stability on arc initiation (i.e., no current surge)
3. Constantly rising test cabin pressure due to nature of vacuum system and cooling/purge flows

The arc heater was initially configured in the longest (46 segment) arrangement and potentially, the most difficult starting condition. The first starting attempt resulted in a large current surge with subsequent failure of arc heater components and an external arc-over. After making adjustments to the power supply controls to prevent further current surges of this magnitude, the arc heater was rebuilt with the following modifications:

1. All potential arc-over sites around and on the arc heater were carefully insulated
2. A small amount of the primary test gas (normally N_2 , but argon during the start sequence) was bypassed and injected over the face of the cathode to increase arc stability

A subsequent checkout test demonstrated the proper arc operation with this 46 segment configuration. The arc was started in this configuration through the use of a small argon flow as the primary gas and sufficient power supply open circuit voltage to initiate the arc. Once the arc was stable, the required primary gas (N_2) was introduced and the argon flow terminated. Later the oxygen was introduced to provide proper simulation of air.

The heater was then reconfigured into the 23 segment constrictor length (Configuration 3). Initial plans called for a separate checkout series followed by a short calibration series to define four test conditions to be used in the subsequent proof tests. The proof tests were designed to expose several different model designs so that the optimum model design would be selected for the primary test series. Due to the unforeseen length of time required to accomplish each test point, the checkout test series was modified significantly. For each arc heater configuration, checkout, calibration and proof test were to be combined into a short two or three test sequence. In this

manner, problems encountered later in the checkout/calibration/proof test sequence would not prevent the successful completion of at least part of the sublimation tests.

With the arc configured with 23 segments (Configuration 3) the test cabin pressure-rise rates were studied while calibration data were taken for the first proof test. Six runs were made to study ways of decreasing the test cabin pressure-rise rate and its effect on the measured heating rate and stagnation pressure. The final two runs in this sequence provided stream profiles used for final quantification of the effect of the pressure variation on stream properties.

At this point in the preliminary test series the radiant source was calibrated and the first proof tests run. A total of four models were tested (Runs 18 and 20) two per run. The first of these became a convection-only test when the radiant source failed to operate throughout the entire test. The second attempt was successful with good pyrometer and film data being obtained.

With the completion of the first proof tests, facility scheduling requirements forced a halt to any further tests. These few tests however, did provide the following information.

1. The variation of the test cabin pressure results in variation of test conditions as the shock/expansion structure of the stream changes (applies to supersonic mode).
2. The Thermogage pyrometer tracked the chopper very well. Alignment was shown to be extremely important due to the erratic behavior of some of the temperature/time history plots.
3. All model designs were structurally adequate, although the hollow models showed a tendency to crack.
4. The model holder was redesigned to prevent damage to the facility sting. The flare angle was increased and a boron nitride shield was added to facilitate removal of model from the sting.

3.3.2 Sublimation Tests

With only one of the six arc heater configurations fully calibrated, as described in the previous section, scheduling restrictions imposed by the AEHS facility resulted in modification to the sublimation test sequence. It became necessary to conduct simultaneous calibration/proof tests and primary sublimation tests at a specific condition. This section includes (1) a description of the testing sequence employed and (2) review of specific problems and their solutions encountered during this second entry into the AEHS facility. Also presented is a summary and data tabulation for each of the ablation test conditions run.

The sequential calibration/proof test procedure resulted in several of the early runs (up through run 47) being far from optimum with respect to the test objective of:

Maximum accuracy of surface temperature data which implies the highest possible surface temperature measurements.

This problem did not affect the later runs because of procedural changes in pyrometer alignment techniques.

After reconfiguring the arc for a specific test condition the procedure followed involved (1) verifying the arc starting techniques and (2) reviewing calibration runs to determine the test condition parameters.

The typical test sequence, after preliminary calibration data had characterized the test condition, was as follows:

- A. Radiant source started and set to the desired source current. Without the chopper running, radiant heating rate data were taken with the steady-state calorimeter and the blackened slug calorimeter.
- B. Douser was closed and the chopper started.
- C. Argon start flow initiated and the arc heater started. With arc running in a stable mode, N_2 and O_2 were injected and the argon flow terminated.
- D. After the predetermined arc current had been achieved and a stable arc established, the convective conditions were measured with the steady-state calorimeter and pitot probe.
- E. The douser was opened and the high speed camera started prior to the model arriving on the stream centerline. The ablation model was positioned. Ablation test duration was automatically controlled to a preset value, with douser closure and removal of the model from the test stream.
- F. While the arc heater continued to run at the test condition, post-test data were taken with the steady-state calorimeter and the pitot probe.
- G. The arc heater was turned off, the chopper stopped, the douser opened and a final radiant measurement taken with the steady-state calorimeter.
- H. Radiant source turned off.
- I. Test chamber vented to atmospheric pressure. Ablation model repositioned and post-test alignment check of pyrometer made and noted. Model removed from sting.

TABLE 4. SUMMARY OF 0.1 ATM, SUPERSONIC SUBLIMATION TESTS (CONFIGURATION 3)

Test Number	Arc Heater					Radiant Source			Remarks	
	\dot{m} (lbm/sec)	I (amps)	V (volts)	H_G (Btu/lbm)	\dot{q}_{conv} (Btu/ft ² -sec)	Pt2 (atm)	I (amps)	V (volts)		\dot{q}_{rad} (Btu/ft ² -sec)
22	0.016	300	415	19790	1879	0.110	—	—	—	Arc Heater Calibration
23	—	—	—	—	—	—	1500	90	2020	Radiant Source Calibration
24	—	—	—	—	—	—	900	75	730	Radiant Source Calibration
25	0.016	300	409	17520	1800	0.136	900	75	930	Model #7
26	0.016	300	425	14870	1743	0.181	900	75	1070	Models #1 & #9; no chopper
28	0.016	320	450	17690	1866	0.138	900	75	880	Models #5 & #8
58	0.016	300	425	24240	3141	0.208	1500	90	1990	Model #2
60	0.016	300	425	18900	2569	0.226	1500	90	—	Model #3
61	0.016	300	425	20800	2749	0.211	1300	85	2670	Model #10
62	0.016	300	425	17120	2619	0.283	1300	85	2710	Model #6
63	0.016	300	425	—	—	0.216	1300	85	—	Model #13
64	0.016	300	425	17370	2233	0.247	1500	90	2650	Model #31

Pre- and post-test data were necessary to completely define the test environment in the changing test cabin pressure situation. While considerable work was done during the checkout/calibration phase to minimize the pressure rise during the nominal 2-minute test sequence, there remained a significant effect on the convective environment. This was due mainly to the change in the test stream shock/expansion wave structure in the supersonic case, i.e., the test rhombus continually changed. Test cabin pressure variations in the subsonic case directly affected the model's stagnation pressure.

Operation of the radiation source was steady as monitored by the controls for the argon arc source. Pre- and post-test radiation calibration data, however showed a consistent decay in the incident radiation due to (1) decay in the reflectance of the imaging mirror due to soot deposition and (2) a general degradation in the transparency of the static gas environment due primarily to soot and NO_2 formation in the test chamber. The incident radiation data reported reflect this degradation.

The 0.1 atm, supersonic sublimation tests are summarized in Table 4. The heating rate and stagnation pressure data are the average of the pre- and post-test measurements. The centerline enthalpy, H_{cl} , is also an average based on the pre- and post-test calorimeter measurements, as determined by a procedure described in Section 3.4.2.1. These comments apply to the summary tables presented in this section. The complete set of data are shown in Appendix B. Test 22 was a final arc heater calibration of this condition, with radiant source calibration being accomplished in tests 23 and 24. Initial sublimation data were obtained from tests 25, 26 and 28. Subsequent analysis of these data revealed that the surface temperature measured was significantly lower than expected. Two possible causes were identified:

1. Misalignment of pyrometer
2. High conduction losses within the model (insufficient incident radiative heating rates)

The radiant source current was increased to the 1300 to 1500 amp level to maximize the radiant energy flux to the model surface. In addition great care was taken in aligning the pyrometer. Subsequently tests 58, 61, 62, 63 and 64 were run. These tests provided excellent ablation data points.

The 0.1 atm, high velocity, subsonic sublimation tests are summarized in Table 5. Since no checkout/calibration tests had been run at this test condition, test 32 (no data shown) was the initial checkout test for the arc heater. Tests 33 to 37 were calibration runs, with various arc heater flowrates and arc currents being used to define the optimum arc combination. Since the test stream was subsonic, changes in the test cabin pressure were directly translated as changes in the model

TABLE 5. SUMMARY OF 0.1 ATM, HIGH VELOCITY, SUBSONIC SUBLIMATION TESTS (CONFIGURATION 2)

Test Number	Arc Heater					Radiant Source			Remarks	
	\dot{m} (lbm/sec)	I (amps)	V (volts)	H_q (Btu/lbm)	\dot{q}_{conv} (Btu/ft ² -sec)	P _{t2} (atm)	I (amps)	V (volts)		\dot{q}_{rad} (Btu/ft ² -sec)
33	0.00084	200	75	—	80	0.101	—	—	—	Arc Heater Calibration
—	0.00126	200	86	—	140	0.120	—	—	—	
34	0.00126	213	75	—	150	0.142	—	—	—	
—	—	300	75	—	300	0.135	—	—	—	
—	—	339	75	—	360	0.189	—	—	—	Calibration
35	0.00084	199	75	—	70	0.119	—	—	—	
—	—	250	75	—	80	0.134	—	—	—	
—	—	296	75	13460	120	0.137	—	—	—	
36	0.00084	300	75	13460	104	0.131	950	75	970	Arc Heater Calibration
37	0.00084	300	75	13460	140	0.148	—	—	—	
38	0.00084	300	75	13460	130	0.160	950	75	940	Models #23 & 25
39	0.00084	300	75	13460	130	0.136	950	75	880	Models #19 & 22
48	0.00084	300	75	16510	170	0.090	1200	80	1760	Model #27
49	0.00084	300	75	16510	190	0.132	1500	90	2500	Model #30
50	0.00084	300	75	16510	170	0.083	1500	90	2600	Model #14

stagnation pressure, which accounts for the large test to test pressure variation. Initial sublimation data were obtained from tests 38 and 39. For the reasons outlined above, these tests were rerun as tests 48, 49 and 50.

The 0.1 atm, low velocity, subsonic sublimation tests are summarized in Table 6. The calibration and initial sublimation tests were tests 43 to 46. Final sublimation data were obtained from tests 51 to 54. Ablation data from these tests are presented in Section 3.4.3.

The 1.0 atm, supersonic sublimation tests are summarized in Table 7. At this condition, the test cabin pressure rise had the least effect on the convective test stream due to the relatively high pressure (70 to 80 torr) required for matched nozzle flow. This allowed for a lower initial cabin pressure, maintaining operation in the underexpanded mode throughout the test. The result was a test rhombus which varied only slightly over the test period. Test 69 provided arc heater calibration data while final sublimation data was obtained from tests 70, 71, 72 and 73. A total of 4 usable data points were obtained at this condition.

The final sublimation tests, 1.0 atm, low velocity, subsonic, are summarized in Table 8. For this condition, the test cabin was vented to the atmosphere, thus maintaining the stagnation pressure at 1.0 atm. The high cabin pressure produced an unexpected side effect. The production of various nitric oxide compounds (NO_x) was very high and appeared to be predominately NO_2 from its reddish-brown color. It is felt this was a result of the high oxygen content of the cabin at this condition reacting with the high temperature nitrogen/oxygen test stream. Since this operating mode was unique, there was no means of evacuating the cabin during the test at a rate sufficient to prevent NO_x formation. Visual observation of tests 76, 77 and 78, which were run with arc heated oxygen and nitrogen, revealed a significant reduction in the radiant levels due to the NO_x buildup. Pre- and post-test measurements of the radiant levels (see Table 8) showed a 40 to 50 percent reduction. Tests 79 and 80 were an attempt to reduce the concentration of NO_x by removing the arc heated oxygen. These two tests were made using arc heated nitrogen. This modification resulted in a radiant reduction of 33 to 35 percent, indicating that arc heated nitrogen was still enabling the NO_x reactions to proceed at a significant rate. It should be noted that the NO_x buildup in the cabin not only reduced the radiant levels incident on the model but also perturbed the pyrometer data (see Section 3.4.1). For this reason, the final test was run with cold argon flowing over the model at a low subsonic velocity of about 2 ft/sec; the only energy input to the ablation model was radiant. The intention of the argon flow was to remove ablation products (i.e., soot formed by condensing carbon vapor species) from the vicinity of the ablating surface which block some of the

TABLE 6. SUMMARY OF 0.1 ATM, LOW VELOCITY, SUBSONIC SUBLIMATION TESTS (CONFIGURATION 1)

Test Number	Arc Heater						Radiant Source			Remarks
	\dot{m} (lbm/sec)	I (amps)	V (volts)	H_G (Btu/lbm)	\dot{q}_{conv} (Btu/ft ² -sec)	P_{t2} (atm)	I (amps)	V (volts)	\dot{q}_{rad} (Btu/ft ² -sec)	
43	0.00084	300	50	—	—	0.131	950	75	1220	Arc Heater/ Rad. Source Calibration
—	0.00126	300	50	—	—	0.165	—	—	—	Arc Heater Calibration
44	0.00126	400	85	—	34	0.147	950	75	—	—
45	0.00126	400	85	—	—	0.163	950	75	1230	Model #21
46	0.00126	400	75	—	—	0.218	950	75	—	Model #28
51	0.0126	300	75	12530	—	0.088	1500	90	2730	Model #24
52	0.0126	300	75	12530	50	0.081	1500	90	2920	Model #29
53	0.0126	300	75	12530	50	0.083	1500	90	2890	Model #20
54	0.0126	300	75	12530	25	0.129	1500	90	2860	Model #26

TABLE 7. SUMMARY OF 1.0 ATM, SUPERSONIC SUBLIMATION TESTS (CONFIGURATION 6)

Test Number	Arc Heater						Radiant Source			Remarks
	\dot{m} (lbm/sec)	I (amps)	V (volts)	H _Q (Btu/lbm)	\dot{q}_{conv} (Btu/ft ² -sec)	P _{t2} (atm)	I (amps)	V (volts)	\dot{q}_{rad} (Btu/ft ² -sec)	
69	0.025	350	1050	17080	4630	0.897	—	—	—	Arc Heater Calibration
70	0.025	375	1050	17900	4903	0.915	—	—	—	Model #12
71	0.023	350	1050	18760	4960	0.852	1500	90	1940	Model #15
72	0.023	350	1050	17880	4750	0.860	1500	90	2040	Model #18
73	0.023	350	1050	18140	4822	0.862	1500	90	1860	Model #17
	0.023	350	1050	17940	4770	0.862	1500	90	2020	

TABLE 8. SUMMARY OF 1.0 ATM, LOW VELOCITY, SUBSONIC SUBLIMATION TESTS (CONFIGURATION 4)

Test Number	Arc Heater					Radiant Source				Remarks
	\dot{m} (lbm/sec)	I (amps)	V (volts)	H_G (Btu/lbm)	\dot{q}_{conv} (Btu/ft ² -sec)	Pt ₂ (atm)	I (amps)	V (volts)	\dot{q}_{rad}^* (Btu/ft ² -sec)	
76	0.0084	200	650	5940	63	1.0	1500	90	2150/1090	Model #11
77	0.0084	200	675	5940	—	1.0	1500	90	1930/1160	Model #16
78	0.0084	200	650	5940	—	1.0	1500	90	2070/1290	Model #35
79	0.0065	200	625	5940	74	1.0	1500	90	1960/1290	Model #34; N ₂ flow
80	0.0065	200	600	5941	81	1.0	1500	90	1920/1290	Model 32; N ₂ flow
81	—	—	—	—	—	1.0	1500	90	1940/1880	Model #33, cold argon flow

*Before/after

emitted radiation. In this test, (#81) the argon flow velocity was apparently too low to be effective and a plume or cloud of carbon soot was observed at the model surface. The effect of this plume is discussed in Section 3.4.

In summary, sublimation data points were obtained at two pressure levels and three distinct flow velocities for a total of five separate convective conditions.

3.4 TEST RESULTS

The results of the graphite vaporization study conducted in the NASA Ames AEHS facility are presented in this section along with a discussion of the techniques used to reduce the data. The test matrix with a tabulation of measured test conditions is presented in Section 3.4.1. The procedures used to characterize the convective environment, verify the pyrometer data, and determine the surface recession rates are discussed in Section 3.4.2. Uncertainties associated with each type of data are analyzed. The ablation response of each test model is presented in Section 3.4.3.

3.4.1 Test Matrix and Test Conditions

Table 9 is the test matrix and tabulation of the average stream and model surface test conditions for all ATJ-S ablation model exposures in this test series. The initial proof model exposures and calibration runs are not presented, but can be found in Appendix B along with actual stream measurements before and after model exposures. The complete tabulation in Appendix B also describes the assumptions required for those data that were unavailable due to data acquisition or probe malfunction.

3.4.2 Data Reduction Techniques

The data reduction procedures, assumptions and uncertainties involved in convective stream characterization, model surface temperature measurements, and recession rates are discussed in the following subsections.

3.4.2.1 Convective Environment Characterization

As mentioned earlier in Section 3.2.3, the arc heater cooling water temperature rise and mass flow rate were not measured in this facility and, therefore, the arc heater efficiency and bulk enthalpy were not known. In addition, the low heating rates encountered in the subsonic portions of this test series, coupled with the necessity to use a 0-5000 Btu/ft² sec steady-state calorimeter (see Section 3.2.3) resulted in cold-wall convective heating measurements corresponding to less than 1 percent of the full range output of the instrument. These two factors affected the characterization of the convective environment at the subsonic conditions. Under both the supersonic and

TABLE 9. TEST CONDITIONS AND ATJ-S SURFACE TEMPERATURE DATA

Test Number	Model Number	Heater Config	\dot{m} N ₂ /O ₂	Exposure Time	\dot{q} Steady-State Calorimeter		P _{t2} (atm)	H _C * (8tu/lbm)	T _s (max) w/o REFL Component (°R)
					Radiation†	Convection			
25	7	3	.016	59.86	930	1800	.136	17521	6489
26	1			45.60	1070	1743	.181	14872	6410
	9			45.80					6321
28	5			30.00	880	1866	.138	17694	6289
	8			30.04					6369
38	23	2	.00084	59.95	940	134	.160	13458	5988
	25			59.70					6135
39	19			59.70	880	134	.134	13458	5855
	22			60.00					5995
45	21	1	.00126	≈120.00	1230	16.3	.163	—	5586
48	27	2	.00084	59.2	1760	172	.090	16505	6017
49	30			29.4	2500	147	.132	16505	6173
50	14			30.15	2600	170	.083	16505	5903
51	24	1	.00126	59.62	2730	—	.089	12527	6680
52	29			29.65	2920	50.5	.081	12527	5974
53	20			29.35	2890	50.5	.083	12527	6684
54	26			30.05	2860	25.3	.129	12527	6658
58	2	3	.016	21.20	1990	3141	.208	24238	6068
60	3			30.00	—	2569	.226	18899	6605
61	10			19.80	2670	2749	.211	20805	6540
62	6			20.10	2710	2619	.283	17118	6579
63	13			21.65	—	—	.216	—	6627
64	31			19.75	2650	2233	.247	17367	6676
70	12	6	.023	15.10	1940	4958	.852	18761	7158
71	15			8.60	2040	4750	.861	17885	7082
72	18			8.70	1860	4822	.863	18137	7092
73	17			8.50	2020	4768	.862	17936	7102
76	11	4	.0084	30.00	1620	36.1	1.0	5941	6618
77	16			45.65	1545	45.4	1.0	5941	6653
78	35			45.95	1680	63.9	1.0	5941	6649
79	34		.0065	45.30	1625	90.5	1.0	5941	6307
80	32		.0065	45.40	1605	54.3	1.0	5941	6762
81	33	RAO ONLY	COLO Ar	45.60	1910	N/A	1.0	N/A	7082

†The copper steady-state calorimeter was not blackened — the \dot{q} data were adjusted by an emissivity of 0.83 based on blackened transient calorimeter data.

*Based on Fay-Riddell theory of stagnation point convective heat transfer to a 5/16" calorimeter.

subsonic flow conditions the arc heater chamber pressure (P_c) was accurately measured by a pressure transducer. The stream stagnation pressure (P_t) was measured with a pitot probe inserted into the stream prior to and immediately following the test model exposure. The determination of the convective flow centerline enthalpy was based on the measured cold wall heat flux but was calculated differently for the subsonic and supersonic cases. These two procedures are described below.

Supersonic Condition

For the two supersonic test conditions (arc heater configurations 3 and 6), the centerline enthalpy was calculated using the Fay-Riddell theory for cold wall stagnation point convective heat transfer to a sphere and the measured cold wall heat flux. The heating rate (\dot{q}) measured by the steady-state calorimeter was in the mid to upper range of the instrument. These data along with the measured stagnation pressure (P_{t2}) were used to compute the centerline enthalpy (H_c) from the following relation (Reference 43):

$$\dot{q} = 0.0462 \sqrt{P_{t2}/R_N} H_0$$

where: R_N = nose radius of the steady-state calorimeter (ft)

P_{t2} = stagnation pressure (atm)

\dot{q} = heating rate (Btu/ft²-sec)

H_0 = stream enthalpy (Btu/lbm)

The measured \dot{q} data at these test conditions are considered accurate and were used to determine the effective centerline enthalpy for each supersonic run.

Subsonic Conditions

The subsonic stream enthalpy was calculated using an iteration technique which required an arc heater efficiency to be assumed and the bulk enthalpy (H_0) calculated using the known input power and gas mass flow rate. This initial enthalpy estimate along with the measured chamber pressure (P_c) was used to define the arc chamber gas state. At these subsonic flow conditions, due to uncertainties in the measured data, the data from all the runs at a particular subsonic condition were used to define an average P_c , H_0 and cold wall heat rate (\dot{q}). The subsonic heat transfer coefficient to an axisymmetric blunt body (Reference 44) was computed and compared to the experimentally determined value based on the average measured \dot{q} and initial effective H based on an assumed efficiency. Various efficiencies were assumed in this iteration until closure was achieved.

and the theoretical and experimental heat transfer coefficients agreed. The following relations were used in the theoretical evaluation of the heat transfer coefficient:

$$Nu_x = 0.76 Re_x^{1/2} Pr^{0.4} = \frac{hx}{k}$$

$$\therefore h = 0.76 \left(\frac{k}{x} \right) \left(\frac{\rho u x}{\mu} \right)^{1/2} (Pr)^{0.4}$$

$$h = 0.76 k \left(\frac{\rho}{\mu} \right)^{1/2} \left(\frac{u}{x} \right)^{1/2} (Pr)^{0.4}$$

$$h = 0.76 k \left(\frac{\rho}{\mu} \right)^{1/2} \sqrt{\frac{du}{ds}} (Pr)^{0.4}$$

$$\text{where: } \frac{du}{ds} = \frac{2}{\pi} \frac{U_{\infty}}{R_c} \sqrt{\frac{\rho_{\infty}}{\rho_0}}$$

These relations assume (1) incompressible flow, (2) no centerline enthalpy peaking, and (3) a fully filled nozzle.

As previously mentioned, the low heating rates of the subsonic test conditions and the relatively high range of the steady-state calorimeter caused substantial uncertainty in the subsonic heating data. Therefore, when the average \dot{q} for runs of similar conditions at each subsonic test point were computed, obviously erroneous data were ignored. The similarity in material response, power input, stream conditions and available convective \dot{q} data from the transient slug calorimeter were used to define an average q for each subsonic condition. Arc heater Configuration 1 is an example of the selection processes used to average the subsonic \dot{q} data. Of the four runs at this condition (runs 51 through 54), only three produced a recorded \dot{q} data. Only two of these were considered valid (runs 52 and 53). The low q data from run 54 were ignored (see Table 9). The low millivolt output resulted in a barely discernible deflection on the CEC recording system. However, the surface recession rates of the four runs were similar. Since the repeatability of the measured \dot{q} (50.5 Btu/ft-sec) was evident throughout the four calorimeter exposure of runs 52 and 53, this value was assumed as the average \dot{q} for Configuration 1. Since the sensitivity of the calorimeter was low at these test conditions, the estimated accuracy of the subsonic \dot{q} data due to deflection measurement uncertainties alone is ± 20 percent. Although these uncertainties are large their effect on the data interpretation isn't too significant as shown in Section 4.

The last series of runs at the 1.0 atm subsonic configuration produced equally suspect steady-state calorimeter data. For these runs the average convective \dot{q} measured by the transient slug calorimeter was also used to estimate the stream enthalpy and subsonic heat and mass transfer rate.

3.4.2.2 Pyrometer Data Reduction

Several potential problem areas that affect the optical pyrometer surface temperature measurements were investigated to determine their impact on the reported data. Potential problems include alignment, gas cap radiation, ablation products in the boundary layer, and the occlusion of the reflected component. Each of these areas is discussed in this section.

Alignment

During the initial runs of the test program pyrometer alignment became a serious problem and resulted in the low temperature data reported in runs 38 through 45. Initially the target was positioned off of the stagnation point along the 45° ray in the horizontal plane (see Figure 12). Thermal and pressurization cycling of the models, as well as slight variations in model length and positioning differences, resulted in rather gross uncertainties in the pyrometer target location on the model surface. When this fluctuation in temperature became apparent, greater care was taken in verifying the pyrometer alignment. The target location was checked and noted prior to each run. After the model exposure the model was reinserted and the target location checked again. The location with respect to the maximum recession area was noted. These steps resulted in highly consistent temperature levels for similar test conditions for runs 48 through the completion of the test series.

Gas Cap and Ablation Products Radiation

A potential source of error in pyrometer data of ablating graphite surfaces is the emission and/or absorption of the high temperature gas cap between the normal shock and the model. Another concern is the radiative properties of the ablation products within the boundary layer. The two effects are shown to be negligible by Rindal, et al. (Reference 45) for carbon sublimation in air under environmental conditions similar to these.

In Reference 45 gas cap radiation was calculated for stagnation pressures (P_{t2}) of 0.05 atm, 0.5 atm, and 100 atm assuming air enthalpies of 30,000 Btu/lbm at the lower pressures and 3000 Btu/lbm at the high pressure condition.

In calculating the radiation from the gas cap, the gas cap was assumed to be optically thin with the radiation being a combination of both continuum and band (line) radiation. The thickness of the gas cap, the shock stand off distance, was calculated from:

$$\delta = 0.78 \frac{\rho_{\infty}}{\rho_0} R_N$$

where R_N = nose radius, 0.5 inch for the AFML study - note that the nose radius for all models of the Aerotherm study reported herein was 0.25 inch

ρ_{∞} = free stream density

ρ_0 = stagnation point density

The radiation from the ablation products was studied for only one condition $P_t = 0.5$ atm and $H_0 = 30,000$ Btu/lbm. The effects of both the ablation products and the gas cap are summarized in Figure 15. The emissive power versus wavelength from the gas cap for two conditions and that from the ablation products at one condition are compared to the emissive power of a blackbody surface at various temperatures. The band radiation component is superimposed upon the continuum radiation; the total radiation power being equal to the sum of these two levels.

As shown in Figure 15, for wavelengths greater than 0.2μ the band contribution was negligible compared to the continuum contribution for both the high and low pressure conditions. Furthermore, at the 100 atm condition, above 0.5μ , the gas cap effects were less than or equal to 2.6 percent of the emissive power of a blackbody at 7000°R (the nominal range of temperatures reported in this investigation). The test pressures of this study were in the range (0.1 to 1.0 atm) which is close to the 0.5 atm curve of Figure 15, where it can be seen that the gas cap effects are even less pronounced.

The ablation products emissive power contribution is less than 1 percent above 0.6μ relative to a 7000°R blackbody. Radiation from the freestream gas upstream of the shock was also found to be negligible in this study.

Reflected Component

As discussed previously in Section 3.2.1, the combined radiation facility utilized a large diameter rotating chopper to occlude the incident radiation from the radiation source and thus eliminate the model surface reflectance component from the pyrometer measurement. This technique is only successful if the pyrometer and associated recording apparatus response time is sufficiently fast

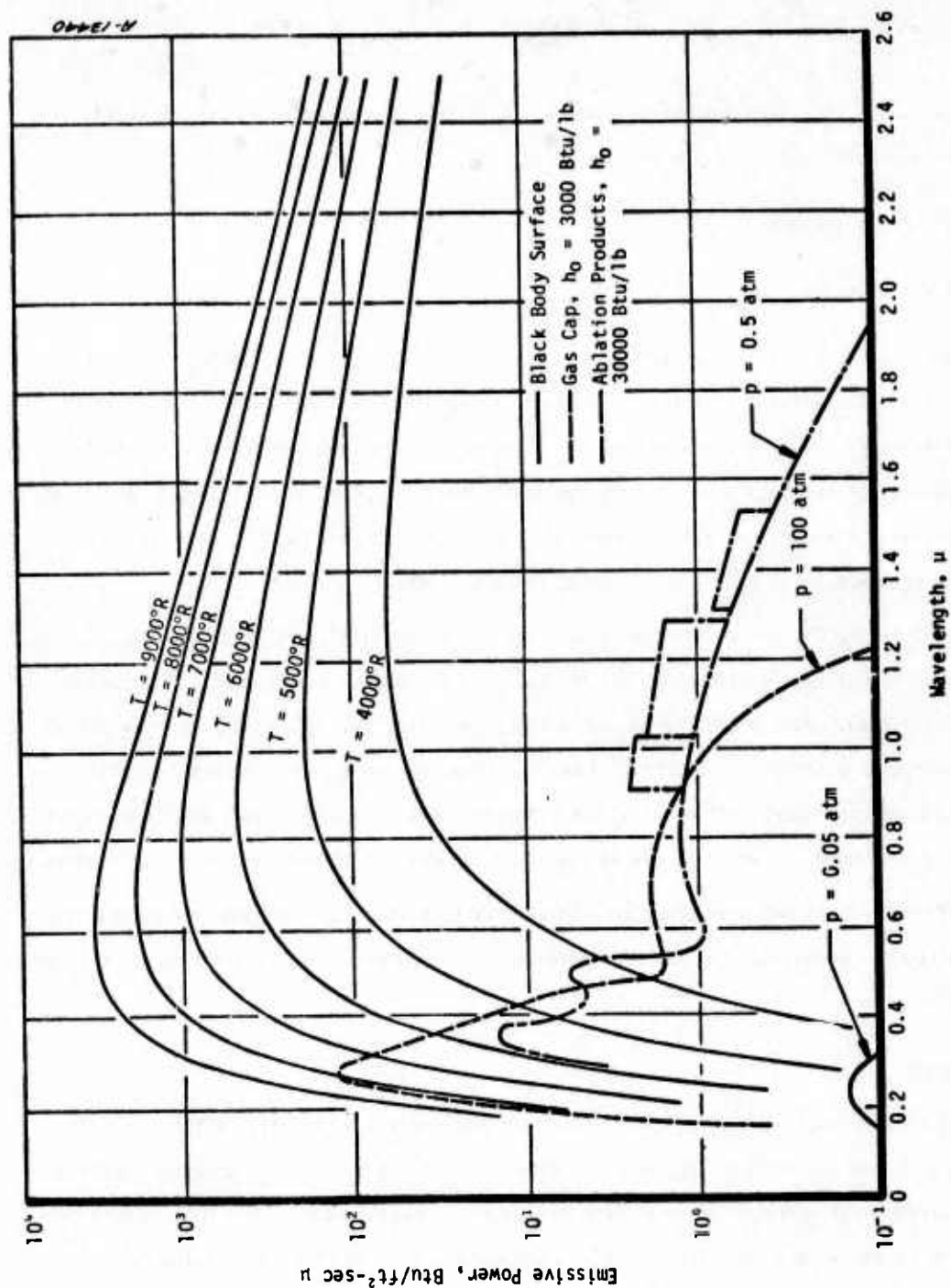


Figure 15. Radiation contributions of surface gas cap and ablation products from AFML-TR-70-133.

to monitor the pyrometer output during the short blockage time. The chopper blades occlude the incident radiation for ~ 3 msec with an interval of about 50 to 60 msec between each blockage. The 10 μ sec response of the pyrometer is more than required for this operation. However the response time of the recording equipment is such that the effective response time of the system is close to 3 msec.

The response time of the pyrometer and recording system was demonstrated by exposing the water cooled steady-state calorimeter to the incident radiation environment while the chopper was operating. The pyrometer output dropped to the cold wall value of the calorimeter during the time when the chopper blades blocked the incident radiation. This response is shown in Figure 16.

3.4.2.3 Recession Data

Model centerline recession rates were generated by reducing the high speed 16mm film data of each model exposure. An L&W photo-optical data analyzer was used to project the model images. The location of the model centerline with respect to a fixed model reference line was noted at several times throughout the test. The times for each location were computed by defining an average framing rate from the projector frame counter and the overall test time from the CEC oscillograph trace. The recession to each profile was computed by measuring the projected images with respect to a fixed reference and converting to actual dimensions through the use of a scale factor. The reference used was the interface between the primary sphere/cylinder portion of the model and the aft cylindrical radiation shield. The scale factor was determined from an average of the projected model diameter over several frames near time 0 (after the model reached test stream centerline) and the known pretest diameter. The scaling factor was determined early in time to reduce the effects of sidewall ablation and thermal expansion. With these phenomena in mind, noting that precise measurements of some projected images were difficult due to film clarity and contrast, the film data length measurements are considered accurate to within about ± 10 percent.

The data from the film reduction procedure were plotted as recession versus time. A straight line was hand-fitted through the data over the steady-state portion of the run. The slope was computed and the results are presented in the following subsection.

For several runs the exposure settings and filtering resulted in poor contrast such that the model reference line could not be clearly identified during the intermediate portion of the test. For these cases an approximate recession rate was evaluated by the ratio of the overall length change to the total test time ($\Delta s / \Delta t$). The length change was the difference between the initial and final lengths as determined from the film data. Initial and final model dimensions were available from the poor quality film data since the reference line was generally visible as the model was moving into and out of the test stream. At these times the model was outside of the high intensity focal point of the radiation source imaging mirror such that the photographic contrast was better.

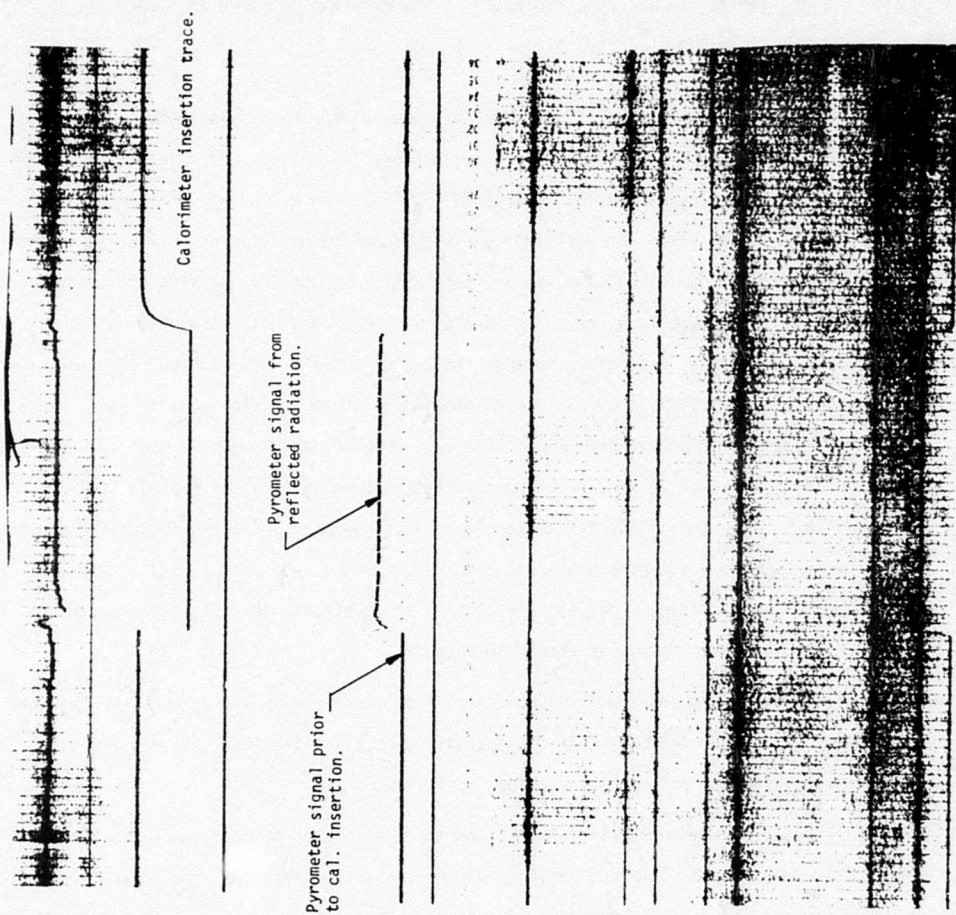


Figure 16. Pyrometer/recording system response to the reflected incident radiation on a "cold" calorimeter.

The $\Delta s/\Delta \theta$ values as determined from the film data were considered more accurate than $\Delta s/\Delta \theta$ values determined from pre- and post-test length measurements of the test samples for the following reasons:

1. The pre- and post-test measurements were made on the overall model length, including the model holder; thermal cycling may have effected the model/model holder junction
2. Some ablation occurred after removal from the test stream
3. Handling, after the exposure and before post-test measurements were taken, may have damaged the surface and affected the Δs measurement

For those runs where no film data are available the \dot{s} data were estimated from other runs at similar conditions. A correlation between \dot{s} as measured by film reduction techniques and $\Delta s/\Delta \theta$ as determined by pre- and post-test length measurements was used to estimate \dot{s} from the $\Delta s/\Delta \theta$ value of the effected model.

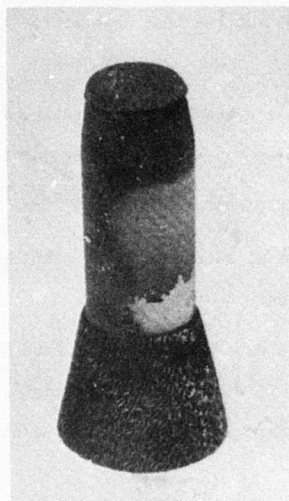
For the subsonic runs the model ablation was slightly asymmetric. This is evident from the photographs in Figure 17 of four ablation models tested at the four primary test conditions. The area off of the model centerline along the 45° ray receded more than the stagnation area. This high recession area was the viewing location of the optical pyrometer but was not viewed by the high speed motion picture camera (see Figure 12, Section 3.2.3). Therefore, the centerline recession rates reduced from the film data were not indicative of the higher recession rates in the location of the surface temperature measurements. To investigate this disparity, the recession rate at the 45° location was estimated from the ratio of recession at the 45° ray (Δs_{45}) to centerline recession (Δs_Q) parallel to the model axis and the centerline recession rate (\dot{s}_Q) as determined from the film data:

$$\dot{s}_{45} = \frac{\Delta s_{45}}{\Delta s_Q} (\dot{s}_{Q-film})$$

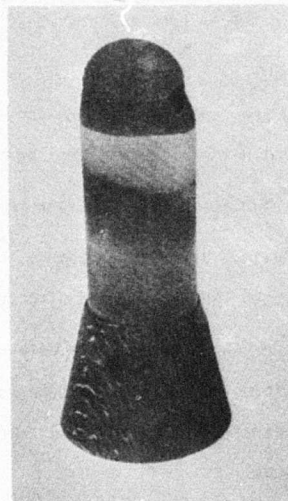
The exposed test models which exhibited significant asymmetries were projected using an optical comparator (10X power) and the image traced in a plane corresponding to the horizontal plane when installed in the test facility. This plane showed the asymmetric ablation shape at the 45° location. In this plane the Δs_Q occurring at the stagnation point was approximately equal to the Δs_Q as viewed by the camera. An unexposed model was then projected and the images superimposed. The overall recession at the centerline and at the 45° position were measured and converted to actual dimensions using the appropriate scaling factor. Figure 18 shows an example of this estimation procedure.

For the subsonic 0.1 atm conditions, runs 38 through 54, the average uncertainty in the reported \dot{s} data and hence the blowing parameter $8'_0$ was approximately 90 percent. It is important

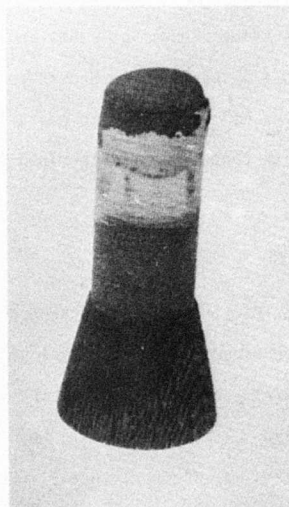
hct106NTT



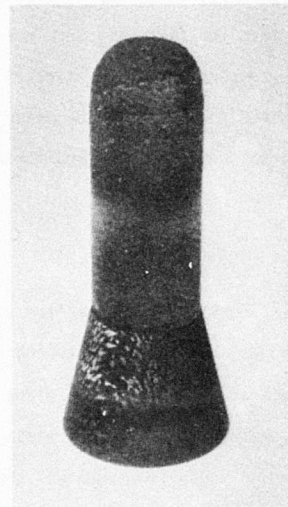
Model #13
Low pressure supersonic



Model #20
Low pressure subsonic



Model #18
Moderate pressure supersonic



Model #33
Moderate pressure subsonic

Figure 17.
Post-test ablation models from the four primary test conditions.

Run 52
Model 29

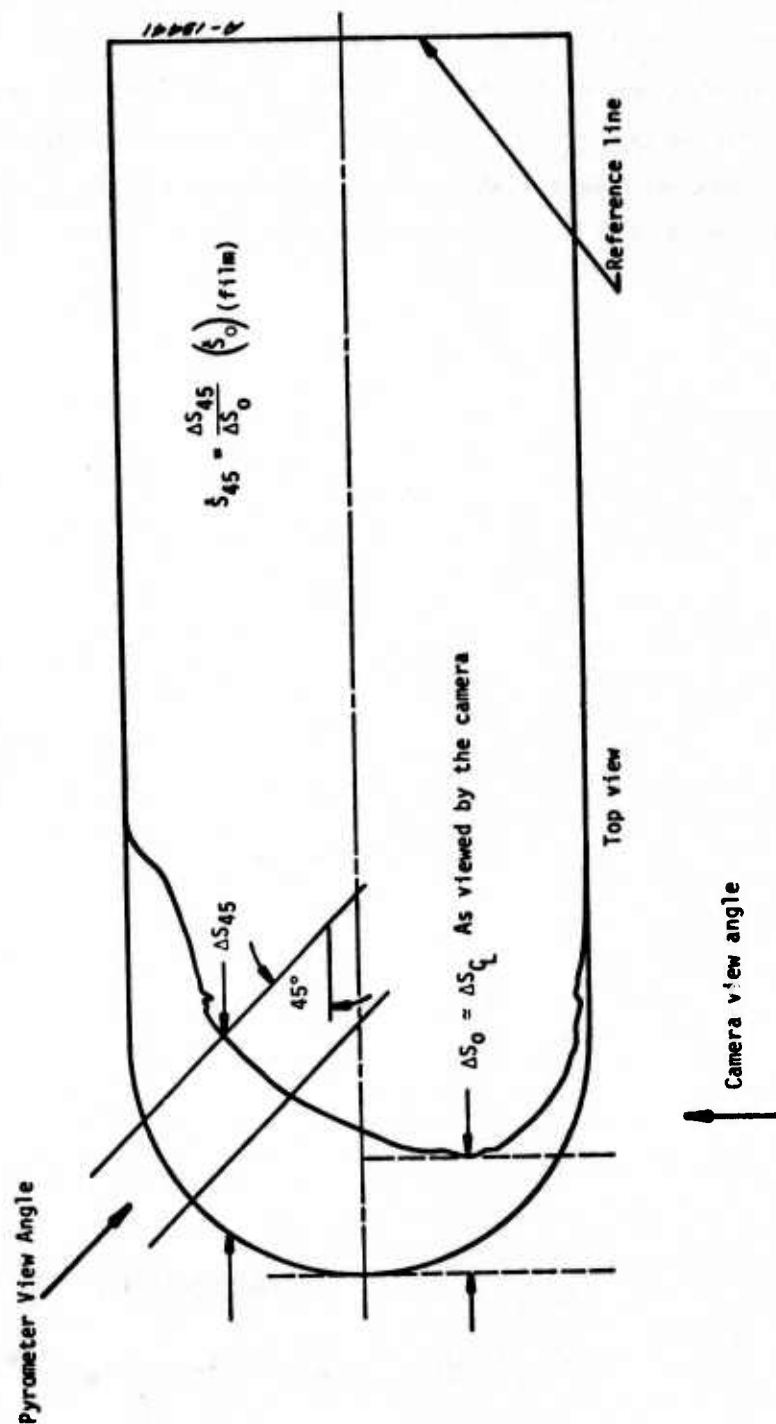


Figure 18. Technique used to correct \dot{S} and B'_0 due to asymmetric ablation.

to note, however that despite the rather large uncertainty in \dot{s} , the effect on the corresponding B' value is not significant since B' values are all $B' > 10$ at these subsonic test conditions.

3.4.3 Ablation Results

The results of the measured and "adjusted" data described in the previous sections are reported in this section in terms of the ablation response of the material. Table 10 is a listing of all successful model exposure runs and the measured or estimated centerline recession rates (\dot{s}), the heat transfer coefficient ($\rho_e u_e C_{H_0}$), and the mass flux (\dot{m}). The maximum surface temperature, without the reflected components, and the calculated blowing parameter ($B'_0 = \dot{m} / \rho_e u_e C_{H_0}$) are also tabulated. These data were derived from the test conditions reported in Table 9 of Section 3.4.1.

TABLE 10. ABLATION RESULTS

Test Number	Model Number	$\rho_e u_e \text{CH}_0$ (lbm/ft ² -sec)	\dot{s} (in/sec)	$(\rho \dot{s})$ (lbm/ft ² -sec)	T_s w/o Reflec (max) (°R)	B_0^I $m/\rho_e u_e \text{CH}_0$
25	7	0.103	0.00342	0.0328	6489	0.318
26	1	0.117	0.00417	0.0400	6410	0.342
	9	0.117	0.00295	0.0283	6321	0.242
28	5	0.105	0.00474	0.0454	6289	0.432
	8	0.105	0.00325	0.0312	6369	0.297
38	23	0.00996	0.000918	0.00880	5988	0.884
	25	0.00996	0.000818	0.00784	6135	0.787
39	19	0.00996	0.00123	0.0118	5855	1.185
	22	0.00996	0.00113	0.0108	5995	1.084
48	27	0.0104	0.000765	0.00733	6017	0.705
49	30	0.0113	0.00434	0.0416	6173	3.680
50	14	0.0103	0.00425	0.0407	5903	3.950
51	24	0.00414	0.00273	0.0262	6680	6.330
52	29	0.00414	0.00332	0.0318	5974	7.680
53	20	0.00414	0.00452	0.0433	6684	10.460
54	26	0.00414	0.00429	0.0411	6658	9.930
58	2	0.130	0.00773	0.0741	6605	0.570
60	3	0.136	0.00915	0.0877	6605	0.640
61	10	0.132	0.00766	0.0734	6540	0.560
62	6	0.153	0.00689	0.0661	6579	0.430
63	13	0.138	0.00690	0.0661	6627	0.480
64	31	0.131	0.00914	0.0876	6676	0.670
70	12	0.264	0.0713	0.204	7158	0.773
71	15	0.266	0.0164	0.157	7082	0.590
72	18	0.265	0.0171	0.164	7092	0.618
73	17	0.266	0.0195	0.187	7102	0.703
76	11	0.0122	0.000428	0.00410	6618	0.336
77	16	0.0122	0.00152	0.0146	6653	1.200
78	35	0.0122	0.00163	0.0156	6649	1.280
79	34	0.0122	0.00163	0.0156	6807	1.280
80	32	0.0122	0.000989	0.00948	6762	0.770
81	33	N/A	0.00145	0.0139	7082	N/A

SECTION 4

SUBLIMATION DATA ANALYSIS

This section reviews analyses of the ATJ-S ablation test results presented in Section 3. In this section the ablation data from the AEHS test series are compared with various thermochemical models to illustrate:

1. Their agreement with the JANAF carbon vapor thermochemical property data, and
2. Their correlation with both equilibrium, diffusion-controlled and kinetically controlled models.

The ablation data generated on this program are unique since tests were run at two pressures (0.1 and ~ 1.0 atmospheres) and two different flow conditions (both subsonic and supersonic) at each pressure. As discussed in Section 3, the variation of the convective flow achieved with the modified constrictor arc heater resulted in about a factor of 40 change in the heat and mass transfer rate. This large variation in $p_e u_e C_m$ is sufficient to cause about a 200°R - 300°R shift to higher surface temperatures if sublimation is rate controlled. Section 4.1 compares the ablation data from the low subsonic (i.e., equilibrium-diffusion controlled) test conditions with various vapor pressure laws. Then, in Section 4.2, the ablation data are compared with the equilibrium and rate controlled thermochemical ablation predictions based on JANAF thermochemistry.

4.1 DATA COMPARISON WITH EQUILIBRIUM CARBON VAPOR PHASE MODELS

The phase diagram of carbon continues to be uncertain as discussed in Section 2. The uncertainty lies principally in:

1. The thermochemical properties of the carbon vapor species above C_2 (i.e., C_3 - C_5) and
2. The triple point state.

Results of the subsonic flow ablation tests are appropriate for establishing the correct carbon vapor species thermochemical model because of their low heat and mass transfer rates (which require that the ablation response be equilibrium diffusion controlled). In addition, these results can be compared with previously reported carbon melt data.

One means of establishing the correct carbon vapor thermochemical properties would be to experimentally construct the B'/T curve at a fixed pressure under a low convective flow condition. The B' curve would be experimentally developed by varying the incident radiative heating so as to generate carbon ablation data in the temperature regime of interest as previously shown in Figure 3.

Another means of establishing the correct carbon vapor thermochemistry would be to establish the asymptotic temperature at a given pressure (i.e., high B' values). At sufficiently high B' values the mass fraction of carbon vapor at the surface approaches unity, as shown by the expression

$$\tilde{K}_{C_w} = \frac{B'}{1+B'} \quad \text{developed in Section 2.2.}$$

Thus, for $B' > 10$, the carbon vapor partial pressure is more than 90 percent of the static pressure and the surface state is controlled by molecular diffusion and chemical equilibrium.

The second method was used in this program to establish the equilibrium carbon vapor state due to the relatively limited number of models and tests available. At both pressures (~ 0.1 and 1.0 atmospheres), the peak incident radiative flux was used to maximize mass flux from the model (i.e., B'). Reference to Table 10 shows that at 0.1 atmospheres the peak B' values are greater than 10^3 . It should be noted that the blowing correction used to arrive at these high B' values is uncertain at these high blowing conditions. This uncertainty is not significant however, for our purposes since the accuracy of the B' value is not critical as long as the B' value is greater than 10. Since the unblown B'_0 values at the ~ 0.1 atmosphere condition are above 6 it is obvious the blown B' values are sufficiently large to assume the carbon vapor is in equilibrium with the surface. Interestingly the B' values at the ~ 1.0 atmosphere test condition are much lower. This occurs for two reasons. First, at 1.0 atmosphere the vapor phase equilibrium temperature is 600°R above the 0.1 atmosphere temperature. The incident radiative flux was the same at both pressures (~ 2200 Btu/ft² sec) thus the surface energy balance dictates that the peak B' value attainable at 1.0 atmosphere must drop appreciably. Secondly, the ablation products at 1 atmosphere formed an opaque smoke pattern much like that of a burning cigarette which blocked some of the incident radiation. In addition NO₂ was formed and blocked incident radiation. As a result, the peak B' values achieved at the 1 atmosphere test condition are in the range 1 to 3. Davy and Bar-Nun (Reference 38) reported a similar soot or smoke plume during their radiation only tests in the AEHS facility. In an attempt to reduce or remove this plume on this series a low subsonic flow of arc heated air was included to reduce the incident and reflected radiation blockage. It is evident from the 1 atmosphere data that the air flow was insufficient to completely remove the plume effects

since the measured surface temperatures are 300°F-500°R below the values measured under supersonic flow conditions. In a further attempt to alleviate this problem the last run (Test 81) used pure argon as the convective gas to reduce the model's mass loss (i.e., the source of the plume) and the potential for NO₂ formation. The surface temperature measured for this run is about 275°R above the temperatures measured for those runs using arc heated air or nitrogen. In addition the B' value is about a factor of 4 above those with the arc heated air. Therefore it appears that if this technique could have been perfected high quality temperature data would have been obtained at 1 atmosphere "equilibrium" test condition. As it stands, however, these surface temperature data are felt to be low.

These equilibrium sublimation data are compared with four carbon phase equilibrium predictions in Figure 19. The equilibrium data in the region of 0.1 atmosphere exhibit excellent agreement with the JANAF phase equilibrium predictions. At the 1.0 atmosphere condition, only the highest temperature data point is included in Figure 10 since the other data are obviously erroneous due to radiation blockage. The highest temperature data point is about 230°R below the JANAF vapor phase equilibrium temperature at the 1.0 atmosphere condition, whereas it is above both the Dolton, et al. and Kratsch, et al. values by about 430°R and 250°R respectively. Interestingly it is only about 70°R below the JANAF/Strauss-Thiele phase equilibrium prediction. It is likely that this surface temperature measurement is also low since although the plume was visually reduced by the cold argon flow and the NO₂ concentration was obviously reduced both were still discernible. In addition the supersonic flow surface temperature data are about 30°R above the peak subsonic flow surface temperature while the B' values are about a factor of 4 lower. Although it is difficult to quantify, all available data suggest that all of the surface temperature data from the subsonic/atmospheric tests are low. Considering this, the peak surface temperature value at one atmosphere tends to verify the JANAF thermochemistry model since the measured value is probably lower than the true surface temperature. Certainly, when taken as a complete set the equilibrium sublimation data support the nominal JANAF thermochemical data.

4.2 DATA COMPARISON WITH EQUILIBRIUM AND RATE CONTROLLED MODELS

The analyses in this section compare the supersonic flow (high mass transfer rate) ATJ-S graphite ablation data presented in Table 10 with equilibrium and kinetically controlled sublimation predictions. The ablation data generated under the high convective conditions are compared with the appropriate JANAF equilibrium diffusion controlled B' curve in Figure 20. The theoretical B' curves included in Figure 20 span the pressure range 0.2 to 1.0 atmospheres as do the data. The impact

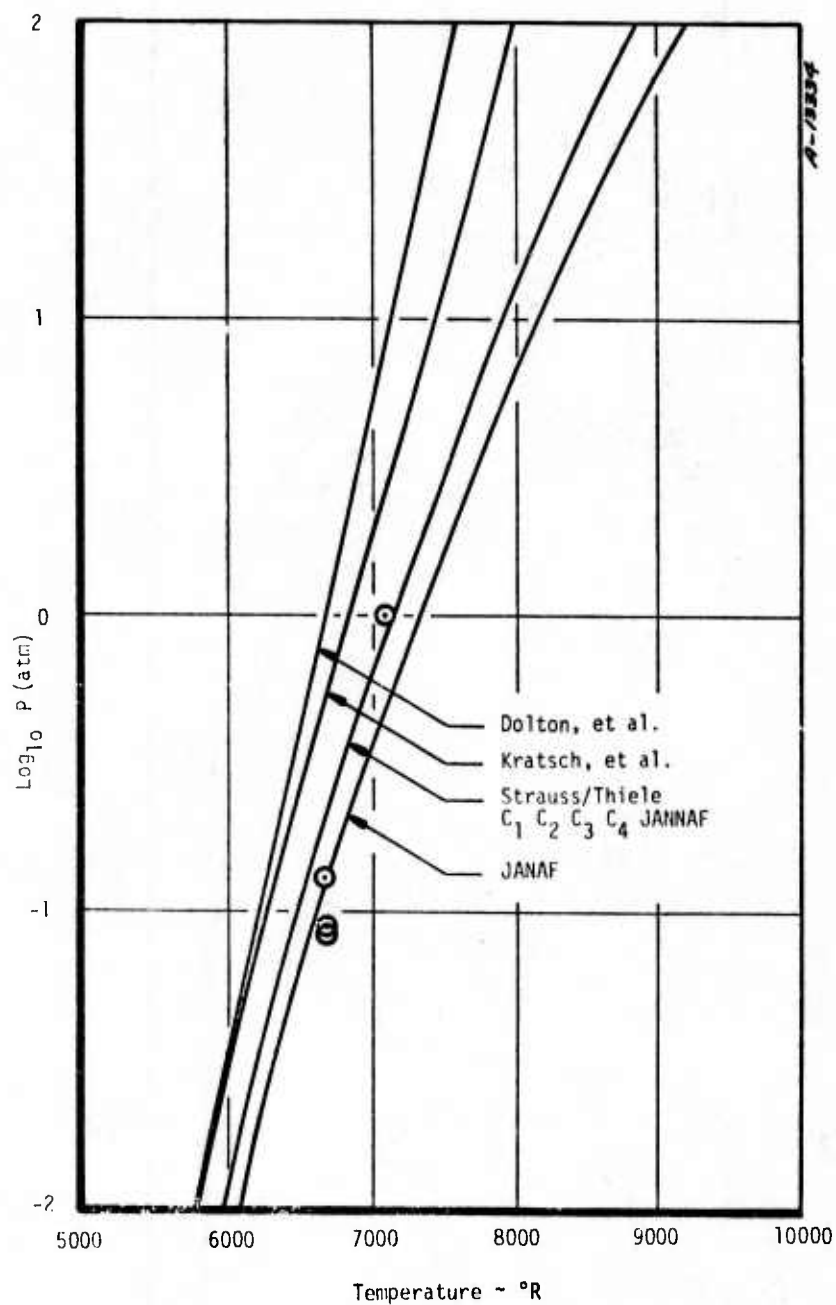


Figure 19. Comparison of phase equilibrium sublimation data with four carbon vapor thermochemical models.

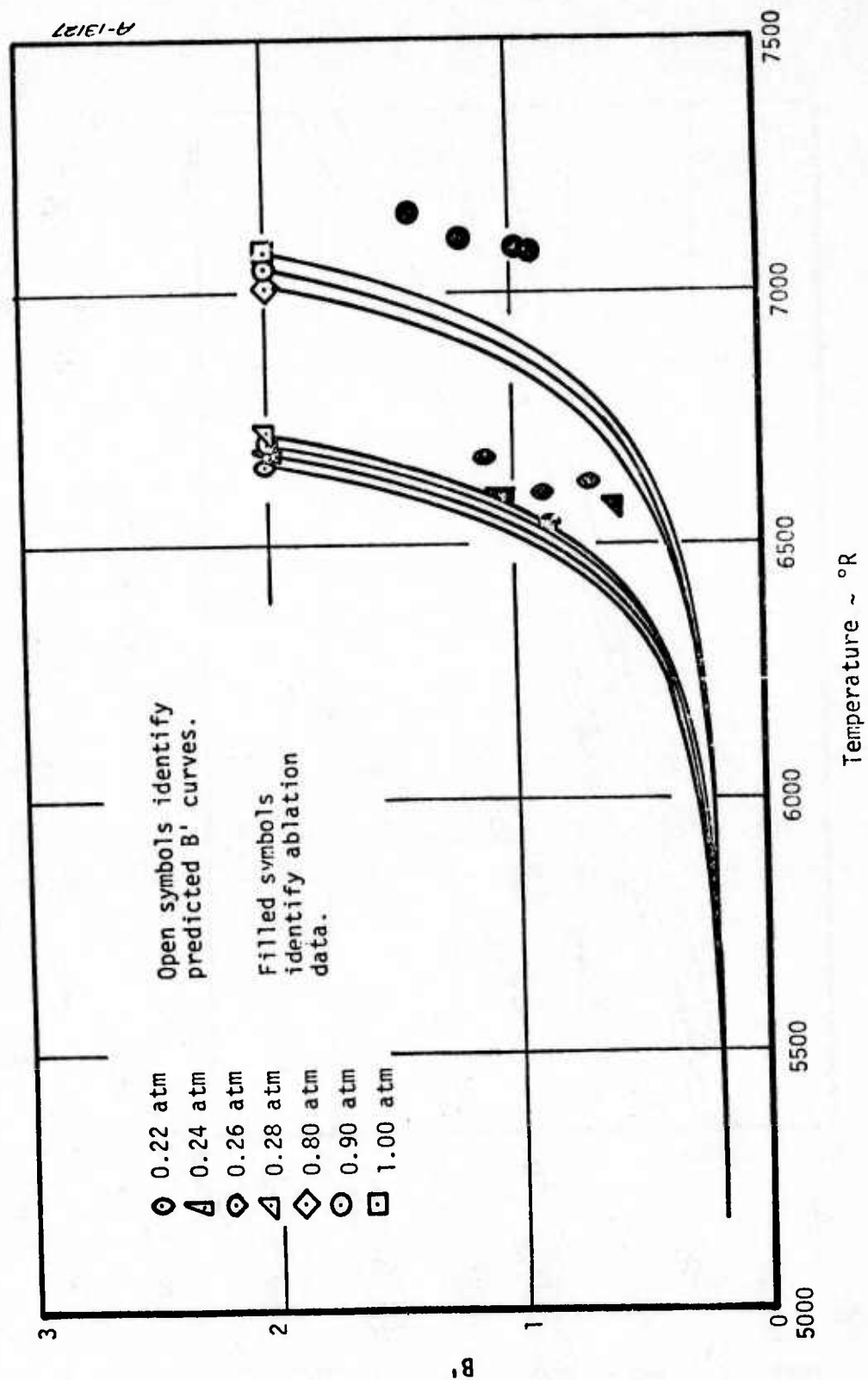


Figure 20. Comparison of ATJ-S ablation data from the AEHS test series with the JANAF equilibrium predictions.

pressures at the supersonic flow conditions for the low (~ 0.2 atmosphere) and moderate (~ 1 atmosphere) pressure tests are in the ranges 0.2 to 0.28 atmospheres and 0.8 to 0.9 atmospheres, respectively. Therefore theoretical B/ curves for these pressures are included in Figure 20 to afford a more accurate comparison.

Comparison of the high convective B' data with the JANAF equilibrium theory shows that the experimental data are consistently at slightly higher temperatures than the theoretical B' curves. Since the agreement between the equilibrium B' data (i.e., $B' \gg 1$) and the JANAF phase equilibrium is good the ablation data comparison in Figure 20 shows a slight, but consistent shift to higher ablation temperatures is occurring with increased heat and mass transfer rates.

Figure 21 shows plots of the temperature shift (defined as $T_s - T_{\text{JANAF}}$) as a function of $p_e u_e C_m$ for the low pressure tests. The results in Figure 21 show that, while the temperature data at a given mass transfer coefficient condition display only about a 2 percent scatter, the ΔT associated with this scatter is similar to the ΔT anticipated due to sublimation kinetics. This result makes firm conclusions regarding kinetic effects difficult. However, considering the low pressure data in Figure 21 in a statistical fashion, it is noted that there is an average temperature shift of about $+65^\circ\text{R}$ with increasing mass transfer coefficient. This average shift is about 30 percent of the predicted shift based on the vaporization coefficients recommended by Dolton, et al. (Reference 22), based on the work of Zavitsanos (Reference 7) for the $C_1 - C_5$ vapor species.

Figure 22 shows the surface temperature shifts at the high convective flow conditions measured from the average of the experimental "equilibrium" surface temperatures at the low pressure test conditions. Included in this figure are the predicted temperature shifts assuming unity vaporization coefficients for each of the carbon vapor species $C_1 - C_5$. It is interesting to note that the bulk of the data lie between the two sets of predictions. Lundell and Dickey (Reference 47) recently completed a graphite sublimation test program using high intensity (25 K watt) CO_2 laser radiation. To interpret their ablation results they assumed unity vaporization coefficients for the vapor species $C_1 - C_5$ which resulted in good agreement with predictions using the JANAF data. The results in Figure 22 show the unity vaporization coefficient kinetic sublimation predictions to be somewhat below the experimental data, but only about $10^\circ\text{R} - 15^\circ\text{R}$ below the average shift of about 65°R at a mass transfer rate of $\sim 0.1 \text{ lbm/ft}^2 \text{ sec}$.

The data plotted in Figure 23 from the moderate pressure tests also exhibit a positive temperature shift with increasing values of $p_e u_e C_m$. Interestingly the magnitude of the shift at these conditions ($P = 0.8$ to 1.0 atmospheres) is in the range 50°R to 150°R , somewhat lower than

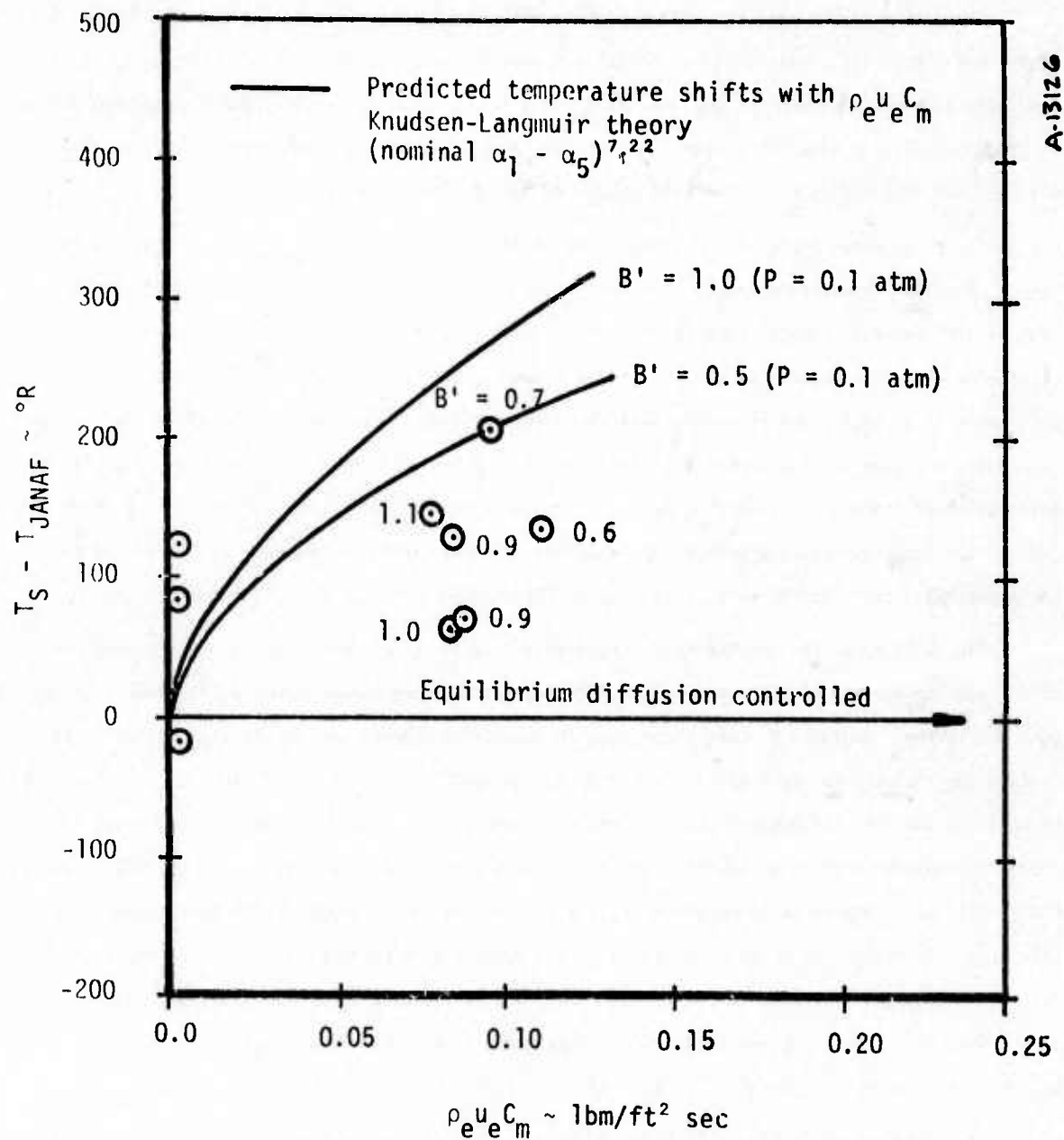


Figure 21. Measured temperature shift with $\rho_e u_e C_m$ for ATJ-S ablation tests in the pressure range of 0.1 to 0.3 atmospheres. (Referenced to theoretical equilibrium temperatures).

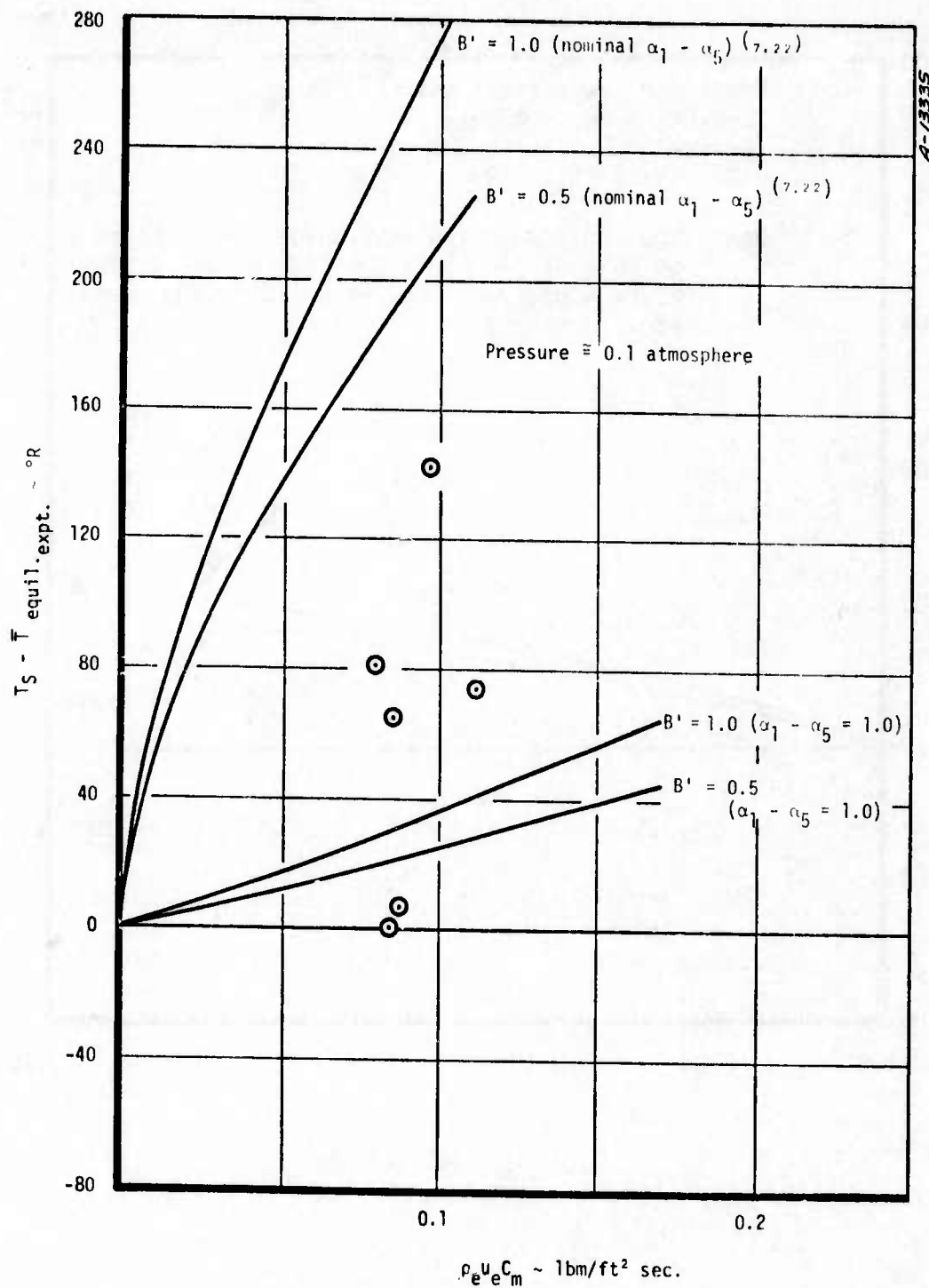


Figure 22. Measured temperature shift with $p_e u_e C_m$ referenced to experimental equilibrium graphite ablation temperatures in the pressure range 0.1 to 0.3 atmospheres.

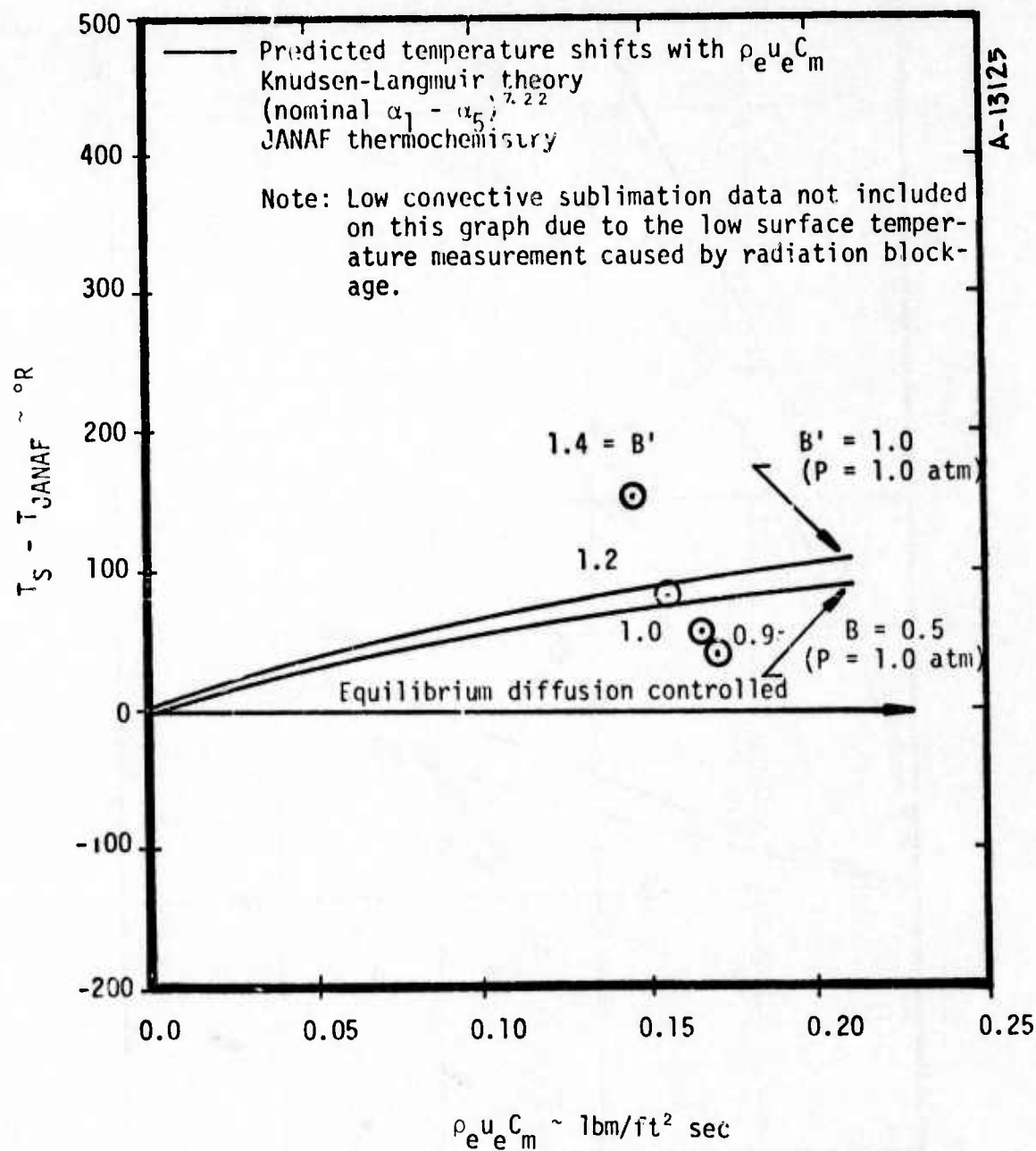


Figure 23. Measured temperature shift with $\rho_e u_e C_m$ for ATJ-S ablation tests in the pressure range 0.8 to 1.0 atmospheres. (Referenced to theoretical equilibrium temperatures).

the shifts at the low pressure test condition. This trend of a decreasing temperature shift with $p_e^{1/2} C_m$ with increasing pressure is in agreement with the Knudsen-Langmuir predictions.

Because the experimental "equilibrium" temperatures are felt to be low due to radiation blockage problems at the moderate pressure test conditions a temperature shift referenced to an average experimental "equilibrium" temperature is not possible. Thus, with the limited data at this condition one can only observe that the experimental shift (referenced to a theoretical equilibrium value) exhibits good agreement with the predicted temperature shift due to sublimation kinetics (assuming nominal vaporization coefficients for the species $C_1 - C_5$). It is important to note, however, that the temperature shifts at this moderate pressure condition are within the ± 2 percent uncertainty of the temperature data. Thus, it is not practical to draw any firm conclusions from the moderate pressure ablation data, despite the fact that the measured surface temperatures are consistently above equilibrium diffusion-controlled predictions.

SECTION 5

ABLATION DATA COMPARISON WITH PREVIOUSLY PUBLISHED RESULTS

This section compares the ATJ-S ablation data from this test series with the ablation data from previous investigations. The results of two ablation test programs, both conducted in the Ames AEHS facility are reviewed and ablation data comparisons made. Data from Wakefield and Petersons (Reference 48) tests of ATJ graphite in the AEHS facility are reviewed and compared with the low pressure supersonic flow ablation data from this series in Section 5.1. Oavy and Bar Nun (Reference 38) also studied graphite ablation under radiation only test conditions in the AEHS facility. Their test results are reviewed and ablation data comparisons made in Section 5.2. In addition, ATJ ablation data from the nominally one atmosphere ablation tests of Lundell and Oickey (Reference 24) which were conducted in the NASA-Ames Heat Transfer Tunnel are reviewed and compared with data selected from this program in Section 5.3.

5.1 WAKEFIELD AND PETERSON'S AEHS ABLATION TEST SERIES

Wakefield and Peterson's ablation tests of hemispherically tipped hollow ATJ graphite ablation models were similar to this test series with the following exceptions:

1. Wakefield and Peterson's ablation tests were limited to the 0.06 to 0.33 atmosphere supersonic flow regime.
2. The Linde arc heater was used in the AEHS facility instead of the constrictor heater used on this program.
3. The optical pyrometer used by Wakefield and Peterson was a monochromatic device (Thermodot TD-9) with a narrow bandpass filter centered at 0.8μ .

The difference between the optical pyrometers used on these two test series provides an interesting check on the accuracy of the pyrometer data from both test series. The response time of the TD-9 pyrometer is reported to be about 100 msec for a 30 percent full scale deflection. Thus one would not expect the pyrometer signal to respond to the 3 msec interval during which the incident radiation is blocked. (Interestingly, Wakefield and Peterson report that the component of reflected radiation is small as one would expect with the TD-9 response.) Results reported in Section 3.2.3

showed the Thermogage pyrometer recorded about a 200°R temperature drop during the 3 msec the incident radiation was blocked. One must consider, however that the optical sensitivity of the Thermogage covers a broader spectral range than that of the TD-9, thus its sensitivity to the reflected radiation is greater (note the spectral distribution of the AEHS radiation source in Figure 8). In addition to these differences in the optical pyrometers, Wakefield and Peterson corrected the measured brightness temperatures by assuming a surface emissivity of 0.9. This corresponds to an "actual" surface temperature about 130°R above the brightness ($\epsilon = 1.0$) temperature for these conditions. Wakefield and Peterson report a 3 percent uncertainty in the surface temperature data, which corresponds to about a 200°R uncertainty. A minimal amount of mass loss in the condensed phase was observed by Wakefield and Peterson, based on their interrogation of film data and observation of the post-test models.

The comparison between Wakefield and Peterson's results and the 0.22 to 0.28 atmosphere supersonic flow results from this test series compared in Figure 24 shows excellent agreement. The surface temperature data in Figure 24 exhibits agreement within $\pm 200^\circ\text{R}$ which is within the basic data uncertainty. Wakefield and Peterson compared their test data with ablation predictions based on JANAF thermochemistry for the carbon vapor species and found excellent agreement. This correlation, however did not conclusively establish the JANAF thermochemistry for the carbon vapor species as being correct, since the tests were conducted under relatively high heat and mass transfer rate conditions which could imply significant sublimation kinetic effects. The excellent corroboration between their ATJ ablation data and the ATJ-S data from this test series further substantiates the accuracy of the reduced data previously reviewed in Section 3.4.3.

5.2 DAVY AND BAR NUN'S AEHS ABLATION TEST SERIES

This ablation test series in the AEHS facility tested ATJ graphite models, in the form of solid 0.4 inch diameter right circular cylinders ~ 1.5 inch long. The ablation tests were radiation only tests in a cold argon environment. The test chamber environment was prepared for each test by pumping down to pressures of 1-10 μ for 10-20 minutes, purging the chamber with argon, and then filling with room temperature argon to the desired test pressure.

Davy and Bar Nun used the same Thermodot TQ-9 FH optical pyrometer as Wakefield and Peterson. During the test series they made both front and sideview readings of the ablating models at various times at comparable test conditions and observed no essential differences in the ablation temperature. They also reported that after the initial heating transient, the pyrometer signal reached a steady state condition in which the chopper modulation was only barely perceptible. This result is

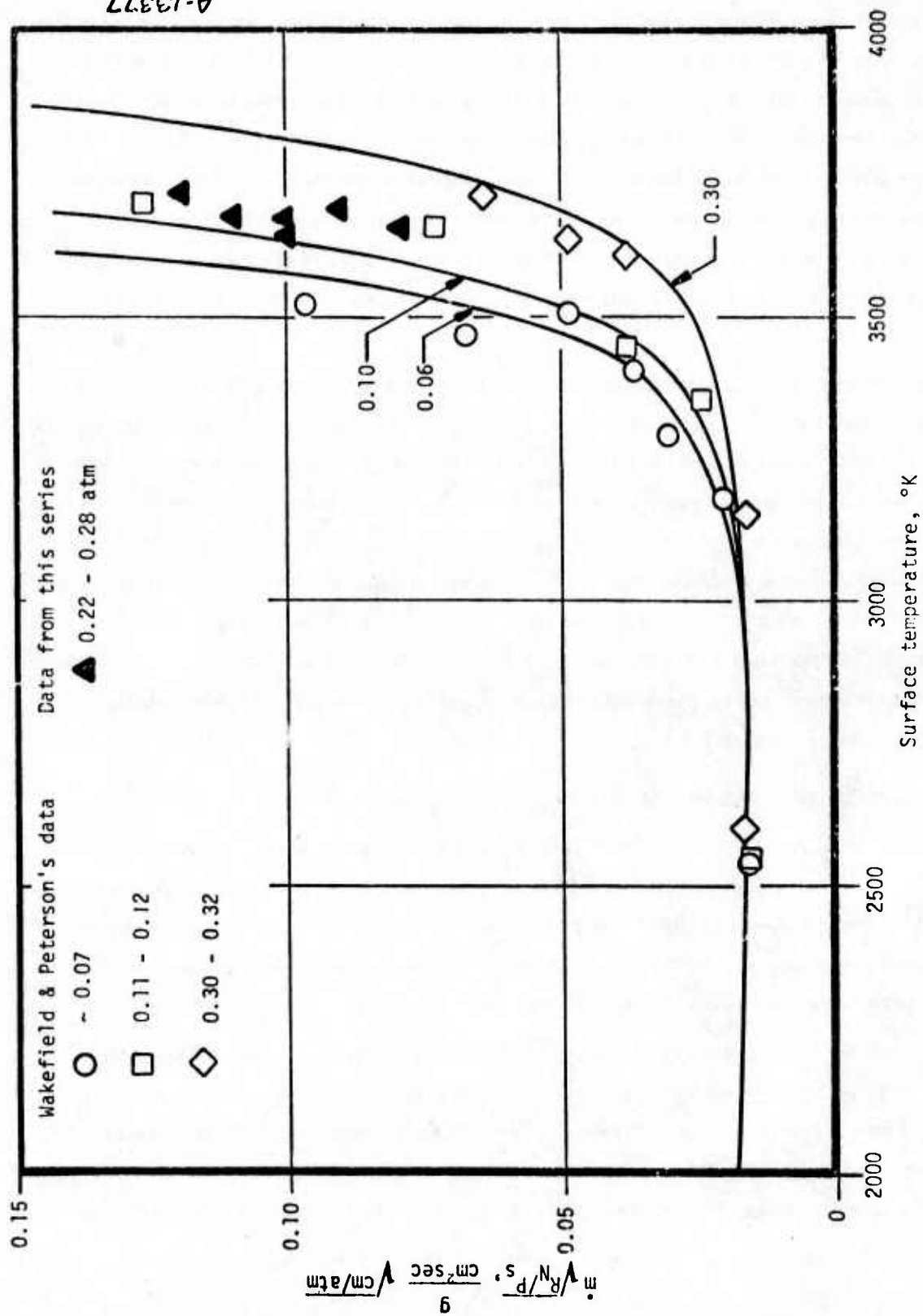


Figure 24. Comparison of Wakefield and Peterson's ablation data from the AEHS facility with ablation data from this series.

in good agreement with that reported by Wakefield and Peterson as would be expected. At pressures above 0.1 atmosphere slight temperature corrections were made due to soot blockage of the incident and emitted surface radiation. In the pressure range 0.1 to 0.3 atmospheres these soot corrections to the measured temperatures were less than 90°R. At the 1.0 atmosphere test condition the soot correction to the measured surface temperature was about 500°R.

The radiation only data from Davy and Bar Nun's ATJ ablation tests are compared with the low subsonic flow test data from this series in Figure 25. Davy and Bar Nun's data in Figure 25 are plotted using the soot corrected surface temperatures and the assumption that the equilibrium carbon vapor pressure is equivalent to the static chamber pressure. Despite Davy and Bar Nun's attempt to correct the measured temperatures (due to soot absorption) their data are consistently about 400°R below the data from this series. The high enthalpy low subsonic flow employed for these tests removed any potential soot film at the 0.2 to 0.3 atmosphere test conditions. At the 1.0 atmosphere test condition (cold subsonic argon flow) some blockage was felt to exist during these tests but no attempt was made to quantify this effect. Despite the fact that the measured surface temperature from this test series at the 1.0 atmosphere test condition is considered low, it is still about 400°R above the highest value reported by Davy and Bar Nun. One can only conclude from this comparison that the soot absorption which occurred due to the cold argon environment was underestimated. In addition, the blunt, solid ATJ graphite ablation models tested by Davy and Bar Nun provided a significantly higher capacitance than the models tested on this series. This difference would cause lower steady state ablation temperatures, which is substantiated by the fact that the mass loss rates reported by Davy and Bar Nun are about an order of magnitude lower than the data from this series.

Based on this ablation data comparison and differences in the two test techniques one can identify several reasons why the ablation temperatures measured by Davy and Bar Nun would be low. Therefore, the conclusions regarding the carbon vapor thermochemistry drawn by these researchers are highly suspect. There still remains the question regarding the degree of incident and emitted radiation blockage which occurred in this test series at the one atmosphere test condition. Suggestions as to possible test techniques available to further study this problem are reviewed in Section 8.

5.3 LUNDELL AND DICKEY'S ATJ ABLATION TEST SERIES

The ATJ ablation test series conducted by Lundell and Dickey (Reference 24) has become a classical reference within the carbon ablation community. This relatively extensive ablation test series covered the pressure range of 0.3 to 4.4 atmospheres and was conducted in the NASA Ames Heat

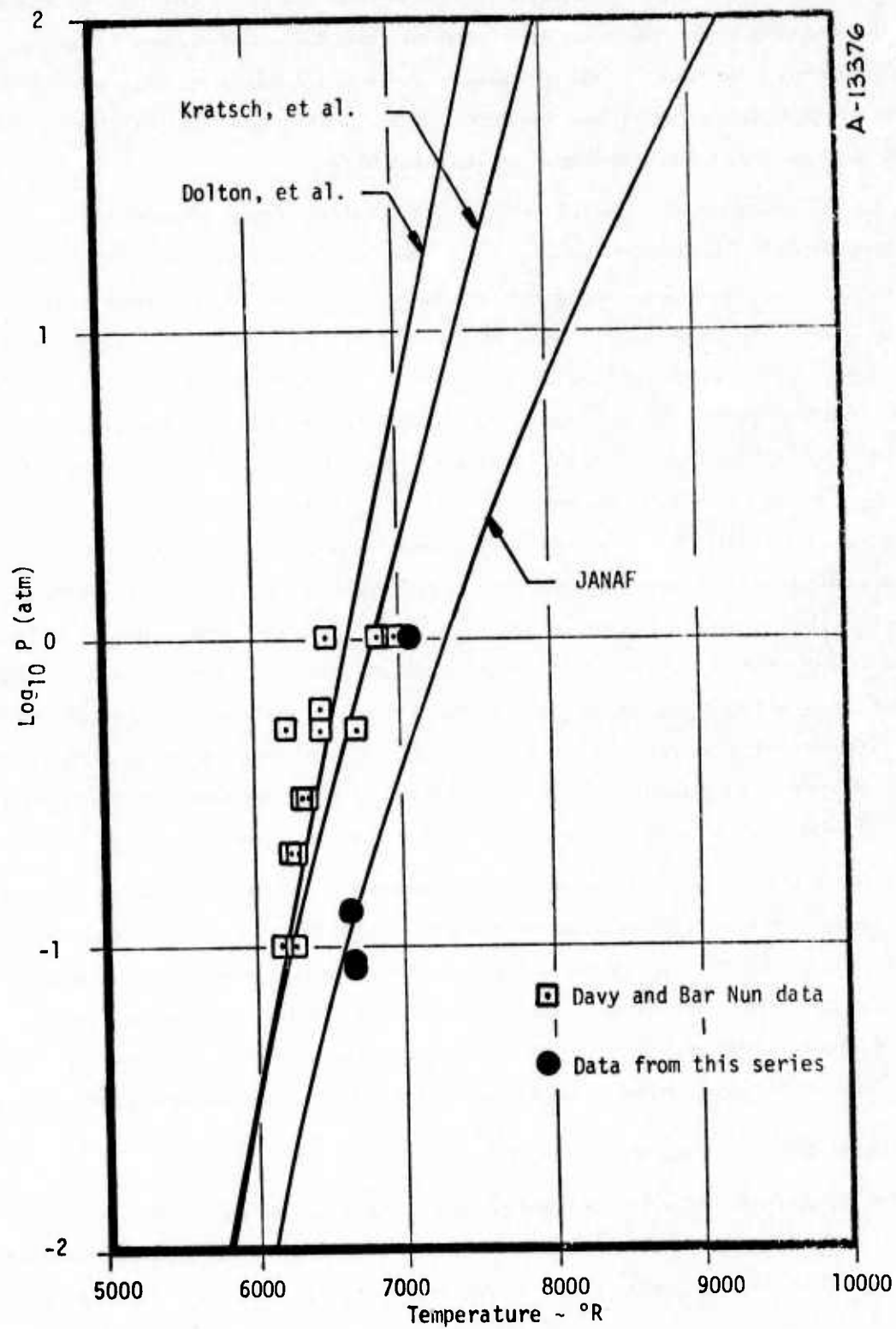


Figure 25. Comparison of phase equilibrium sublimation data from Davy and Bar Nun's tests with data from this series.

Transfer Tunnel. The intent of their test program was the generation of high quality ATJ ablation data in the sublimation regime. A further objective of their program was to determine if significant ablation mechanisms other than the classical thermochemical phenomena exist (e.g., particulate mass loss).

The Ames Heat Transfer Tunnel is a conventional arc-driven wind tunnel. For these tests a Linde arc heater (Model N4001) was used. The flow over the models varied from Mach 3.1 to 3.8. During a run as many as 18 separate support arms are available for insertion into the flow. Instrumentation inserted into the test stream during each run included calorimeters (both slug type and steady state) and pressure probes. Instrumentation external to the test chamber included optical pyrometers and a motion picture camera. Two pyrometers were used so that the monochromatic brightness temperature would be measured at two different wavelengths. The pyrometers used were a Thermodot Model TD-9 with a bandpass at 0.8μ and a Pyro 650 with a bandpass filter at 0.65μ . Both pyrometers were calibrated to 6100°R through use of a conventional disappearing-filament optical pyrometer.

Lundell and Dickey's ATJ ablation data at a nominal surface pressure of 1 atmosphere are shown in Figure 26. The raw ablation data were transformed into B' values through use of the following equations. The nondimensional mass transfer parameter B' is defined as, $B' = \dot{m}/\rho_e u_e C_H$ where:

$$\rho_e u_e C_{H_0} = 0.113 \sqrt{P_s/R_n} \quad \text{Reference 24}$$

and

$$C_H/C_{H_0} = \frac{1.48 B_0'}{(e^{1.4 B_0'} - 1)}$$

The nose radius (R_n) used in the expression for the convective heat transfer coefficient ($\rho_e u_e C_{H_0}$) was the effective value which Lundell evaluated and reported for each ablation model (based on the initial and final nose radius). Included in Figure 26 is the predicted JANAF equilibrium and kinetic sublimation B' curves. The agreement between the equilibrium prediction and the data is excellent. Also included in Figure 26 are the 1 atmosphere ablation data from this test series. These data are at B' values nearly a factor of two above the highest Lundell and Dickey value. This data comparison shows the measured ablation temperatures on this test series to be about 300°R above the values of Lundell and Dickey. The ablation data from this series exhibit good agreement with the kinetic sublimation prediction in Figure 26.

The convective flow environments over the models in both tests are extremely similar as shown by the data in Table 11.

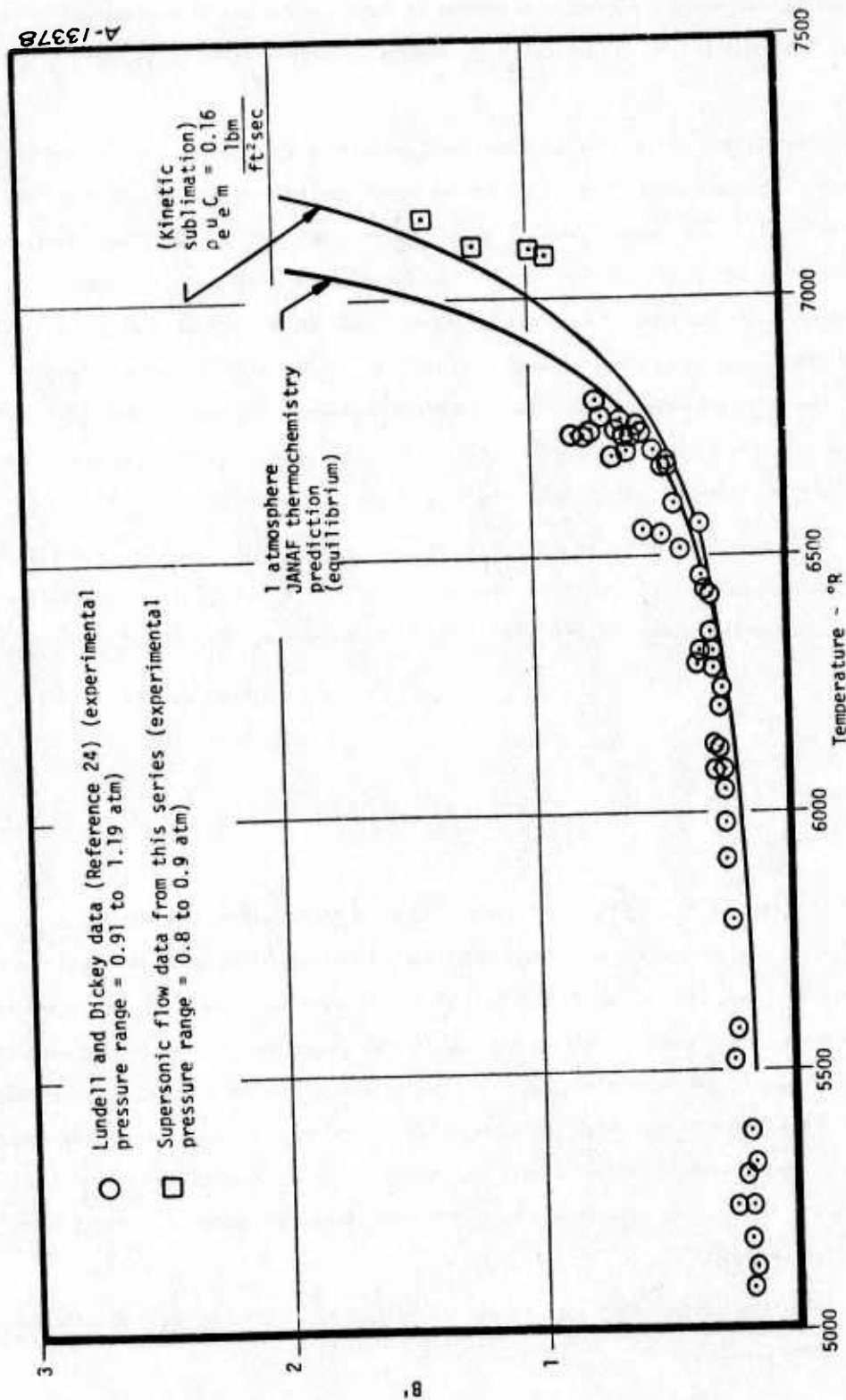


Figure 26. Comparison of ablation data from this series with the data of Lundell and Dickey.

TABLE 11. COMPARISON OF 1 ATMOSPHERE
SUPERSONIC FLOW CONVECTIVE
ENVIRONMENTAL PARAMETERS.

	This Series	Lundell & Dickey's Series
Gas	air	air
$H_c \left(\frac{\text{Btu}}{\text{lbm}} \right)$	~18,000	~17,000
Mach no.	~2.6	~3.5
Model size (in.)	D = 0.5	D = 0.6 to 1.2

The principal difference between the two test series results from the high radiant flux in the AEHS facility. The temperature data in Figure 26 from this test series have been corrected for the reflected component of the incident radiation. Similar ablation data from the low pressure (~0.1 atm.) supersonic flow condition were compared with the results of Wakefield and Peterson in Section 5.1 and shown to exhibit excellent agreement. Thus the data quality from this series is substantiated by these direct comparisons with other ablation data.

Lundell and Dickey did report a significant amount of particulate mass loss from their blunt cylindrical models. Although the cause of this particulate mass flux is not understood, the effect of particulate mass loss on the surface energy balance is to lower the ablation temperature. Therefore, the most probable explanation for the ~300°R surface temperature difference between these two sets of ablation data is the particulate mass loss which Lundell and Dickey observed from their models in the Ames Heat Transfer Tunnel. The data from this test series suggest negligible particulate mass loss occurred which corroborates well with the results of Wakefield and Peterson. The surfaces of the ablation models were all smooth indicative of no gross spallation and review of the high speed motion picture data showed virtually no particulate mass loss. The only particulate mass flux evident from the high speed film data occurred during Run 81 which was unique since cold argon was flowing over the radiatively heated ablation model. Close examination of this post-test model showed a rough irregular surface around the periphery of the front ablative surface where the particulate mass loss obviously occurred. In this rather singular case the severe thermal gradients in the region of the interface between the front ablating surface and the cooler cylindrical afterbody resulted in material spallation. A similar phenomenon, but less severe than this in Lundell and Dickey's ablation tests may have caused the rather significant particulate mass flux which they observed. Thus, the lack of agreement between these two sets of data is best rationalized by the particulate mass flux which was

observed to occur in the Ames Heat Transfer Tunnel ablation tests. It should be stressed, however that this is purely speculation and cannot be proven due to the lack of quantitative data from which the effect of the observed particulate mass loss can be quantified.

SECTION 6

IMPLICATIONS OF SUBLIMATION KINETICS ON HIGH PRESSURE ABLATION RESPONSE

The ATJ-S ablation data analyses in Section 4 show that the kinetic sublimation predictions (using the JANAF thermochemistry data and the vaporization coefficients of Zavitsanos (Reference 7) extended by Dolton, et al. (Reference 22)) slightly overpredict the measured temperature shifts from the theoretical equilibrium ablation temperatures. These analyses were restricted to the low and moderate pressure regime since the ablation data were restricted to this regime.

The intent of this section is to extrapolate these low and moderate pressure ablation results to the high pressure regime of interest. The kinetically controlled sublimation predictions are made using the JANAF thermochemical properties, the Knudsen-Langmuir kinetic model, and the vaporization coefficients of Zavitsanos (Reference 7) extended to C_4 and C_5 by Dolton, et al., (Reference 22). The thermochemical B' curves presented in this section were predicted with the modified version of the Aerotherm Chemical Equilibrium (ACE) computer code (Reference 35). The assessment of the high pressure sublimation kinetic effects are made for typical AFFDL 50 MW ablation environmental conditions and a typical flight environment. In addition, analyses are summarized which illustrate the sensitivity of kinetic sublimation predictions to the state of the carbon vapor species (i.e., whether frozen or equilibrium). In total, these analyses illustrate the potential effect of carbon sublimation uncertainties in the high pressure regime (i.e., $p > 10$ atm) as extrapolated from the low pressure ablation data from this program's AEHS facility test series.

The generalized kinetic sublimation predictions are reviewed in Section 6.1 where comparisons are made with the equilibrium predictions and the sensitivity of kinetic predictions to the carbon vapor state are studied. Results of analyses showing the effect of uncertainties in the carbon vapor state are reviewed in substantially more detail than the cursory review presented in Section 2.3.3. Section 6.2 then compares the effect of sublimation kinetics on the predicted ablation response of selected high pressure 50 MW ablation data and a typical reentry condition.

6.1 GENERALIZED KINETIC SUBLIMATION ABLATION PREDICTIONS

The kinetic sublimation predictions presented in this section are restricted to moderate and high pressures (i.e., 1 - 300 atm) since over 90 percent of nosetip recession generally occurs in this pressure regime. These predictions are designed to answer the question: "What is the most probable effect of carbon sublimation kinetics on the predicted ablation response for current environmental conditions of interest?"

Results of these calculations in the form of $B'/\text{temperature}$ plots are shown in Figure 27. Pressures from 1 to 300 atmospheres and mass transfer coefficients covering the range of 0.1 to 10 $\text{lbm}/\text{ft}^2\text{sec}$ were assumed to generate these results. The carbon vapor species were assumed to be either frozen (as was assumed in Section 4) or to equilibrate in the vapor state. The frozen vapor predictions are used for comparison, however since this assumption maximizes the shift from the equilibrium diffusion controlled ablation state.

It is clear from these results that at high pressure ablation conditions of interest (i.e., $P_{t2} > 50$ atmospheres) the uncertainty in the surface temperature resulting from an uncertainty in the sublimation response of carbon is probably below 100°R (based on an extrapolation of the data analyses in Section 4 and the high pressure predictions shown in Figure 27).

Not only does the kinetic sublimation response of graphitic materials present an uncertainty in ablation predictions (although the results in Section 4 put a bound on the kinetic effects) but the state of the carbon vapor species at the surface continues to be uncertain as discussed in Section 2. Early kinetic sublimation models assumed the carbon vapor species to be frozen. More recent kinetic sublimation models have assumed the carbon vapor to be in equilibrium. A direct comparison of these two assumptions has been made to assess the effect of the carbon vapor chemical state on the predicted ablation response. These results are shown in Figure 27. The comparison is made for a mass transfer coefficient of 10 $\text{lbm}/\text{ft}^2\text{sec}$ since sublimation kinetic effects are greatest at high mass transfer conditions.

The significance of the assumed carbon vapor state increases with temperature and pressure. Little difference exists between the equilibrium and frozen carbon vapor solutions at 1 atmosphere, whereas at 300 atmospheres the equilibrium vapor case corresponds more closely to the equilibrium/diffusion controlled solution than the kinetic sublimation/frozen vapor solution. This results for the following reasons. When the vapor state is frozen each kinetic reaction controls a portion of the total sublimation response. However, when the vapor species can equilibrate the sublimation response becomes controlled by only the fastest kinetic reaction. This shift is maximized at high pressures because of the increased significance of the higher order vapor species (e.g., C_5) which has an

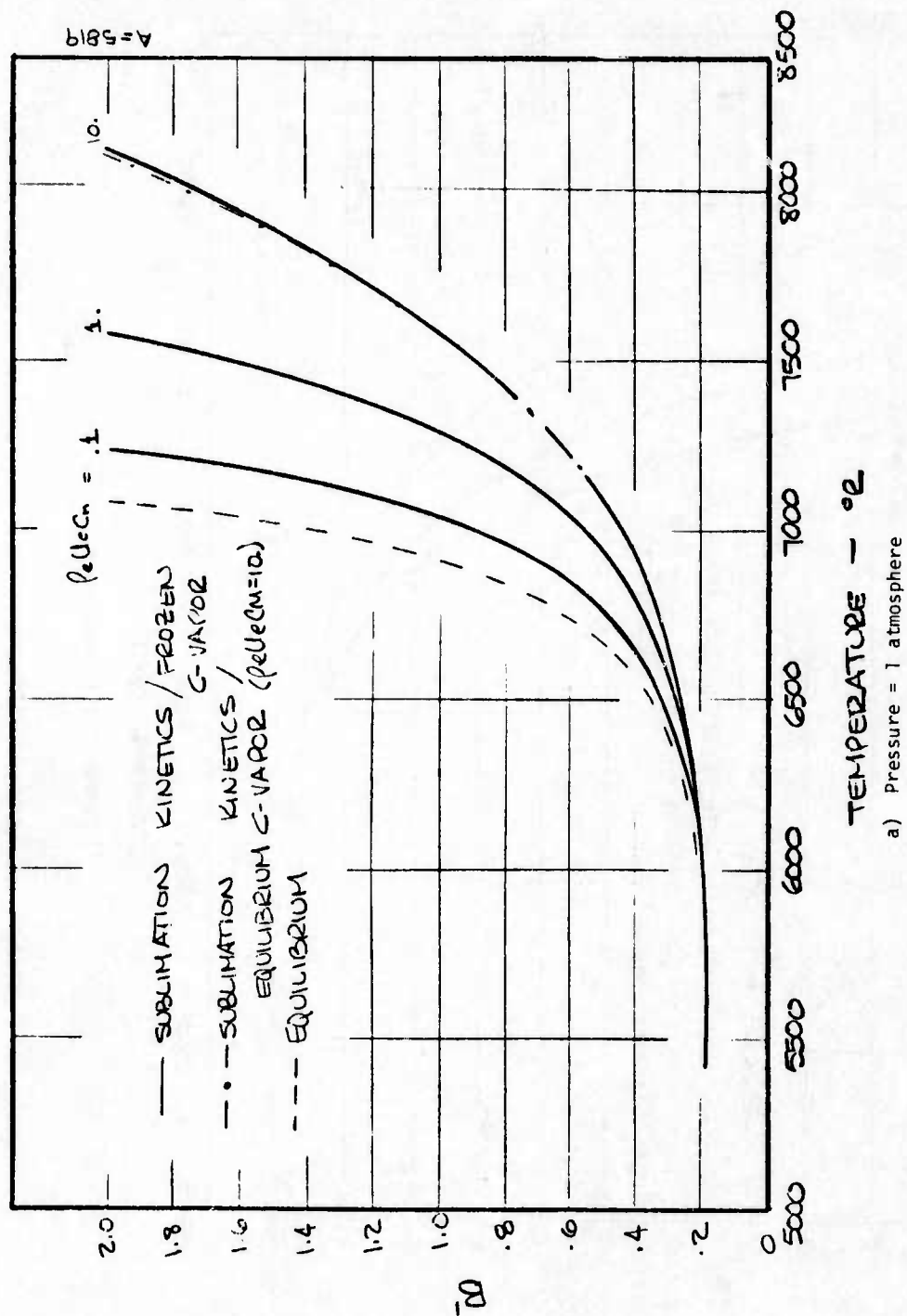


Figure 27. Mass transfer predictions for graphite ablation in air assuming equilibrium and frozen carbon vapor species with kinetically controlled sublimation.

a) Pressure = 1 atmosphere

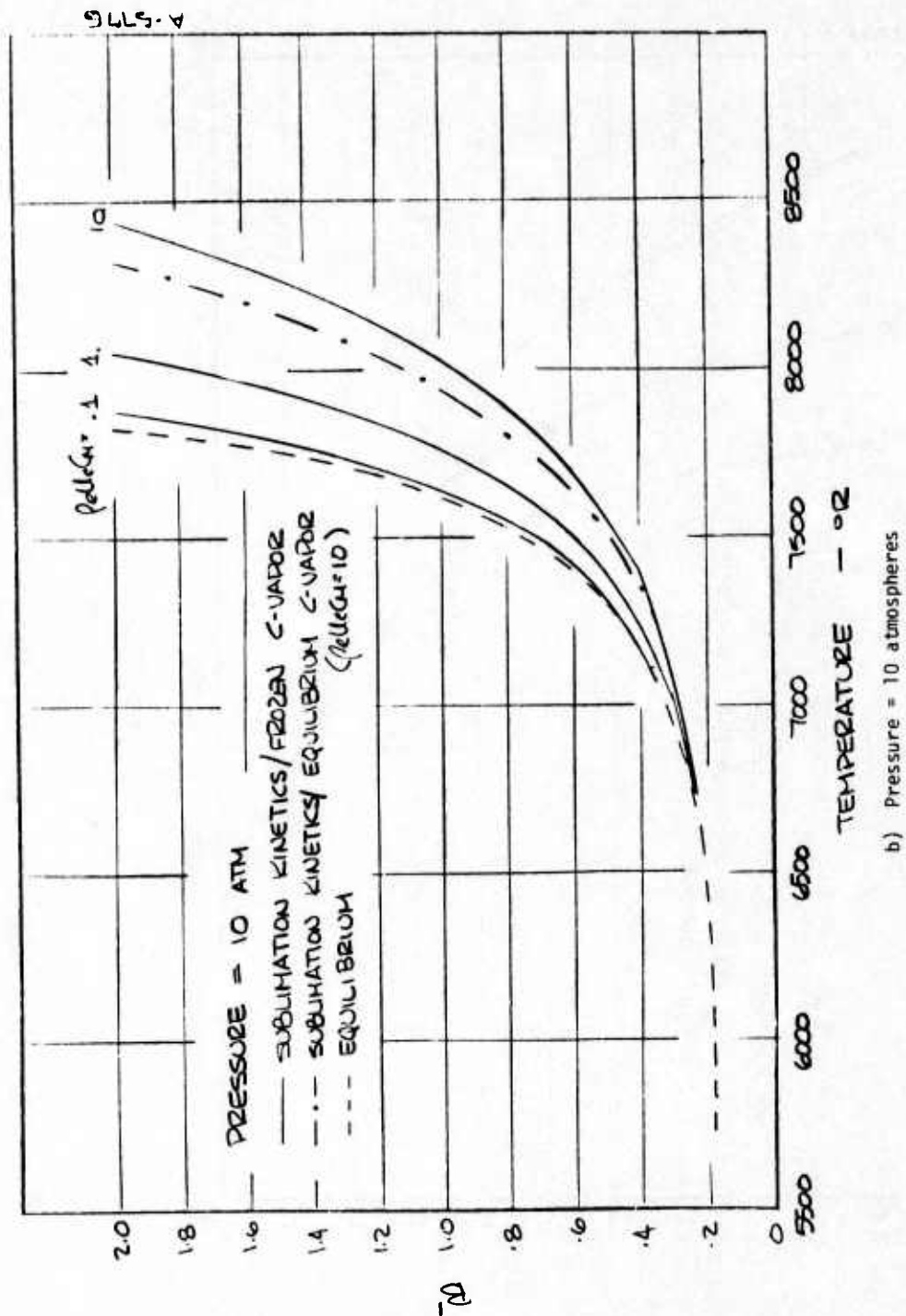


Figure 27. Continued.

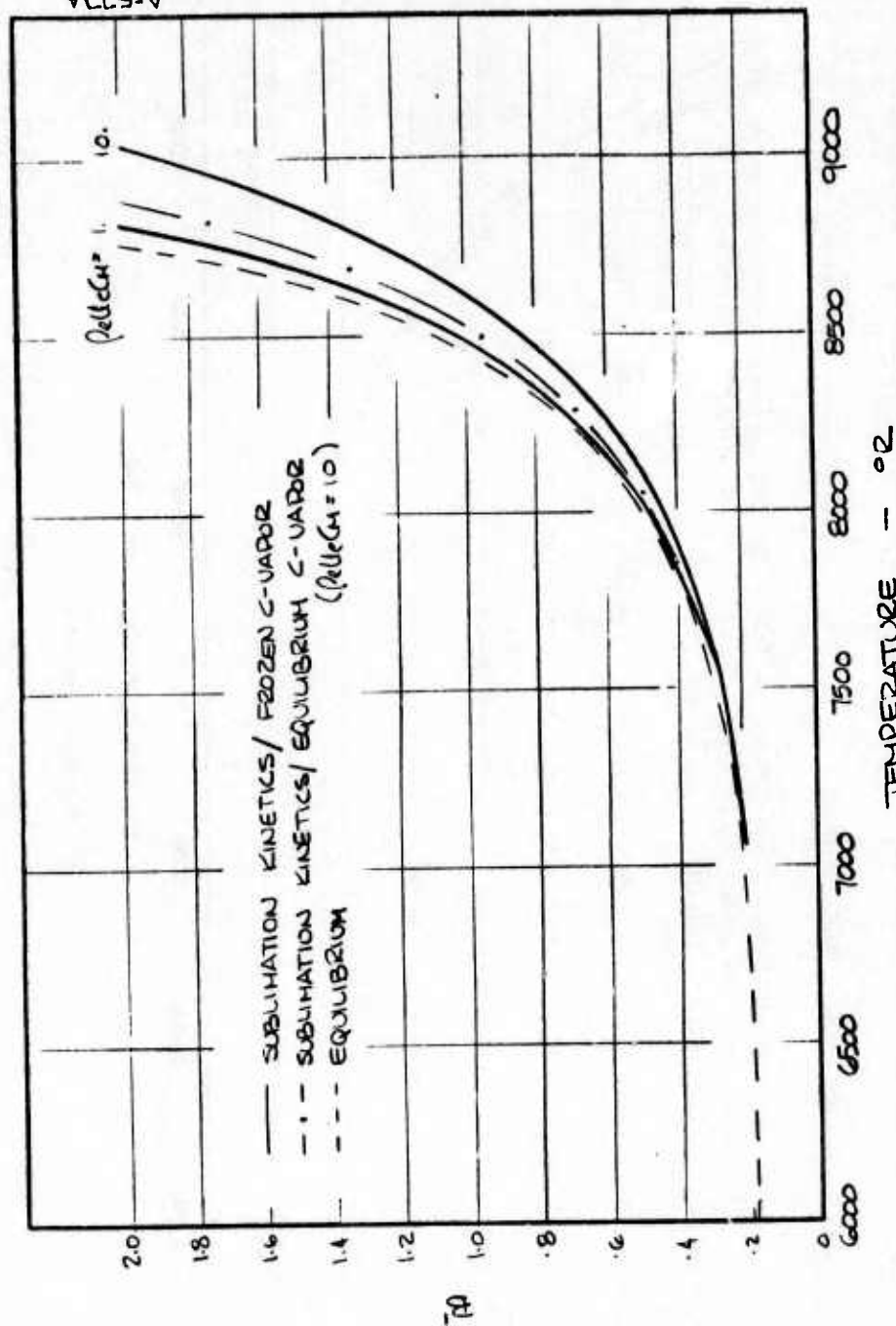
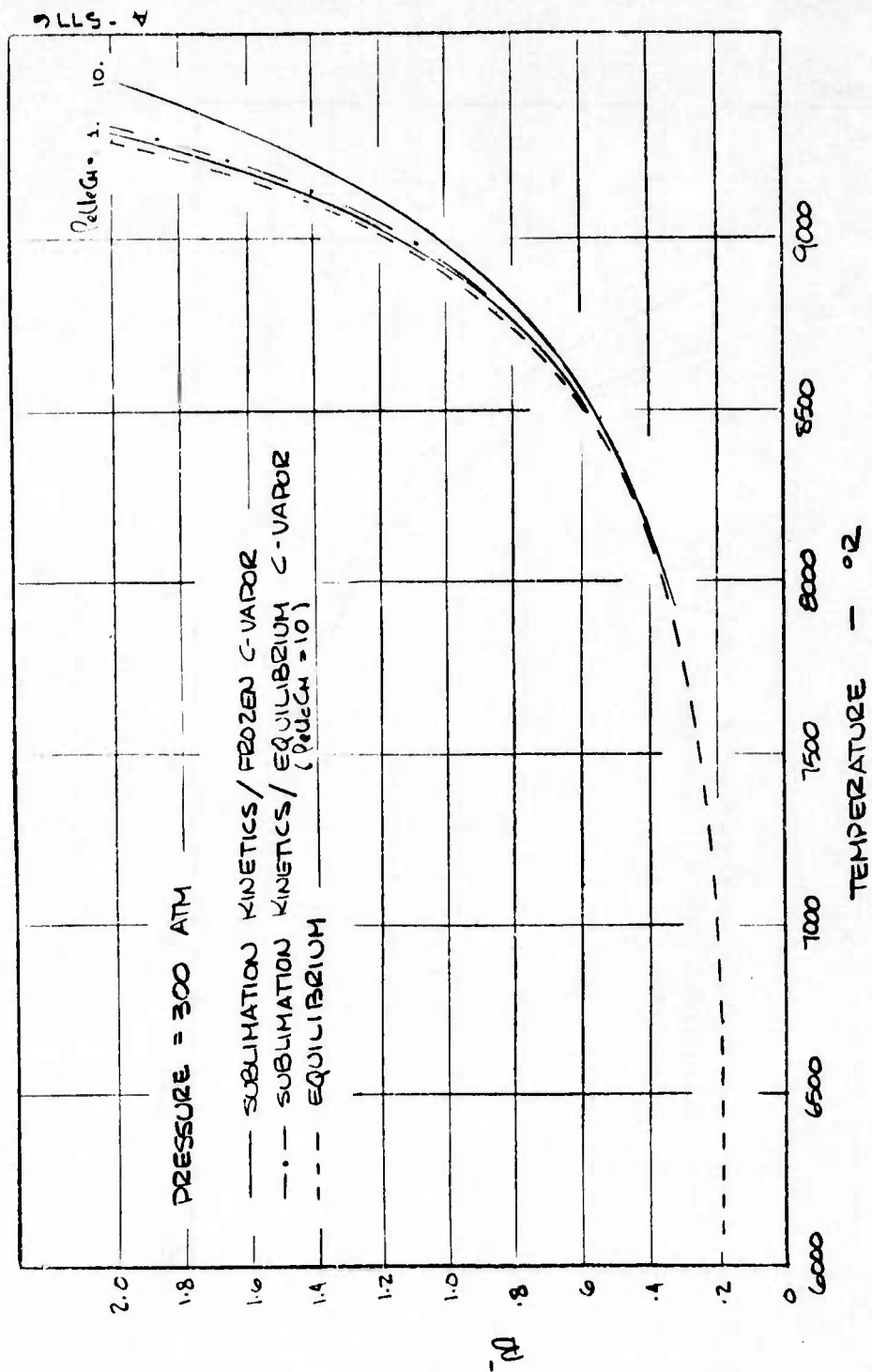


Figure 27 Continued



d) Pressure = 300 atmospheres

Figure 27. Concluded.

extremely small vaporization coefficient. Thus, when the vapor is frozen, kinetic sublimation of C_5 is greatly restricted. Conversely, when the vapor can equilibrate the partial pressure potential of the faster sublimation reactions is increased due to the gas phase reactions which increase the concentration of those vapor species restricted by their slow sublimation rates (i.e., C_3 and C_5) while reducing the concentration of the faster subliming species (i.e., C_2).

This is readily shown by the predicted ablation data summarized in Table 12. At the 300 atmosphere condition the kinetic sublimation rates of C_2 and C_3 change by factors of 5 and 1/3 respectively when shifting from an assumed frozen to equilibrium vapor at the surface. Thus, the equilibrium vapor assumption causes the C_2 concentration to be reduced while the C_3 and C_5 concentrations are substantially increased (particularly at higher temperatures). For this reason, kinetic sublimation predictions based on an assumed equilibrium carbon vapor at the surface are shifted back toward the equilibrium/diffusion controlled predictions as the temperature increases (i.e., higher pressures).

Relating this result to the ablation data generated in this program in a precise quantitative manner is not possible. However, the data analyses in Section 4 show a consistent shift to temperatures above the equilibrium diffusion controlled temperature predictions under high heat and mass transfer conditions. The data from this program however are insufficient to back out either vaporization coefficients or to assess whether the carbon vapor species are frozen or chemically equilibrate. The data suggests an upper bound of these chemical kinetic effects and this is evaluated in the next section.

6.2 KINETIC SUBLIMATION PREDICTIONS APPLIED TO 50 MW ABLATION DATA AND FLIGHT

To quantitatively assess the effects of sublimation kinetics on the predicted ablation response of graphitic materials, kinetic predictions were compared with equilibrium/diffusion controlled predictions of recent 50 MW ATJ-S and C/C tests. The kinetic predictions assumed a frozen carbon vapor in order to maximize kinetic effects. Only the high pressure turbulent tests were analyzed since the ablation response and temperature measurements are both definitely steady state and easily related to the ablation model due to the turbulent biconic shape which develops. Rough wall heating, based on a micro roughness height of 1 mil were assumed for these analyses. The correction factor (K_r) to the smooth wall heat and mass transfer coefficient was based on the correlation of Powars (Reference 49).

The kinetic and equilibrium/diffusion controlled predictions are compared in Figure 2B. Both sublimation modeling techniques are seen to predict the measured ablation temperature within a $\pm 200^\circ R$ (i.e., ± 2.5 percent) uncertainty band. Kinetically controlled sublimation predicts ablation temperatures about $45^\circ R$ (0.5 percent) above the diffusion controlled values. The decrease in the predicted recession rate with sublimation kinetics is less than 2 percent for the test conditions.

TABLE 12. SENSITIVITY OF CARBON VAPOR SPECIES CONCENTRATIONS AND SUBLIMATION RATES WITH THE ASSUMED CARBON VAPOR STATE AND WITH PRESSURE.

Pressure - 1 atm
T = 7605°R

	State of Carbon Vapor	
	Frozen	Equilibrium
B'_{C_1}	.02722	.0186
B'_{C_2}	.11756	.13784
B'_{C_3}	.04481	.04408
B'_{C_4}	.00801	.00877
B'_{C_5}	.00017	.00017
$\sum_{j=1}^5 B'_{C_j}$.1978	.2136
B'_{total}	1.0	1.018

Species	Mole Fraction	
	State of Carbon Vapor	
	Frozen	Equilibrium
C_1	.3387-1	.6204-1
C_2	.7205-1	.2929-1
C_3	.1856-1	.4663-1
C_4	.2515-2	.2172-3
C_5	.6771-4	.1502-3
CN	.2259	.2205
C_2N	.2694	.2669
C_2N_2	.4516-2	.4432-2
C_4N_2	.1280-2	.1256-2
CO	.2181	.2153

Pressure - 300 atm
T = 8993°R

	State of Carbon Vapor	
	Frozen	Equilibrium
B'_{C_1}	.0112	.0186
B'_{C_2}	.0553	.2689
B'_{C_3}	.2510	.0896
B'_{C_4}	.0145	.0508
B'_{C_5}	.0079	.0013
$\sum_{j=1}^5 B'_{C_j}$.3399	.4292
B'_{total}	1.0	1.094

	Mole Fraction	
	State of Carbon Vapor	
	Frozen	Equilibrium
C_1	.1507-1	.1490-1
C_2	.3707-1	.3544-1
C_3	.1120	.1331
C_4	.4871-2	.4489-2
C_5	.2139-2	.1032-1
CN	.1035	.1012
C_2N	.2046	.2002
C_2N_2	.2655-1	.2542-1
C_4N_2	.1990-1	.1905-1
CO	.2342	.2259

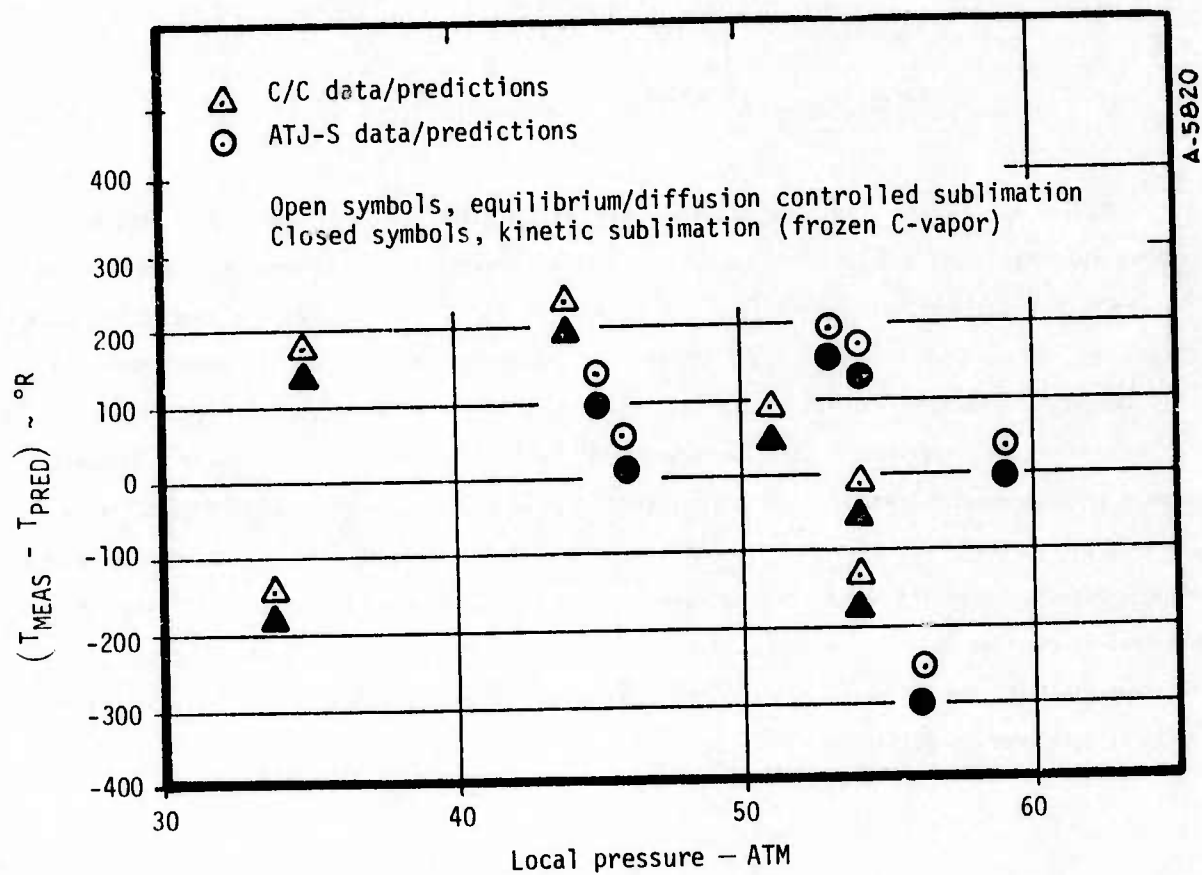


Figure 28. Effect of sublimation kinetics on predicted graphite ablation temperatures in the 50 MW arc.

Table 13 compares the surface ablation states predicted for flight conditions assuming both equilibrium and kinetically controlled sublimation. The entry environmental parameters assumed for these analyses correspond to a high ballistic coefficient reentry configuration which has developed a fully turbulent biconic shape. The static pressure on the biconic surface was assumed to be 100 atmospheres. The blown value of the convective heat and mass transfer coefficient was assumed to be 6 lbm/ft² sec. The total enthalpy assumed for the reentry condition was 10,000 Btu/lbm.

TABLE 13. COMPARISON OF EQUILIBRIUM AND KINETICALLY CONTROLLED SUBLIMATION PREDICTIONS FOR A TYPICAL HIGH β HIGH REENTRY CONDITION

Sublimation Model	T_w ($^{\circ}$ R)	\dot{S} (in/sec)	% ΔT_w	% $\Delta \dot{S}$
Equilibrium	8285	.459	—	—
Kinetic	8320	.457	.42%	-.44%

Both of these analyses demonstrate that the effects of sublimation kinetics (assuming the physics are as modeled) are small (slightly less than 0.5 percent for both temperature and recession) for the high pressure ablation conditions considered. The ATJ-S ablation data analyses in Section 4 showed that the measured effects of sublimation kinetics were no greater than the predictions, using this same model. Thus, extrapolating the low and moderate pressure ablation data from this program to the high pressure regime in this manner shows that the existence or non-existence of sublimation kinetic effects could not be inferred from ablation data at these high pressure conditions (since the data uncertainty is greater than the anticipated magnitude of the effect). Also, if sublimation kinetic effects are of the magnitude calculated here, and if there are no "secondary effects" of sublimation kinetics (e.g., increased particulate mass loss), then for engineering purposes, sublimation kinetics need not be included in the modeling of the ablation response of graphitic materials at high pressure conditions.

SECTION 7

CONCLUSIONS

Conclusions regarding the thermochemical sublimation response of ATJ-S graphite derived from high temperature ablation tests under low and high mass transfer environments in the NASA Ames AEHS facility are summarized below.

1. The variable velocity flow (subsonic to supersonic) test procedure designed for the NASA Ames AEHS facility proved to be a viable test technique for studying the detailed thermochemistry of graphite sublimation in the low to moderate pressure regime.
2. The high B' , low $\rho_e u_e C_M$ equilibrium data generated on this program exhibit very good agreement with the carbon vapor pressure curve predicted by the JANAF thermochemical data for carbon vapor species C_1 through C_5 .
3. The ablation data generated on this program displayed, on the average, an increasing shift in surface temperature above the theoretical (JANAF) equilibrium value with increasing convective mass transfer coefficient. This shift is in the direction to substantiate that the graphite ablation rate is being partially controlled by sublimation kinetics.
4. The measured temperature shifts with increasing mass transfer coefficient were relatively small. At the low pressure condition (0.22 to 0.28 atm.), the average shift in $T_{\text{measured}} - T_{\text{JANAF}}$ was about 150°R as $\rho_e u_e C_M$ increased from near zero to 0.08 - 0.11 lbm/ft²sec. The shift predicted using the kinetic sublimation coefficients reported by Zavitsanos as extended by Dolton, et al., for these conditions is $\sim 200^\circ\text{R}$. Thus, it may be concluded that graphite sublimation kinetics effects in the moderate pressure regime are probably no greater than predicted by Dolton, et al.
5. While the surface temperature measurements were judged to be quite accurate (± 2 percent) the temperature data scatter on an absolute scale was about 100°R which is similar to the measured temperature shifts. Thus, the data are felt to be too imprecise to "back out" quantitative sublimation coefficients or to determine the thermodynamic state of the carbon vapor near the surface (i.e., equilibrium or frozen).

6. Based on the results of this program, the most appropriate thermochemical model for graphite nosetip flight performance predictions is equilibrium diffusion controlled ablation using the JANAF thermochemical data.

SECTION 8

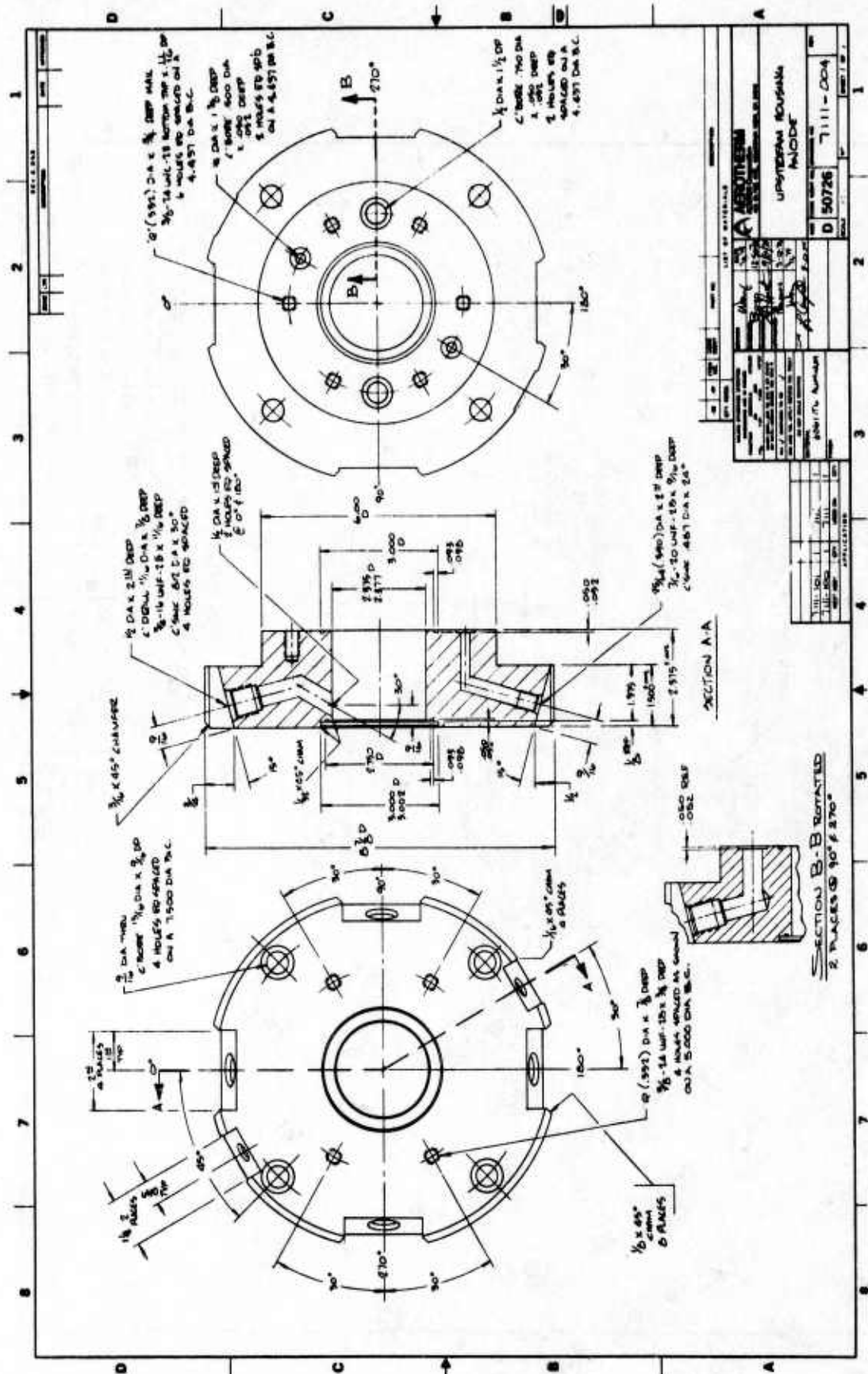
RECOMMENDATIONS

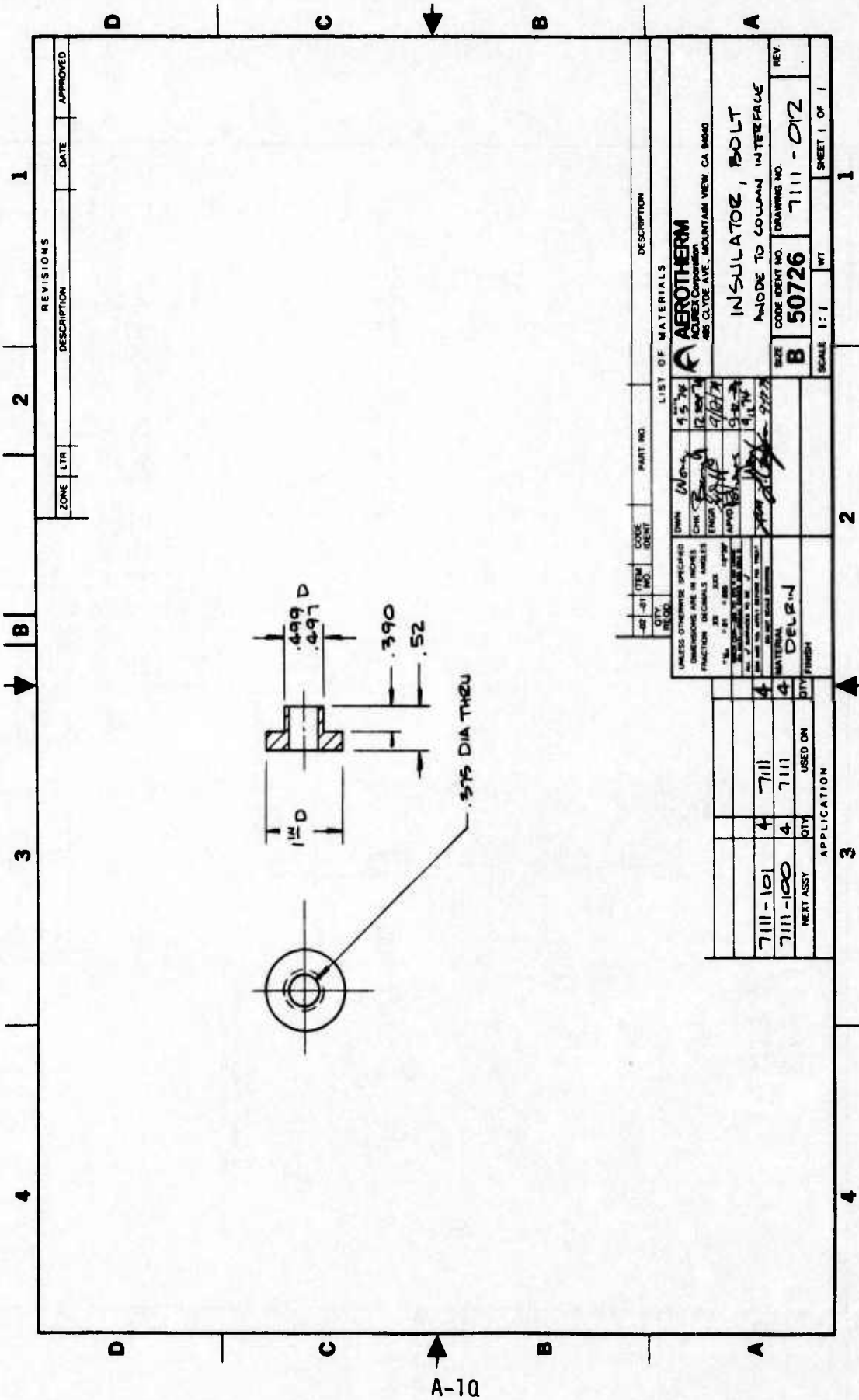
The recommendations for further studies of the thermochemical ablation response of graphitic materials address two areas of the problem. The first addresses the more detailed thermochemical events which control graphite sublimation in air (much in the same manner as this program did). The second is a more practical extension of the work of Lundell and Dickey (References 24 and 25) to the higher pressure regime of interest for reentry. Both recommendations are listed below.

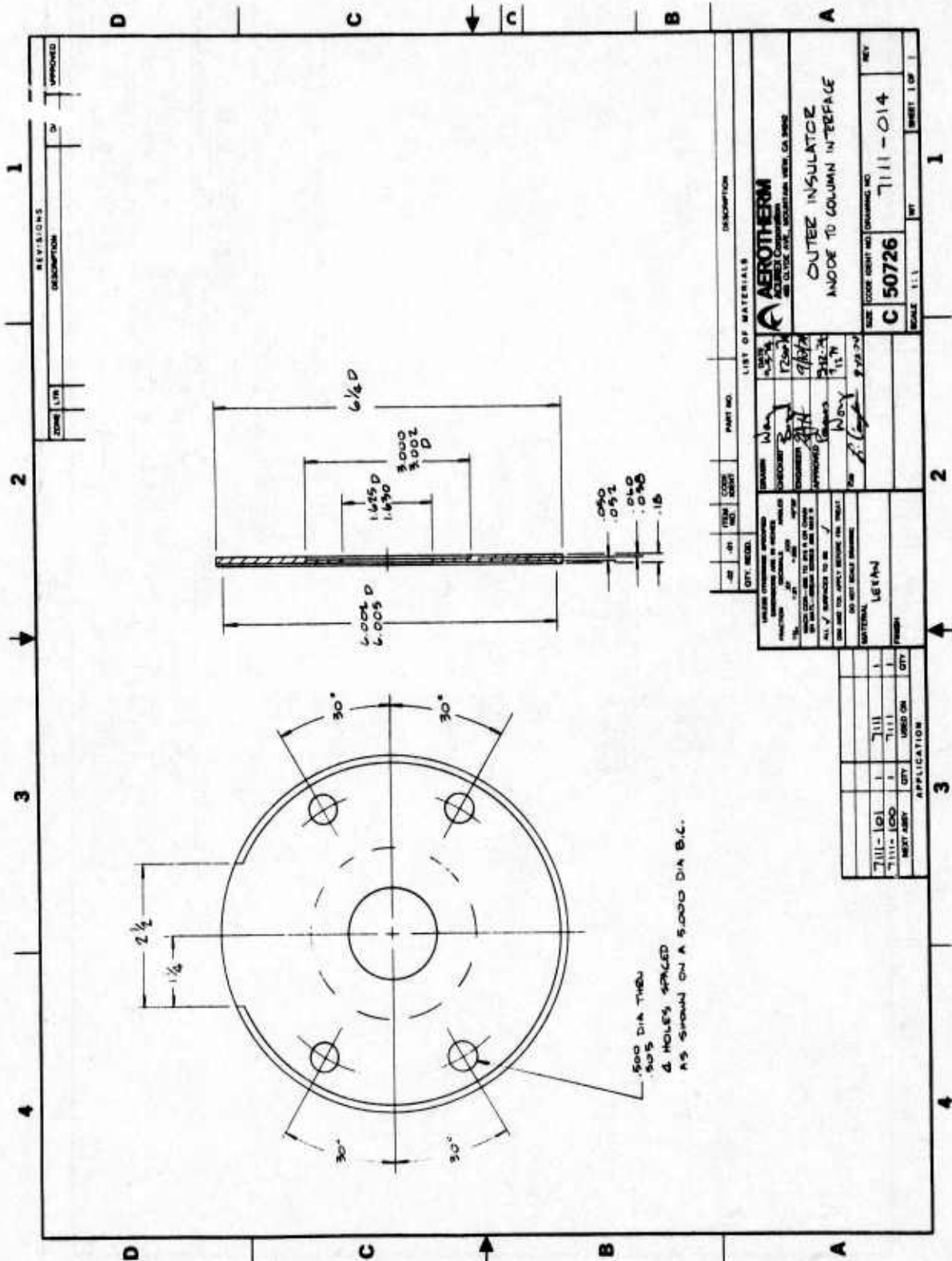
1. The work accomplished on this program has established the AEHS ablation test facility as a useful tool for studying graphite sublimation under low and high mass transfer environments. The test techniques have been established and thoroughly checked out. The data base established on this program, however, is not sufficient for meaningful statistical analyses. Additional ablation testing in the AEHS facility is recommended to provide the data necessary for more quantitative conclusions to be drawn.
2. During the course of this program a study was conducted to assess the capability of existing high pressure ablation test facilities with respect to successfully conducting graphite sublimation tests in the 20 to 40 atmosphere pressure range. Results of this study are documented in References 50 and 51. These studies showed that all existing facilities were inadequate in this regard, due mainly to enthalpy limitations which restrict the achievable B' levels. However, there are currently two arc heaters under construction which may have the requisite pressure and enthalpy capabilities to study graphite sublimation at these higher pressures; these are the KBC-100 arc at AFFDL and the HEAT arc at AEDC. It is recommended that if the required enthalpy levels are demonstrated in either of these facilities then moderate to high pressure graphite vaporization tests should be conducted. These data would serve to extend the results of Lundell and Dickey to higher pressures and would have very practical implications on graphite ablation thermochemistry in the range of interest for flight nosetip ablation predictions.

APPENDIX A

DESIGN DETAILS OF AEHS
CONSTRUCTOR ARC MODIFICATIONS



[illegible]



REVISED		DESCRIPTION		APPROVED	
DATE	BY	DATE	BY	DATE	BY

QTY.	RECD.	DATE	QTY.	RECD.	DATE	QTY.	RECD.	DATE	QTY.	RECD.	DATE

LIST OF MATERIALS		PART NO.		DESCRIPTION	
QTY. <td>RECD. <td>DATE <td>QTY. <td>RECD. <td>DATE</td> </td></td></td></td>	RECD. <td>DATE <td>QTY. <td>RECD. <td>DATE</td> </td></td></td>	DATE <td>QTY. <td>RECD. <td>DATE</td> </td></td>	QTY. <td>RECD. <td>DATE</td> </td>	RECD. <td>DATE</td>	DATE

AEROTHERM		AEROTHERM		AEROTHERM	
AEROTHERM		AEROTHERM		AEROTHERM	
AEROTHERM		AEROTHERM		AEROTHERM	
OUTER INSULATOR					
ANODE TO COLUMN INTERFACE					
KEY					
C 50726					
7111-014					
SCALE 1:1					
SHEET 1 OF 1					

APPLICATION		QTY.		QTY.	
7111-101	1	7111	1	7111	1
7111-100	1	7111	1	7111	1
MST ARRY	1	7111	1	7111	1

APPENDIX B

COMPLETE DATA SET FROM CALIBRATION AND
ATJ-S ABLATION TESTS IN THE NASA AMES ACHS FACILITY

TABLE B-1. AEHS ATJ-S ABLATION TEST DATA

Test Model Number	Date 19:5	Exposure Time (sec)	Heater Config	Arc Current (Amps)	Arc Voltage (volts)	P _{cham} (atm)	q _{HTCL} Before (BTU/ft ² -sec)	q _{HTCL} After (BTU/ft ² -sec)	P ₂ Before (atm)	P ₂ After (atm)	N _B (BTU/lbm)	N _C Before (BTU/lbm)	N _C After (BTU/lbm)	q _{SLUG} RAD, BLK (BTU/ft ² -sec)	Source Current (Amps)	Source Voltage (volts)	P _{90X} Start (mm)	P _{90X} End (mm)	Δ P _{90X} (mm)	N ₂ O ₂ (lbm/sec)	q _{SLUG} CONV (BTU/ft ² -sec)	T ₅ (max) W/O REFL Component (°R)	
1-15 ¹	4/18 to 5/16	N/A	3																				
16	5/20																						
17																							
18 ²	5/20	30		252	413	NO DEFL	1981	1907	781														
20 ³	5/21	30.86/29.80		315	413	7	1860	2130	670														
22 ⁴	7/21	N/A		300	415	.86	1879	N/A	N/A														
23	7/22	N/A		N/A	N/A	N/A	1610	N/A	N/A														
24	7/22	N/A		N/A	N/A	N/A	670	N/A	N/A														
25	7/22	59.86		300	409	.936	1807	1792	784														
26	7/23	45.5/45.8		300	425	.962	1661	1824	875														
28 ⁶	7/28	30.0/30.4		320	450	.962	726	2043	1688														
32 ⁷	8/1	N/A	2	200	75	.116	55	N/A	N/A														
				228	75	.120	55																
				228	97	.194	315																
				200	97	.192	261																
33	8/1	N/A		200	75	.129	82	N/A	N/A														
				200	86	.149	137																
				213	75	.144	150	N/A	N/A														
34	8/5	N/A		300	75	.168	300																
				339	75	.184	360																
				199	75	.111	66	N/A	N/A														
35	6/5	N/A		250	75	.121	80																
				296	75	.133	120																
36	8/5	N/A		300	75	.145	833	104	967 ^B	967 ^B													
37	8/7	N/A		300	75	.126 & .132	150	120	N/A														
38	23825	59.95/59.70		300	75	.110	806	134	806														
39	19422	59.7/60.0		300	75	.110	731	134	836 ^B	731													
41 ⁹	8/12	N/A	1	300	50	.132	752	NO DEFL	N/A	N/A													
42	8/13	N/A		300	50	.162	NO DEFL	N/A	N/A	N/A													
43 ¹⁰	8/13	N/A		300	50	.134	1014	NO DEFL	N/A	N/A													
				300	50	.165	N/A																
44	8/13	N/A		400	85	.149	N/A	NO DEFL	N/A	N/A													
45	8/14	N/A		400	85	.152	997	15.2 ¹¹	17.4 ¹¹	1045													
46 ¹⁴	8/18	128.7		400	75	.211	103 ¹³	4.2 ¹³	7.3 ¹³	1793													

TABLE B-1. CONCLUDED

Test Model Number	Date	Exposure Time (sec)	Heater Config	Arc Current (amps)	Arc Voltage (volts)	P _{chan} (ATM)	RAO Before (BTU/ft ² -sec)	q _{HYCAL} CONW Before (BTU/ft ² -sec)	q _{HYCAL} CONW After (BTU/ft ² -sec)	H _g Before (BTU/lbm)	H _g After (BTU/lbm)	P _g Before (ATM)	P _g After (ATM)	h _g Before (BTU/lbm)	h _g After (BTU/lbm)	q _{SLUG} RAD, BLK (ft ² -sec)	Source Current (amps)	Source Voltage (volts)	P _{BOX} (mW)	L _{in} (m)	Δ P _{BOX} (mW)	Δ P _{BOX} (mW)	Δ P _{BOX} (mW)	q _{SLUG} CONW (BTU/ft ² -sec)	T _g (°K)
48	27	8/27/75	59.2	2	300	75	1476	189	154	1441	16505.18	.089 ¹⁷	.090 ¹⁷	23662	24814	1320A	1200	80	56	67	11	.00084	N/A	6017	
49	30	8/27	29.4	300	75	1.05	2210	204	170	1938	16505.18	.120	.144	23797	15000	N/A	1500	90	58.5	67	8.5		N/A	6173	
50	14	8/28	30.15	300	75	1.07	2189	170	170	2121	16505.18	.05	.083	23890	17719	1263A	1500	90	56	65	9		N/A	5993	
51	24	8/28	59.62	1	300	75	2287	—	NO OEFL	2237	12527.28	.087 ¹⁷	.090 ¹⁷	23890	17719	1263A	1500	90	57	66.5	9.5	.00126	N/A	6680	
52	29	8/29	29.65	300	75	1.06	2510	50.5	50.5	2342	12527.28	.078 ¹⁷	.083 ¹⁷	23890	17719	1271A	1500	90	57	62.4	5.4		N/A	5974	
53	20	8/29	29.35	300	75	1.03	2460	50.5	50.5	2342	12527.28	.081 ¹⁷	.084 ¹⁷	23890	17719	1284A	1500	90	54.5	64	9.5		N/A	6684	
54	26	9/2	30.05	300	75	1.094	2460	16.8	33.7	2291	12527.28	.115	.143	23890	17719	1390A	1500	90	58	65.2	7.2		N/A	6658	
58 ⁹	2	9/5	21.20	3	300	425	2082	3353	2929	1880	12527.28	.245	.170	23662	24814	1022A	1500	90	1	6.4	5.4	.016	N/A	6068 ²⁰	
60 ²¹	3	9/8	30.00	300	425	1.841	2923	3082	2055	—	—	.223	.229	23890	17719	1500	1500	90	4	12.8	8.8		N/A	6605 ²²	
61	10	9/8	19.30	300	425	1.841	2217	3280	2172	2217	—	.230	.191	23890	17719	1217A	1300	85	2.5	12.1	9.6		N/A	6540	
62	6	9/8	20.10	300	425	1.770	2329	3065	2172	2172	—	.305	.261	23890	17719	1237A	1300	85	4	21.3	17.3		N/A	6579	
63	13	9/8	21.65	300	425	1.771	—	—	—	—	—	.254	.178	23890	17719	1130A	1300	85	3	10.4	7.4		N/A	6627	
64	31	9/9	19.75	300	425	1.960	2233	2471	1995	2160	—	.247	—	23890	17719	—	1500	90	1.5	10.0	8.5		N/A	6676	
69 ²³	CAL	9/12	NA	6	350	1050	1.841	4632	N/A	N/A	—	.897	N/A	17083	N/A	N/A	N/A	N/A	54.5	64	9.5	.025	N/A	N/A	N/A
70	12	9/12	15.10	375	1050	1.841	N/A	4903	N/A	N/A	—	.915	N/A	17904	N/A	N/A	N/A	N/A	54	54	NO OEFL	.023	N/A	N/A	7158
71	15	9/16	8.60	350	1050	1.730	1610	4921	4994	—	—	.852	.852	18622	18899	—	1500	90	54	64	11		N/A	7082	
72	18	9/16	8.70	350	1050	1.770	1809	4740	4759	1574	—	.864	.857	17812	17957	—	1500	90	54	63.5	9.5		N/A	7092	
73	17	9/16	8.50	350	1050	1.735	1590	4759	4885	1502	—	.865	.860	17873	18400	1101A	1500	90	53	61.5	8.5		N/A	7102	
76 ²⁴	11	9/17	30.00	4	200	650	1788	36.1	N/A	903	5941 ²⁹	1.0	1.0	17684	18188	1493A	1500	90	54 ²⁵	760	0.0	.0084	N/A	6618	
77	16	9/17	45.65	200	675	1.060	1598	36.3	54.5	903	5941 ²⁹	1.0	1.0	17684	18188	1587A	1500	90	52 ²⁵	760	0.0		—	6653	
78	35	9/17	45.95	200	650	0.992	1719	54.3	73.4	1068	5941 ²⁹	1.0	1.0	17684	18188	1645A	1500	90	59 ²⁵	760	0.0		—	6649	
79	34	9/18	45.30	200	625	1.060	1628	90.5	—	1060	5941 ²⁹	1.0	1.0	17684	18188	1320B	1500	90	60 ²⁵	760	0.0	.0065 ²⁷	—	6807	
80	32	9/18	45.40	200	600	0.950	1592	36.2	72.4	1068	5941 ²⁹	1.0	1.0	17684	18188	1181B	1500	90	59 ²⁵	760	0.0	.0065 ²⁷	—	6762	
																1402B	1500	90	760	760	0.0	COLD	N/A	7062	

A = INJECTION AFTER MODELS B = INJECTION BEFORE MODELS

COMPIC NUMBER	DESCRIPTION			
	N	P _g (ATM)	u _g (ft./sec)	Q _g (ft. ³ /sec)
1	SUBSONIC	0.1	120	
2	SUBSONIC	0.1	890	
3	SUBSONIC	0.1	Q _g = 2.75*	
4	SUBSONIC	1.0	120	
6	SUBSONIC	1.0	Q _g = 1.00*	

TABLE B-2. AEHS TEST CONDITIONS AND REDUCED HTJ-S ABLATION DATA

Model Number	Test Number	Date	P _{t2} Before (ATM)	P _{t2} After (ATM)	H ₈ (BTU/lbm)	H ₈ Before (BTU/lbm)	H ₈ After (BTU/lbm)	$\rho_e U C_M^{14}$ (lbm/ft ² -sec)	\dot{s} (in/sec)	\dot{m} (ps) (lbm/ft ² -sec)	T _s (w/o REFL) (max) (°R)	$\rho_e U C_M^0$ 8' 0
8 Proof	18	5/20	—	—	—	—	—	—	.00278	.0266	—	—
2 Proof	—	—	—	—	—	—	—	—	.00498	.0477	—	.422
1 Proof	20	5/21	.128	.188 ¹⁵	—	18160	17159	.113	.00434	.0416	—	.368
4 Proof	—	—	.128	.188	—	18160	17159	.113	.00342	.0328	6489	.318
7	25	7/22	.101	.170	—	19861	15181	.103	.00417	.0400	6410 ⁵	.342
1	26	7/23	.119	.243	—	16819	12925	.117	.00295	.0283	6321 ⁵	.242
9	—	—	.119	.243	—	16819	12925	.117	.00474	.0454	6289	.432
5	28 ⁶	7/28	.124	.152	—	20265	15123	.105	.00325	.0312	6369	.297
8	—	—	.124	.152	—	20265	15123	.105	.000918	.00880	5988	.884
23	38	8/8	.122	.198	13458 ¹⁶	—	—	.00996	.000818	.00784	6135	.787
25	—	—	.122	.198	13458 ¹⁶	—	—	.00996	.00123	.0118	5855	1.185
19	39	8/8	.103	.168	13458 ¹⁶	—	—	.00996	.00113	.0108	5995	1.084
22	—	—	.103	.168	13458 ¹⁶	—	—	.00996	.000521	.00499	5536	—
21	45	8/14	.130	.195	—	—	—	—	.000423	.00405	5744	—
28	46	8/18	.157 ³⁰	.157 ³⁰	—	—	—	—	—	—	—	—

TABLE 8-2. CONCLUDED

Test Number	Date	P_{t_2} Before After (ATM)		H_B (BTU/lbm)	H_C Before After (BTU/lbm)		$\rho_{Ue}^{Ue} M_0^{14}$ (lbm/ft ² -sec)	\dot{s} (in/sec)	\dot{m} (ps) (lbm/ft ² -sec)	T_s (w/o REFL) (max) (=R)	$\rho_{Ue}^{Ue} M_0$ m/ e ^{Ue} M ₀
48	8/27/75	.089	.090	16505 ¹⁸			.0104	.000765 ³³	.00733	6017	0.705
49	8/27	.120	.144	16505 ¹⁸			.0113	.00434 ³³	.0416	6173	3.68
50	8/28	.081 ³¹	.083	16505 ¹⁸			.0103	.00425 ³³	.0407	5903	3.95
51	8/28	.087	.090	12527 ²⁶			.00414 ³²	.00273 ³³	.0262	5680	6.33 ³²
52	8/29	.078	.083	12527 ²⁸			.00414 ³²	.00332 ³³	.0318	5974	7.68 ³²
53	8/29	.081	.084	12527 ²⁸			.00414 ³²	.00452	.0433	6684	10.46 ³²
54	9/2	.115	.143	12527 ²⁸			.00414 ³²	.00429 ³³	.0411	6655	9.93 ³²
58	9/5	.245	.170		23662	24814	.130	.00773	.0741	6605 ¹⁷	0.57
60	9/8	.223	.229		22797	15000	.136	.00915	.0877	6605 ⁶	0.64
61	9/8	.230	.191		23890	17719	.132	.00766	.0734	6540	0.56
62	9/8	.305	.201		19386	14850	.153	.00689 ³⁴	.0661 ³⁴	6579	0.43 ³⁴
63	9/8	.254	.178		22434 ³⁵	18096 ³⁵	.138 ³⁵	.00690	.0661	6627	0.48
64	9/9	.247	.173 ³⁶		17367	16754	.131	.00914	.0876	6676	0.67
70	9/12	.852	.852		18622	18899	.264	.0213	.204	7158	0.773
71	9/16	.864	.857		17812	17957	.266	.0164	.157	7082	0.590
72	9/16	.865	.860		17873	18400	.265	.0171	.164	7092	0.618
73	9/16	.860	.864		17684	18188	.266	.0195	.187	7102	0.703
76	9/17	1.0	1.0	5941			.0122	.000428 ³³	.00410	6612	0.336
77	9/17	1.0	1.0	5941			.0122	.00152	.0146	6653	1.200
78	9/17	1.0	1.0	5941			.0122	.00163 ³⁷	.0156 ³⁷	6649	1.280 ³⁷
79	9/18	1.0	1.0	5941			.0122	.00163	.0156	6507	1.280
80	9/18	1.0	1.0	5941			.0122	.000989 ³³	.00948	6762	0.770
81	9/18	1.0	1.0	N/A			N/A	.00145 ³³	.0139	7022	N/A

FOOTNOTES TO TABLES B-1 AND B-2

APPENDIX B

1. Initial system checkout runs: starting procedure verified, P_{BO} rise calibrated - pumps required defined, exposure time determined, instrumentation verified.
2. Radiation source went out during model exposure, restarted after models.
3. Runs 19 & 21 - no data available.
4. Two injections, Hy-Cal data repeated.
5. Radiation chopper not on for this test. T_{MAX} w/o RELF estimated from runs 25 & 28.
6. Main valve closed - data not reduced.
7. Run 29: starting procedure; run 30: no data available; run 31: N_2 load pressure fell off - main supply closed.
8. Exposed to combined convective and radiative flow.
9. Run 40: no deflection - no data.
10. New slug calorimeter installed.
11. Medtherm - 12 calorimeter - questionable data.
12. Slug exposed to convective flow, therefore not blacked for radiation after measurement.
13. All probes injected downstream of test station ≈ 1.0 ".
14. Run 47: no deflection on data channels.
15. Based on average of P_t after from runs 25, 26, 28.
16. H_B value assuming 54 percent arc heater efficiency (η). No enthalpy peaking, and fully filled nozzle.
17. Initial P_{t2} trace off scale. $P_{t2} = \Delta P_{t2} + P_{BOX}$ @ injection.
18. H_B value assuming 65 percent arc heater efficiency (η), no enthalpy peaking, and fully filled nozzle.

19. Runs 55-57 starting procedure verified.
20. Bad CEC galvo.
21. Run 59 laser not on, pyro not visible on CEC, proof test model exposed data not reduced.
22. Chopper effect not visible on O'graph, max temperature curve was estimated from reflective component of similar runs.
23. Runs 65-68 starting procedure verified.
24. Runs 74-75 starting procedure verified.
25. Reduced cabin pressure for start only, bleed up to 1.0 atm for test.
26. New slug calorimeter installed for remainder of test.
27. N_2 only.
28. H_B value assuming 74 percent arc heater efficiency (η), no enthalpy peaking, and fully filled nozzle.
29. H_B value assuming 40 percent arc heater efficiency (η), no enthalpy peaking, and fully filled nozzle and average of voltages for this condition.
30. Based on average P_{t2} values from runs 44 & 45.
31. Estimated from run 48 P_{t2} .
32. Estimated from $\dot{q} = 50.5$ BTU/ft²-sec on run 53.
33. \dot{s} data from $\Delta s/\Delta \theta)_f$, based on film pre- and post-profile measurements. No reference line available for film \dot{s} reduction.
34. Estimated from average ratio of \dot{s} nom film/ $(\Delta s/\Delta \theta)$ for runs 61 and 63.
35. Estimated from average of runs 58, 60-62.
36. Estimated from previous run.
37. Based on average \dot{s} nom/ $\Delta s/\Delta \theta$ ratio from runs 77 and 79; 76 and 80 not included because no \dot{s} nom was available and $\Delta s/\Delta \theta$ was significantly different than $\Delta s/\Delta \theta$ film.

REFERENCES

1. Drowart, J., Burns, R. P., DeMaria, G., and Inghram, M. G., "Mass Spectrometric Study of Carbon Vapor," The Journal of Chemical Physics, Vol. 31, 1959, p. 1131.
2. Brewer, L., Gilles, P., and Jenkins, F., "Vapor Pressure and Heat of Sublimation of Graphite," Journal of Chemistry and Physics, Vol. 16, 1948, pp. 797-807.
3. Doehaerd, T. H., Goldfinger, P., and Waelbroeck, F., "La Tension de Vapeur et la Chaleur de Sublimation du Carbon III," Bulletin, Soc. Chim. Belg., Vol. 62, 1953, pp. 498-544.
4. Thorn, R. J. and Winslow, G. H., "Vaporization Coefficients of Graphite and Composition of the Equilibrium Vapor," The Journal of Chemical Physics, Vol. 26, 1957, p. 186.
5. Noda, T., reported by Mii, H., Proceedings of the International Symposium on High Temperature Technology, Asilomar Conf. Grounds, Calif., Oct. 6-9, 1959; Stanford Research Inst., Menlo Park, McGraw-Hill, N.Y., 1959.
6. Beque, J., Thesis, Paris 1945, as discussed by P. Goldfinger and F. Waelbroeck, "La Tension de Vapeur et la Chaleur de Sublimation du Carbon IV," Bulletin Soc. Chim. Belg., Vol. 62, 1953, p. 545.
7. Zavitsanos, P.D., "The Vaporization of Pyrolytic Graphite," R66S031, May 1966, General Electric Co.
8. Chupka, W. A. and Inghram, M. G., "Direct Determination of the Heat of Sublimation of Carbon with the Mass Spectrometer," The Journal of Physical Chemistry, Vol. 59, 1955, pp. 100-104.
9. Pitzer, K.S. and Clementi, L., "Large Molecules in Carbon Vapor," Journal of the American Chemical Society, Vol. 81, 1959, p. 4477.
10. Schoessow, G. J., "Graphite Tripole Point and Solidus-Liquidus Interface Experimentally Determined Up to 1000 Atmospheres," NASA CR-1148, July 1968, University of Florida.
11. Jones, M. T., "The Phase Diagram of Carbon," National Carbon Research Laboratories, PRG-3, January 1958.
12. Bundy, F. P., "Melting of Graphite at Very High Pressure," Journal of Chemical Physics, Vol. 18, No. 3, 1 February 1963.
13. Vereshchagin, L. F. and Fateeva, N. S., "Melting Curves of Graphite, Tungsten, and Platinum Up to 60 KBar," Soviet Physics JETP, Vol. 28, No. 4, April 1969.
14. Milne, T. A., Beachey, J. E., and Greene, F. T., "Vaporization Kinetics and Thermodynamics of Graphite Using the High Pressure Mass Spectrometer," Final Technical Report AFML-TR-74-57, May 1974.
15. Wachi, F. M. and Gilmartin, D. E., "High-Temperature Mass Spectrometry-I. Free Vaporization Studies of Graphites," Carbon, Vol. 8, pp. 141-154, 1970.
16. Basset, J., "Fusion of Graphite Under Pressure of Argon of 1 to 11,500 Kg So Cm, Determination of the Triple Point, and the Establishment of a Provisional Diagram for the Solid, Liquid and Gaseous States of Carbon," Journal de Physique et Le Radium, Vol. 10, 1939, pp. 217-228.
17. Steele, W. C., "Studies of Gas-Solid Interactions Using a Modulated Beam Mass Spectrometer," Technical Report AFML-TR-69-80, April 1969.
18. Konig, Hans, "The Melting of Carbon," Naturwissenschaften, 34, pp. 108-111, 1947.
19. Whittaker, A. G., Kinter, P. L., Nelson, L. S., and Richardson, N., "Determination of Carbon Vapor Pressure in the Region of the Solid-Liquid-Vapor Triple Point and the Formation of Unusual Carbon Polymorphs by Use of CO₂ Laser Radiation," Paper given in Dallas, 9 October 1975.
20. Wachi, F. M. and Gilmartin, D. E., "Heat of Formation and Entropy of C₃ Molecule," Aerospace Report No. TR-0172 (2250-40)-7, May 1972.

21. "JANAF Thermochemical Tables," 1971, Dow Chemical Co., Midland, Michigan.
22. Dolton, T. A., Goldstein, H. E., Maurer, R. E., AIAA 3rd Thermophysics Conference, Paper No. 68-754, Los Angeles, California, June 1968.
23. Kratsch, K. M., Martinez, M. R., Clayton, F. I., Green, R. B., and Wuerer, J. S., Graphite Ablation in High-Pressure Environments. AIAA Entry Vehicle Systems and Technology Conference, Williamsburg, Virginia, December 1968.
24. Lundell, J. H. and Dickey, R. R., "Ablation of ATJ Graphite at High Temperatures," AIAA Journal, Vol. 11, No. 2, February 1973.
25. Lundell, J. H. and Dickey, R. R., "Ablation of Graphite Materials in the Sublimation Regime," Vol. 13, No. 8, August 1975.
26. Strauss, H. L. and Thiele, E., "Thermodynamics of C_3 . II, General Methods for Non-rigid Molecules at High Temperatures," The Journal of Chemical Physics, Vol. 46, No. 7, 1 April 1967.
27. Diaconis, N. S., Stover, E. R., Hook, J., and Catalano, G. J., "Graphite Melting Behavior," AFML-TR-71-119, July 1971.
28. Van Vechten, J. A., "Scaling Theory of Melting Temperatures of Covalent Crystals," Physical Review Letters, Vol. 29, No. 12, 18 September, 1972.
29. Maurer, R. E., Wool, M. R., and Rindal, R. A., "Experimental and Analytical Evaluation of Graphite Ablation Utilizing the Ballistic Range," Technical Report AFML-TR-72-176, September 1972. (Confidential)
30. Powars, C. A., "Reduced Data Report: Fall 1971 AFML/SAMSO Ablation Tests in the AFFDL 50 MW Rent Arc," Aerotherm Project 7035, August 1972. (Confidential)
31. Lees, L., "Convective Heat Transfer with Mass Ablation and Chemical Reactions," Third AGARD Combustion and Propulsion Colloquium, May 1958.
32. Putz, K. E. and Bartlett, E. P., "Heat-Transfer and Ablation-Rate Correlations for Reentry Heat-Shield and Nostip Applications," Journal of Spacecraft and Rockets, Vol. 10, No. 1, January 1973.
33. Ziering, M., "Thermochemical Ablation of Carbon Base Heat Shields," AVCO Technical Release, K230-70-MZ-69, May 1970.
34. Kratsch, K. M., Dirling, R. B., Jr., and Swain, C. E., "Erosion Mechanisms and Improvement of Graphitic Materials, Volume III. Thermochemical and Micromechanical Erosion of Graphite," AFML-TR-70-307, August 1972. (Confidential)
35. Kelly, J. T., "User's Manual General Nonequilibrium Ablation Thermochemistry (GNAT) Computer Program," Aerotherm Report UM-74-54, October 1974.
36. Maurer, R. E., "An Evaluation of Some Uncertainties in Carbon Sublimation Kinetics," Aerotherm TM-73-28, January 1973.
37. Baker, R. L., "Graphite Ablation Chemistry Nonequilibrium Effects," AIAA Pre-Print No. 75-735, October 1975.
38. Davy, W. C., and Bar-Nun, A., "Vaporization Characteristics of Carbon Heat Shields Under Radiative Heating," AIAA Pre-Print 72-296, AIAA 7th Thermophysics Conference, San Antonio, Texas, April 10-12, 1972.
39. Peterson, D. L., Gowen, F. E., and Richardson, C., "Design and Performance of a Combined Radiative-Convective Heating Facility," AIAA Pre-Print No. 71-255, AIAA 6th Aerodynamic Testing Conference, Albuquerque, New Mexico, March 10-12, 1971.
40. Whittaker, A. G. and Kintner, P. L., "Particle Emission and Related Morphological Changes Occuring During the Sublimation of Graphitic Carbons," Report of Work Supported Under SAMSO Contract F04701-75-C-0076, The Aerospace Corp., El Segundo, California.

41. Maahs, H. G. and Schryer, D. R., "Particle Removal in the Ablation of Artificial Graphite," AIAA Journal, Vol. 7, No. 11, Nov. 1969, pp. 2178-2179.
42. Maurer, R. E., "Interim Report Passive Nostip Technology (PANT) Program Volume VI - Graphite Ablation Data Correlation and Analysis," SAMSO-TR-74-86, January 1974.
43. Zoby, E. V., "Empirical Stagnation-Point Heat-Transfer Relation in Several Gas Mixtures at High Enthalpy Levels," NASA-TN-D-4799, Langley Research Center, Langley Air Force Base.
44. Kays, W. M., Convective Heat and Mass Transfer, McGraw-Hill Series in Mechanical Engineering, McGraw-Hill Book Company, 1966.
45. Forney, D. M., editor, "Graphite Materials for Advanced Reentry Vehicles, Part 1 - Analytical Techniques and Material Characterization," AFML-TR-70-133, August 1970.
46. Moeckel, W. L. and Weston, K. C., "Composition and Thermodynamic Properties of Air in Chemical Equilibrium," NACA TN 4265, Lewis Flight Propulsion Laboratory, Ohio, April 1958.
47. Lundell, J. H. and Dickey, R. R., "Vaporization of Graphite in the Temperature Range of 4000° to 4500°K," AIAA Paper 76-166, AIAA 14th Aerospace Sciences Meeting, Washington, D.C., January 26-28, 1976.
48. Wakefield, R. M. and Peterson, D. L., "A Study of Graphite Ablation in Combined Convective and Radiative Heating," AIAA Paper No. 72-88, AIAA 10th Aerospace Sciences Meeting, San Diego, Calif. 1972.
49. Powars, C. A., "Analysis of PANT Series A Rough Wall Calorimeter Data, Part I. Surface Roughness Effects on Heat Transfer," Aerotherm Report 73-80, C/N 7040.273, September, 1973.
50. Maurer, R. E., Cangie, C. D., and Powars, C. A., "The Feasibility of Carbon Sublimation Tests in the 50 MW Arc," Aerotherm Report No. TM-74-46, July 1974.
51. Hartman, C., Cangie, C. D., and Lee, K., "Assessment of Applicability of Martin-Marietta 6 MW Constrictor Arc to Task I Graphite Vaporization Tests,"

AD

BO14238

AUTHORITY:

AFWAL

1tr, 19 NOV 82

